INTERNATIONAL ATOMIC ENERGY AGENCY
UNITED NATIONS EDUCATIONAL, SCIENTIFIC AND CULTURAL ORGANIZATION
INTERNATIONAL CENTRE FOR THEORETICAL PHYSICS
I.C.T.P., P.O. BOX 586, 34100 TRIESTE, ITALY, CABLE: CENTRATOM TRIESTE

SMR.755/19

Workshop on Fluid Mechanics

(7 - 25 March 1994)

Pattern forming instabilities

S. Fauve
Ecole Normale Supérieure de Lyon
46, allée d'Italie
69364 Lyon
France

Stéphan Fauve
Ecole Normale Supérieure de Lyon
46, allée d'Italie 69364 Lyon France

1. Pattern Forming Instabilities

Instabilities in nonlinear systems driven far from equilibrium often consist of a transition from a motionless state to one varying periodically in space or time. Various examples, widely studied in the past years, are, Rayleigh-Benard convection, Couette-Taylor flow, waves in shear flows, instabilities of liquid cristals, oscillatory chemical reactions, ... The appearence of periodic structures in these systems driven externally by a forcing homogeneous in space or constant in time, corresponds to a bifurcation, characterized by one or several modes that becomes unstable as a control parameter is varied. Linear stability analysis of the basic state gives the critical value of the control parameter for the primary instability onset, the nature of the most unstable modes and their growthrate above criticality. Many examples have been studied for a long time and can be found for instance in the books of Chandrasekhar (1961) or Drazin and Reid (1981). However, linear stability analysis does not describe the saturation mechanism of the primary instability, and thus a nonlinear analysis should be performed to determine the selected pattern, its dynamics and in particular the secondary instabilities that occur as the control parameter is increased above criticality. Before considering these problems, we present some examples of the charateristic phenomena that occur above a pattern-forming instability onset.

1.1 Example : The Faraday instability

As a first example, consider a cylindrical vessel containing a liquid and its vapour (or any other gas), vertically vibrated at frequency ω_e (Figure 1.1).

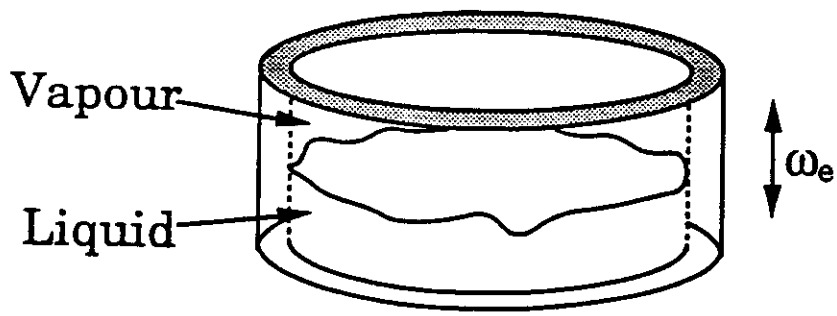

Figure 1.1. Sketch of the apparatus for the Faraday instability.

It was discovered by Faraday (1831) that when the vibration amplitude exceeds a critical value, the flat liquid-gas interface becomes unstable to standing waves. Figures 1.2 a and 1.2 b display the surface waves excited by vertical shaking, seen from above. The axisymmetric standing wave of Figure 1.2 a is observed as a transient at instability onset; the shape of this mode is due to the circular geometry of the vessel. This is the most unstable linear eigenmode of the flat interface. However, this axisymmetric pattern is not nonlinearly stable; in a large enough container, nonlinear interactions select the square pattern of Figure 1.2 b, which is the stable stationary state just above the instability onset. Thus, from this first example, one observes that the patterns ultimately selected by the instability do not generally correspond to the most unstable linear mode. Here, nonlinear effects are strong enough to overcome boundary effects that trigger the axisymmetric pattern.

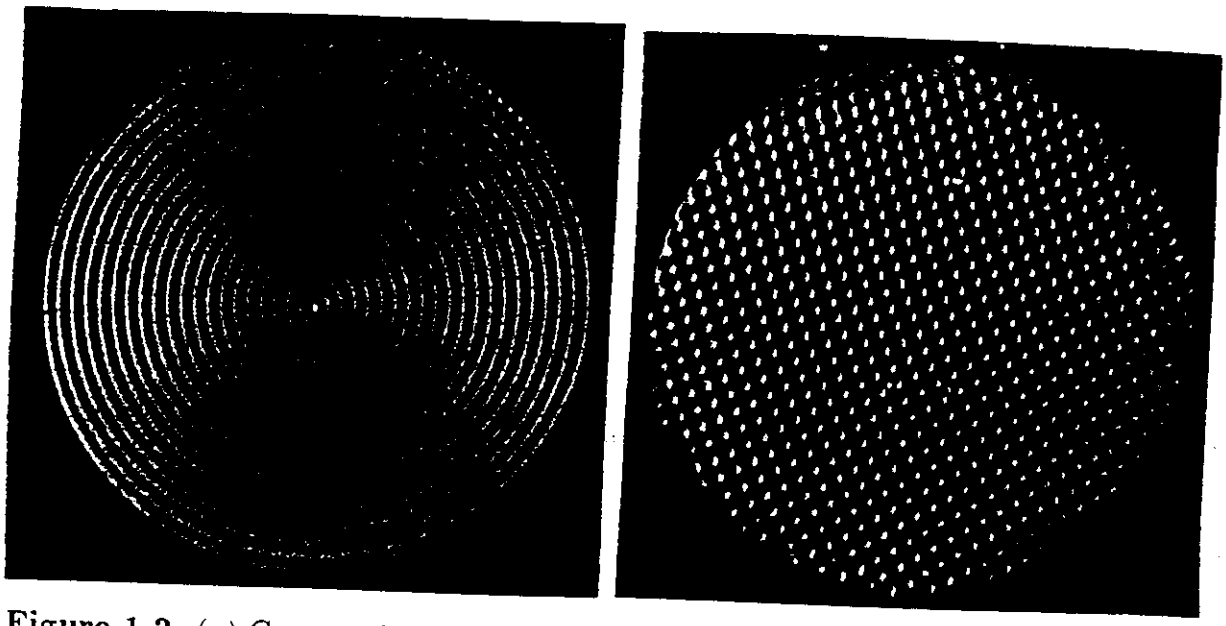

Figure 1.2. (a) Concentric circular standing waves at the interface between liquid CO_2 and its vapour submitted to vertical vibrations. This pattern is only observed as a transient regime at instability onset; it is unstable to modulations perpendicular to the wave crests (already apparent) and the final stable stationary standing wave pattern is the square array (b).

We can think of the square pattern as the result of two sets of counter-propagating waves, perpendicular to each other and of equal amplitudes. When we have a liquid-vapour system, we can approach the critical point at which the liquid-vapour interface disappears. Near this critical point, the nonlinear interaction between the intersecting waves changes so that they cannot both remain stable, and one set vanishes. We then get a one-dimensional standing wave pattern (Figure 1.3). Thus nonlinear effects not only saturate the growth of the linearly unstable modes but they also act as a selection mechanism for the pattern.

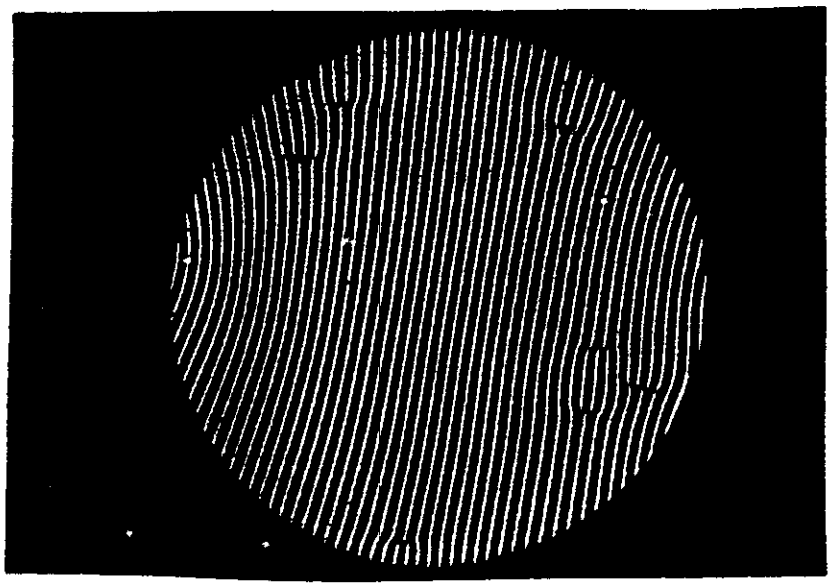

Figure 1.3. Near the critical liquid-vapour point of CO_2, only one of the perpendicular sets of waves can remain. Note the defects in the wave pattern.

In Figure 1.3 we see that some of the wave-crests do not reach all the way across the vessel. The endpoint of a crest is called a *defect*. If one integrates the phase-gradient along a closed curve around one of these defects, the integral comes to $\pm 2\pi$ instead of 0, because one passes more waves on one side of the defect than on the other. At the defect itself, the amplitude of the wave vanishes, so that at this point the phase is undefined. Defects are widely observed when a periodic pattern undergoes a secondary instability. In the above example, they nucleate or annihilate by pair or at the lateral boundary and during their life-time, move in the underlying periodic pattern. Their dynamics plays an important rôle in the transition to spatiotemporal disorder. Their shape traces back to the pattern symmetries. For instance, defects of the square standing wave pattern consist of lines instead of points; they separate two regions of the wave-field that oscillate out of phase (Figure 1.4).

Secondary instabilities of periodic patterns do not always generate defects. An important class of secondary instabilities consists of long-wavelength modulations of the primary pattern. The surface wave pattern in an elongated rectangular geometry or in an annular container, i.e. when a one-dimensional wave is forced by the boundary conditions, exhibits a secondary instability consisting of a long wavelength spatiotemporal modulation of the primary pattern wavelength (Figure 1.5).

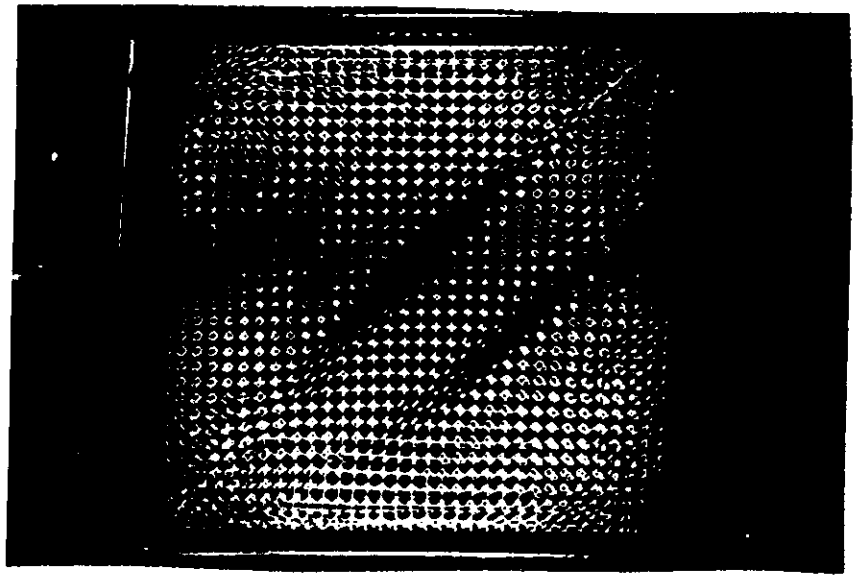

Figure 1.4. Line-defects in surface waves on vertically-shaken mercury. The regions on opposite sides of the lines are out of phase with one another.

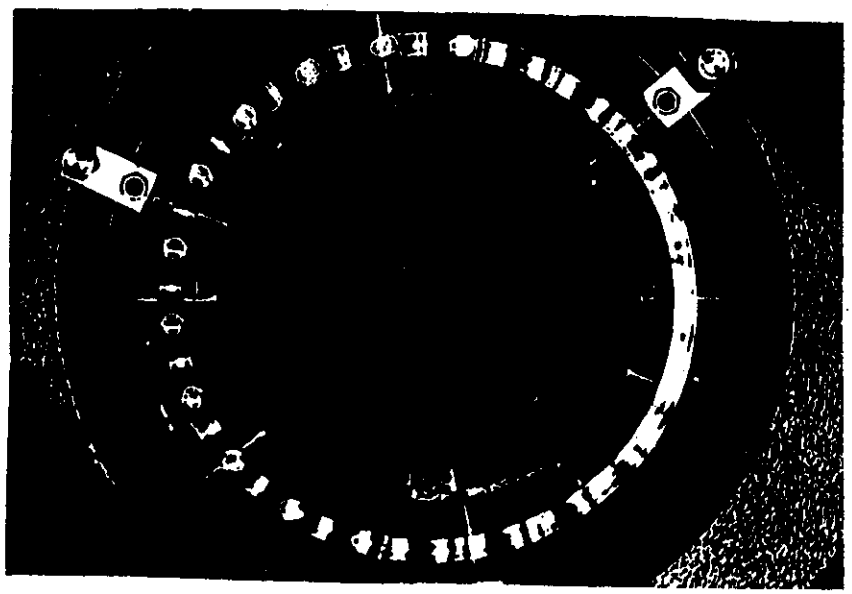

Figure 1.5. Snapshot of the long wavelength modulation of the basic standing wave in an annular geometry. The basic standing wave consists of 21 wavelengths and the wavelength of the modulation is equal to the perimeter of the annulus.

1.2 Analogy with phase-transitions : amplitude equations

The different phenomena described above are not particular to parametrically generated surface waves; long-wavelength instabilities or defect-dynamics are widely observed above the onset of most pattern-forming instabilities (Wesfreid and Zaleski, 1984 ; Wesfreid et al., 1988). An obvious unifying description consists of looking for evolution equations for the

amplitude and the phase, i.e. for the complex amplitude of the periodic pattern generated by the primary instability. Indeed, at the primary instability onset, the critical modes have, by definition, a vanishing growth-rate ; we will show that adiabatic elimination of all the other (faster) modes leads to nonlinear partial differential equations that govern the amplitude of the critical modes, and so describes the slow modulations in space or time of the periodic structure envelope : these are the *amplitude equations*. We will see that the form of the amplitude equations can be derived simply from symmetry considerations, and that the underlying detailed equations are needed only to evaluate parameters in the amplitude equations. Another possible way is to use experiments to determine the parameters in an amplitude equation, because we can know the form of the equation without knowing all the details of the microscopic dynamics. This is similar to the description of a fluid flow using Navier-Stokes equation the form of which traces back to conservation laws ; the coefficients, viscosity for instance, depend on the microscopic dynamics and might be computed using the Boltzmann equation; it is however simpler and more reliable to use the experimentally measured coefficients.

We will mainly be studying amplitude equations, rather than the microscopic governing equations of the underlying systems. We take this approach because similar patterns are observed in a wide range of systems, and their behaviour is a result of the broken symmetries at the primary instability onset rather than of the microscopic dynamics. Systems with different microscopic description frequently exhibit, on a macroscopic level, similar patterns which are governed by the same amplitude equation. The situation is analogous to the one we encounter in phase-transions in condensed-matter physics where the behaviour of the order parameter is governed by symmetries and does not depend on the "chemical details" of the system. The close analogy between instabilities in nonlinear systems driven far from equilibrium and phase transitions is now well documented experimentally as well as theoretically. This idea was fathered by Landau (1941), and developed by several people in the context of hydrodynamics, electric circuits, nonlinear optics and chemical instabilities. In this context, the complex amplitude of the periodic pattern plays the role of an order parameter and characterizes the broken symmetries at instability onset. Amplitude equations are analogous to the Ginzburg-Landau description of phase transitions.

1.3 Long wavelength neutral modes : phase dynamics

The second area that we will study is the disorganization of the primary pattern through secondary instabilities. When the primary instability saturates nonlinearly and gives rise to a finite amplitude periodic pattern, only its phase remains neutral in the long-wavelength limit. Indeed, a spatially uniform modification of the phase corresponds to a shift of the periodic pattern, and thus is neutral because of translational invariance in space. Likewise, other broken symmetries, translational invariance in time at the onset of an oscillatory instability, Galilean invariance at the onset of a pattern-forming instability, etc ..., may

generate long-wavelength neutral modes, i.e. modes that are neither dissipated nor amplified at zero wavenumber. These modes are analogous to Goldstone modes in particle physics or condensed-matter physics, and often lead to secondary instabilities of the primary pattern. Because their growthrate vanishes in the long wavelength limit, we eliminate adiabatically the other fast modes in order to obtain evolution equations that describe pattern-dynamics through its slowly varying phases. Thus, contrary to the situation at instability onset, the pattern amplitude is no longer a neutral mode above criticality; for a perfectly periodic pattern, it saturates at a finite value. However, phase instabilities, that usually occur at zero wavenumber do not always saturate in the long wavelength limit; they often cascade to short scales, leading to defect nucleation in the primary pattern. Although non-neutral, the pattern amplitude locally vanishes, thus breaking the long-wavelength approximation. A consistant description of this type of pattern-dynamics is still an open problem.

1.4 Localized nonlinear structures

Shock-waves or solitons are well known examples of nonlinear localized structures. Defects of periodic patterns are another class of localized structures. Although incompletely, we will define the main characteristics of these objects, try to classify them and to understand their dynamics.

Another type of localized structure is well known in fluid dynamics and illustrated by plate 109 in Van Dyke (1982), reproduced here as Figure 1.6. It is a turbulent spot, i.e. a region of turbulent flow advected in a laminar flow. This type of structure is widely observed in pipe flows or boundary layers. The turbulent region can expand when moving, but there are also solutions where the spot keeps a nearly constant size.

Similarly, pattern forming instabilities can display localized structures consisting of a region in the bifurcated state surrounded by the basic state. This occurs when there is a parameter range in which the system has two stable states of different form; then one might observe both of them in separate regions. Thermal convection of a binary fluid mixture in an annulus, studied by Kolodner, Bensimon and Surko (1988), displays such localized patterns (Figure 1.7).

An earlier example is the localized standing wave observed in Faraday instability (Wu, Keolian and Rudnick, 1984). In the limit of small dissipation, we will show that these structures trace back to the solitary waves of conservative systems.

Figure 1.6. Emmons spot in the boundary layer over a flat plate.

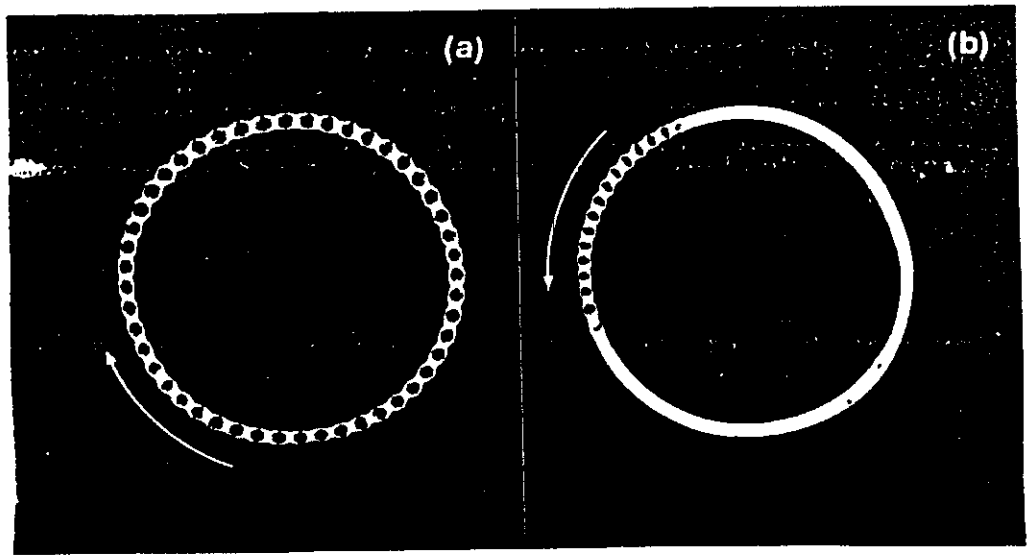

Figure 1.7. (a) Periodic pattern of travelling convection rolls (b) The travelling rolls fill only part of the annulus ; both the conducting and convecting states are stable and coexist in different regions of the annulus.

References

Chandrasekhar, S. (1961) *Hydrodynamic and Hydromagnetic Stability*, Clarendon Press, Oxford.

Drazin, P. G. and Reid, W. H. (1981) *Hydrodynamic Stability*, Cambridge University Press.

Faraday, M. (1831) Phil. Trans. R. Soc. London, **52**, 319.

Kolodner, P., Bensimon, D. and Surko, C.M. (1988). *Travelling-wave convection in an annulus*, Phys. Rev. Lett. **60**, 17.

Landau, L., (1967) *On the theory of phase transitions, On the problem of turbulence*, Collected papers of L. Landau, Gordon and Breach .

Van Dyke, M. (1982). *An Album of Fluid Motion*

Wesfreid, J. E. and Zaleski, S., (1984) *Cellular Structures in Instabilities*, Lectures Notes in Physics, Springer Verlag

Wesfreid, J. E., Brand, H. R., Manneville, P., Albinet, G. and Boccara, N., (1988) *Propagation in Systems far from Equilibrium*, Springer Verlag.

Wu, J., Keolian, R. and Rudnick, I. (1984). *Phys. Rev. Lett.* **52**, 1421.

2. Nonlinear Oscillators

In this lecture we study simple dissipative nonlinear oscillators as the simplest examples of temporal patterns, i.e. periodic limit cycles, quasiperiodic regimes and frequency locking phenomena. Two different amplification mechanisms are considered to balance dissipation and sustain an oscillatory regime:

- "negative dissipation", for which the system is autonomous,

- parametric forcing, where an external time dependent perturbation is applied.

Our objective is to find an amplitude equation for the amplitude and phase of the oscillation. We show that its form depends on the amplification mechanism, because the broken symmetries at the oscillatory instability onset are different, but that universal behaviour of the oscillation amplitude and the frequency exists in both types of oscillator. We next consider a negative dissipation oscillator with an external time-dependent forcing, and study frequency-locking phenomena.

2.1 Van der Pol Oscillator

We begin with an autonomous system with negative dissipation. The canonical example is the Van der Pol oscillator, introduced in electronics a long time ago (Van der Pol, 1934). The governing equation is

$$\ddot{u} - 2\lambda\dot{u} + u^2\dot{u} + \omega_0^2 u = 0.$$

Here, the dissipation is negative if $\lambda > 0$ and the nonlinear term causes the system to saturate when $u^2 \sim \lambda$.

2.1.1 Global or linear stability

Some insight into the behavior of this equation can be obtained by studying the total energy of the system, which is here a simple example of Liapunov functional. This is a useful first

step before attempting a more detailed analysis. The sum of potential and kinetic energies is

$$E = \omega_0^2 \frac{u^2}{2} + \frac{\dot{u}^2}{2}$$

and the time derivative of the energy is

$$\dot{E} = \omega_0^2 u\dot{u} + \dot{u}\ddot{u} = (2\lambda - u^2)\dot{u}^2.$$

Thus if $\lambda < 0$ (linear damping), $\dot{E} < 0$. Moreover, there is a lower bound, $E = 0$, which occurs if and only if $u = \dot{u} = 0$, and consequently the motionless state is globally stable.

We are interested in the case $\lambda > 0$. A linear stability analysis about u = 0 is done by taking $u \propto \exp(\eta t)$, and if $\mathcal{R}e(\eta) > 0$ the system is unstable. Substituting into the Van der Pol equation and linearizing gives the characteristic polynomial

$$\eta^2 - 2\lambda\eta + \omega_0^2 = 0$$

or $\eta = \lambda \pm \sqrt{\lambda^2 - \omega_0^2}$. If we let $\lambda = \mu\epsilon$ where ϵ is small, $\eta \simeq \mu\epsilon \pm i\omega_0^2$ and the system becomes unstable as λ changes sign; this is a Hopf bifurcation and the system's behavior changes from a damped oscillation to an amplified oscillation as λ increases. Near the bifurcation point, the growth rate is small and the time scale of the growth is $T \sim 1/\epsilon$).

2.1.2 Nonlinear effects

The linear analysis predicts exponential growth, but this is eventually checked by the nonlinear term, which leads to saturation when $u^2 \simeq \epsilon$. We can see this by studying the energy balance of the system. We suppose that there is a harmonic limit cycle when λ is small and so we are close to the bifurcation, and we also presume that the amplitude of the oscillation varies on a slow time scale, thus

$$u \approx a(t)\cos\omega_0 t \quad \text{and} \quad \dot{u} \approx -\omega_0 a(t)\sin\omega_0 t.$$

The energy balance over one cycle requires

$$\frac{1}{T}\int_0^T \dot{E}dt = 0 \quad \text{or} \quad 2\lambda\overline{\dot{u}^2} - \overline{u^2\dot{u}^2} = 0,$$

where the overbar denotes averaging over one cycle.

Using the above expressions for u, we find $a^2 = 8\lambda = 8\mu\epsilon$, and so the oscillation amplitude above criticality is, $u \sim \sqrt{\epsilon}$.

A second rôle of the nonlinearity is the production of higher harmonics and the subsequent shift of the fundamental frequency. We show next that these effects are connected. If the governing equation is multiplied by u and averaged over one cycle, the terms involving $\dot{u}$ all average to zero and we are left with the virial equation

$$\overline{\dot{u}^2} = \omega_0^2 \overline{u^2}.$$

Note that both the nonlinear and dissipative terms have averaged to zero. However, the effect of nonlinearity still enters, since we assume that u contains some higher harmonic components:

$$u = \sum_{n=1}^{\infty} a_n \cos(n\omega t + \phi_n).$$

When this is substituted into the virial equation, we obtain

$$\sum n^2 \omega^2 a_n^2 = \omega_0^2 \sum a_n^2.$$

and this can be written as

$$\frac{(\omega^2 - \omega_0^2)}{\omega_0^2} = -\frac{\sum (n^2 - 1) a_n^2}{\sum n^2 a_n^2}.$$

Assuming that the successive harmonics amplitude decreases fast enough with increasing n, the frequency shift, $\Delta\omega \equiv \omega - \omega_0$, is to leading orders,

$$\frac{\Delta\omega}{\omega_0} \simeq -\frac{3}{2}\frac{a_2^2}{a_1^2} - 4\frac{a_3^2}{a_1^2} + \ldots.$$

Thus the shift of the fundamental frequency is related to the existence of higher order harmonics. For the Van der Pol equation, there is no quadratic nonlinearity and $a_2 = 0$; thus there is no frequency correction to leading order. Note however that the relationship between the fundamental frequency shift and the harmonics amplitude, is in general not so simple as the one above. For instance, replace $\omega_0^2 u$ by $\omega_0^2 \sin u$ in the Van der Pol equation and try the same exercise.

2.1.3 Amplitude equations : the multiple-scale method

In cases where the amplitude varies much more slowly than the underlying oscillation, we can use the disparity in temporal scale to obtain a simplified description of amplitude variations independently of the faster time scale. This is sketched schematically in Figure 2.1. The oscillation has time scale t. We introduce a second time variable, $T = \epsilon t$, to parameterize the slow variation in amplitude; indeed, in the vicinity of instability onset, $\lambda = \mu\epsilon$, the instability growth-rate scales like ϵ.

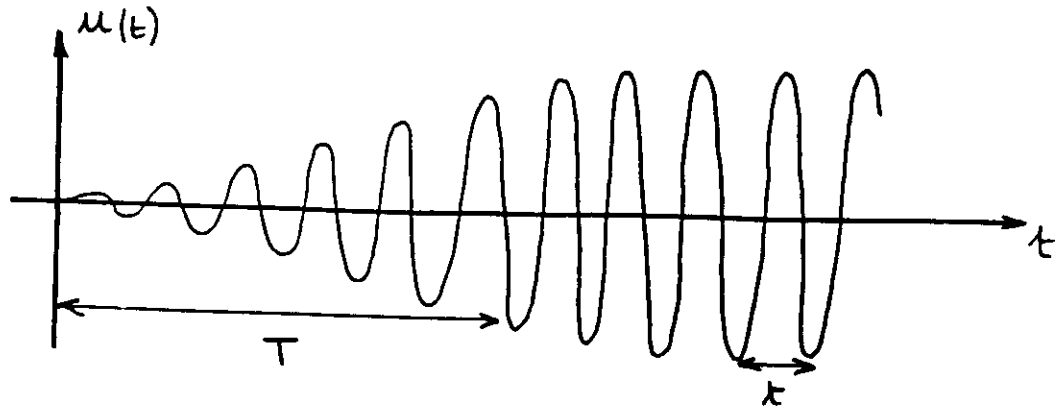

Figure 2.1. Amplitude varying much more slowly than the oscillation gives multiple time scales.

We have already seen that the saturation amplitude for u scales like $\sqrt{\epsilon}$, so we take

$$u(t) \to \sqrt{\epsilon}\tilde{u}(t, T).$$

Using

$$\frac{\partial}{\partial t} \to \frac{\partial}{\partial t} + \epsilon\frac{\partial}{\partial T}$$

we rewrite the Van der Pol equation:

$$\epsilon^{1/2}\frac{\partial^2\tilde{u}}{\partial t^2} + 2\epsilon^{3/2}\frac{\partial^2\tilde{u}}{\partial t\partial T} + \epsilon^{5/2}\frac{\partial^2\tilde{u}}{\partial T^2} + (\epsilon\tilde{u}^2 - 2\mu\epsilon)(\epsilon^{1/2}\frac{\partial\tilde{u}}{\partial t} + \epsilon^{3/2}\frac{\partial\tilde{u}}{\partial T}) + \epsilon^{1/2}\omega_0^2\tilde{u} = 0.$$

We can factor $\sqrt{\epsilon}$ out of every term in this equation; then to order ϵ^0, we have a simple harmonic oscillator:

$$(\frac{\partial^2}{\partial t^2} + \omega_0^2)\tilde{u} = 0$$

It will prove convenient to define $\mathcal{L} = \frac{\partial^2}{\partial t^2} + \omega_0^2$. We can now introduce a perturbation expansion

$$\tilde{u} = \tilde{u}_0 + \epsilon^{1/2}\tilde{u}_1 + \epsilon\tilde{u}_2 + \ldots$$

and collect terms in increasing powers of ϵ:

$$\epsilon^0 : \mathcal{L}\tilde{u}_0 = 0$$

$$\epsilon^{1/2} : \mathcal{L}\tilde{u}_1 = 0$$

$$\epsilon^1 : \mathcal{L}\tilde{u}_2 = -2\frac{\partial^2\tilde{u}_0}{\partial t\partial T} - \tilde{u}_0^2\frac{\partial\tilde{u}_0}{\partial t} + 2\mu\frac{\partial\tilde{u}_0}{\partial t}$$

and so forth. The ϵ^0 equation is easily solved:

$$\tilde{u}_0 = A(T)e^{i\omega_0 t} + \bar{A}(T)e^{-i\omega_0 t},$$

where $A(T)$ is the slowly-varying amplitude of the oscillation. We could write such a solution to the $\epsilon^{1/2}$ equation as well, but since $\tilde{u}_1$ does not appear in the equation for $\tilde{u}_2$, we don't need it until we go to higher order. Substituting the leading order solution into the ϵ^1 equation yields

$$\mathcal{L}\tilde{u}_2 = 2i\omega_0(\mu A(T) - \frac{dA}{dT})e^{i\omega_0 t} - i\omega_0(|A|^2 Ae^{i\omega_0 t} + A^3 e^{3i\omega_0 t}) + cc$$

"cc" in this (and subsequent) equations refers not to a specific expression, but to the complex conjugate of the preceding expression.

In order to avoid secular growth of $\tilde{u}_2$, it is necessary to set the resonant terms—the terms in $e^{i\omega_0 t}$—to zero. Doing so yields

$$(2(\mu A(T) - \frac{dA}{dT}) - |A|^2 A)e^{it} - cc = 0$$

Since e^{it} and e^{-it} are linearly independent, we can set the displayed expression and its complex conjugate to zero independently. Hence,

$$\frac{dA}{dT} = \mu A - \frac{1}{2}|A|^2 A.$$

Taking $A = Re^{i\theta}$, factoring out $e^{i\theta}$ and separating real and imaginary parts, gives

$$\frac{dR}{dT} = (\mu - \frac{1}{2}R^2)R$$

$$\frac{d\theta}{dT} = 0,$$

The amplitude R approaches $\sqrt{2\mu}$ when $\mu > 0$ and the phase θ does not vary with the slow time scale at all. This second feature is not generic for a Hopf bifurcation and traces back to the absence of frequency shift to leading order. As a simple exercise, you can again consider the Van der Pol equation with $\omega_0^2 \sin u$ instead of $\omega_0^2 u$, and show that a term proportional to R^2 occurs the θ equation.

Generically, the amplitude equation for a Hopf bifurcation is of the form

$$\frac{dA}{dT} = \mu A - \beta|A|^2 A$$

with $\beta = \beta_r + i\beta_i$ some complex number. Then, the equations for R and θ become

$$\frac{dR}{dT} = (\mu - \beta_r R^2)R$$

$$\frac{d\theta}{dT} = -\beta_i R^2.$$

If $\beta_r > 0$, The leading order nonlinearity saturates the instability and the bifurcation is said "direct" or "supercritical". Above instability onset, the oscillation amplitude is proportional to $\sqrt{\mu}$. Otherwise, the bifurcation is "inverse" or "subcritical". In the supercritical situation, the phase increases linearly in time, indicating the fundamental frequency shift proportional to μ. Oscillatory instabilities observed experimentally often display this characteristic behaviour for the oscillation amplitude and frequency slightly above criticality. The correponding measurements are a useful check that the system undergoes a Hopf bifurcation. Note however, that the frequency ω_0 itself usually depends on the experimental control parameter (proportional to μ); this dependence is generally linear to leading order and adds to the one due to β_i. This makes β_i difficult to measure precisely.

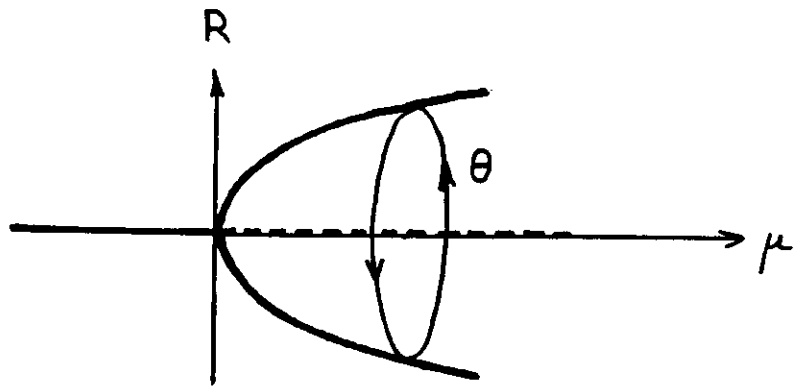

Figure 2.2. Diagram of the supercritical Hopf bifurcation.

2.1.4 Symmetry arguments

We show next that the form of the evolution equation for the oscillation complex amplitude A is determined by symmetry constraints. It is clear that the original Van der Pol equation

$$\ddot{u} - 2\lambda\dot{u} + u^2\dot{u} + \omega_0^2 u = 0$$

describes an autonomous system, i.e. it is invariant under translation in time and is unaffected by a change of variables $t \to t + \theta$. This does not mean that any solution should be translationaly invariant in time; any oscillatory solution, and in particular the expansion we used for u

$$u = \sqrt{\epsilon}[A(T)e^{i\omega_0 t} + \bar{A}(T)e^{-i\omega_0 t}] + \epsilon u_1 + \ldots,$$

obviously breaks translational invariance in time. However, the ensemble of possible solutions should have this invariance. In other words, any image of an oscillatory solution under the transformation corresponding to the broken symmetry must be a solution of the autonomous

system. Thus, if $u(t)$ is an oscillatory solution, so is $u(t+\theta)$. This obvious requirement is enough to determine the form of the amplitude equation, if one assumes, and this is a crucial assumption, that dA/dT can be expanded in powers of A and $\bar{A}$ in the vicinity of instability onset.

Making the transformation $t \to t + \theta/\omega_0$, one get

$$u(t+\theta/\omega_0) = \sqrt{\epsilon}[A(T)e^{i\omega_0 t}e^{i\theta} + \bar{A}(T)e^{-i\omega_0 t}e^{-i\theta}] + \epsilon u_1 + \dots$$

The dynamics of the transformed u is to be the same as the original u, therefore the dynamics of A should be invariant under the transformation,

$$A(T) \to A(T)e^{i\theta}.$$

This transformation selects the combinations of A and $\bar{A}$ that can appear in the amplitude equation: only those which also transform with a factor of $e^{i\theta}$ will do. Consider all the possibilities up to cubic terms:

$$\boxed{A \to Ae^{i\theta}} \qquad \bar{A} \to \bar{A}e^{-i\theta}$$

$$A^2 \to A^2e^{2i\theta} \qquad A\bar{A} \to A\bar{A} \qquad \bar{A}^2 \to \bar{A}^2e^{-2i\theta}$$

$$A^3 \to A^3e^{3i\theta} \qquad \boxed{A^2\bar{A} \to A^2\bar{A}e^{i\theta}} \qquad A\bar{A}^2 \to A\bar{A}^2e^{-i\theta} \qquad \bar{A}^3 \to \bar{A}^3e^{-3i\theta}$$

Only the boxed terms scale appropriately, so only they can appear in the amplitude equation. Hence, we could have deduced the form of the amplitude equation simply from the symmetry of the original equation and the solution to the zeroth-order equation that fixes the broken-symmetry.

Note that we consider t and T as independent variables and did not change $A(T) \to A(T + \epsilon\theta/\omega_0)$. This is only approximately correct, and if we sought higher order perturbations, we would have to make the more complete substitution.

2.1.5 Discussion about symmetry arguments

A. Roberts pointed out that symmetry is not sufficient to reduce the possibilities to the few mentioned above. Rather, there is an implicit assumption that there are no memory effects. He presented an example term

$$A(T)\int_{-\infty}^{T} A(T')\bar{A}(T')K(T-T')dT'$$

which would satisfy the symmetry requirement but include memory effects.

The locality assumption is obviously made when one looks for dA/dT as an expansion in powers of A and $\bar{A}$. It would be interesting to work out a simple example with memory effects.

R. Salmon argued about the relevance of the symmetry requirement. He said that a differential equation has many symmetries, and that any solution can break some of these symmetries. He felt that the reason we consider time-translation symmetry and not some other symmetry is physical rather than mathematical.

The symmetries that have to be considered are the ones that are broken by the linearly unstable solution. The symmetry requirement for the ensemble of possible bifurcated solutions constraints the form of the amplitude equation. A symmetry of the original problem that is not broken by the linearly unstable mode gives no constraint on the amplitude equation. Amplitude equations can also have symmetries that are not forced by the original equation. As we will see when studying frequency-locking phenomena, the form of the linearly unstable mode is of crucial importance ;an amplitude equation is meaningless without the expression of the original field as a function of the amplitude.

2.2 Parametric Oscillators

We will now discuss the bifurcation structure of parametric oscillators. Parametric amplification occurs widely in physical situations. Examples include Langmuir waves in plasmas, spin waves in ferromagnets, surface waves on a ferrofluid in a time-dependent magnetic field, or on a liquid dielectric in an alterning electric field. As shown in the first section, parametric amplification of surface waves on a horizontal layer of fluid vertically vibrated, is a simple experimental model of pattern dynamics. Let us mention also that parametric amplifiers were widely used in electronics. We study here the simplest example which is a pendulum whose support is vibrated. The pendulum angle $u(t)$ from the vertical axis, is governed by the damped Mathieu equation

$$\ddot{u} + 2\lambda\dot{u} + \omega_0^2(1 + f\sin\omega_e t)\sin u = 0,$$

where λ is the damping, ω_0 is the natural frequency, f is the forcing amplitude and ω_e is the external forcing frequency. The resonance characteristics of the Mathieu equation are well known to occur whenever $n\omega_e - \omega_0 = \omega_0$ and are shown in Figure 2.3.

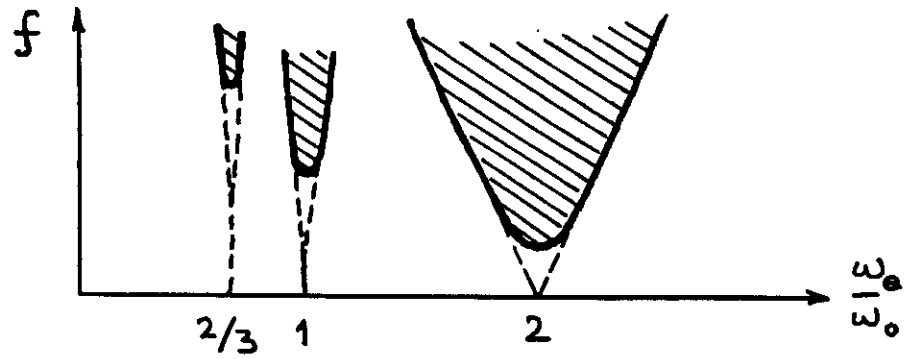

Figure 2.3. Resonance tongues of the Mathieu equation (unstable regions are hatched).

We now examine the strongest resonance $\omega_e = 2\omega_0$ in detail. We obtain the amplitude equation by the method of multiple scales. The three parameters in the equation are damping, forcing and detuning $\delta = \frac{\omega_0^2}{\omega_e^2} - \frac{1}{4}$. To bring in all the effects at the same order we use the scaling $\delta = \epsilon\Delta$, $\lambda = \epsilon\Lambda$, $f = \epsilon F$ and let

$$u(t) = \sqrt{\epsilon}\left[u_0(t,T) + \sqrt{\epsilon}u_1(t,T) + \ldots\right],$$

where the slow time is $T = \epsilon t$.

After substituting these in the equation and collecting terms we obtain at the zeroth order

$$\mathcal{L}u_0 \equiv (\frac{d^2}{dt^2} + \omega_0^2)u_0 = 0,$$

which has the solution

$$u_0 = A(T)e^{i\omega_0 t} + \bar{A}(T)e^{-i\omega_0 t}.$$

The first order equation is the same and its solution can be incorporated into u_0. The second order (ϵ^1) problem is

$$\mathcal{L}u_2 = -2\frac{\partial^2 u_0}{\partial t \partial T} - 2\Lambda\frac{\partial u_0}{\partial t} - \omega_0^2 F u_0 \sin\omega_e t + \frac{1}{6}\omega_0^2 u_0^3.$$

Using the fact that $\omega_e = 2\omega_0 - 4\epsilon\Delta\omega_0 + O(\epsilon^2)$ the solvability condition to eliminate resonant terms is

$$\frac{dA}{dT} = -\Lambda A + \frac{\omega_0 F}{4}\bar{A}e^{-4i\Delta\omega_0 T} - \frac{\omega_0}{4}iA^2\bar{A}.$$

By moving to a frame of reference rotating with $\omega_e/2$ (instead of ω_0) with the transformation $A = Be^{-2i\Delta\omega_0 T}$ we obtain the autonomous amplitude equation

$$\frac{dB}{dT} = (-\Lambda + i\nu)B + \mu\bar{B} + i\beta|B|^2 B$$

where $\nu = 2\Delta\omega_0$, $\mu = \omega_0 F/4$ and $\beta = -\omega_0/4$.

The form of this equation could have been guessed by using symmetry arguments, the relevant symmetry of the Mathieu equation being $t \to t + \frac{2\pi}{\omega_e}$, which restricts terms in the amplitude equation to be invarient under $B \to -B$. This symmetry is a much weaker restriction than the one for the Van der Pol equation ($A \to Ae^{i\theta}$). The term proportional to iB in the amplitude equation corresponds to a rotation of B at constant velocity in the complex plane and thus to a detuning. In other words, $\nu \neq 0$ indicates that $\omega_e/2$ and ω_0) are slighty different, thus that the forcing frequency is not exactly at parametric resonance. Moreover, collecting all the terms with pure imaginary coefficients, $i(\nu + \beta|B|^2)B$, shows that $\beta|B|^2$ is a nonlinear detuning. It is associated with the amplitude dependence of the oscillator frequency, and this nonlinear effect is the one that saturates the instability, by shifting the oscillator away from parametric resonance. This is to be contrasted to the Van der Pol oscillator where the instability is saturated by nonlinear damping. The term $\mu\bar{A}$, that breaks rotational invariance in the complex plane of the amplitude equation, is precisely the one that results from the parametric forcing.

Let us now study the linear stability of the solution $u = 0$. Writing $A = X + iY$ and inserting a mode proportional to $e^{\eta t}$ we obtain the following quadratic for the eigenvalues:

$$\eta^2 + 2\Lambda\eta + (\Lambda^2 - \mu^2 + \nu^2) = 0.$$

Since the damping, Λ, is positive, we see that there is no Hopf bifurcation contrary to the Van der Pol case. There is a stationary bifurcation at a threshold forcing amplitude $\mu_c = \sqrt{\Lambda^2 + \nu^2}$. This is shown in Figure 2.4 which reproduces the 2 : 1 resonance curve of Figure 2.1.

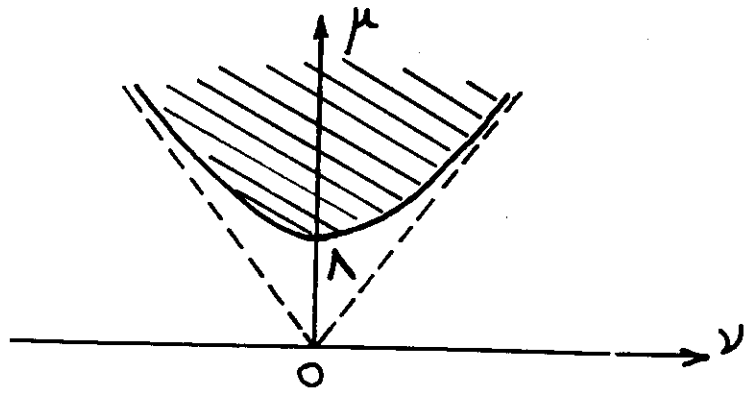

Figure 2.4. Linear stability in parameter space of $u = 0$ with 2 : 1 forcing

The nonlinear stability is only slightly more complicated. We write $A = Re^{i\theta}$ and obtain the equations

$$\frac{dR}{d\tau} = (-\Lambda + \mu\cos 2\theta)R,$$

$$\frac{d\theta}{d\tau} = \nu - \mu\sin 2\theta + \beta R^2.$$

To find the stationary solutions we set the right hand side of the equations to zero. Defining the finite amplitude stationary solution to be R_0 we obtain

$$\beta R_0^2 = -\nu \pm \sqrt{\mu^2 - \Lambda^2}.$$

Without loss of generality we take $\beta > 0$ (otherwise we consider the complex conjugate equation). For real solutions we need $\mu > \Lambda$. Then if $\nu > 0$ only the positive sign is valid and there is one solution for the amplitude, i.e. two solutions with different phases labeled here by 2×1). If $\nu < 0$, then for $\mu < \sqrt{\nu^2 + \Lambda^2}$ we can have 4 solutions (2 solutions with 2 phases). Figure 2.5 shows these different regions.

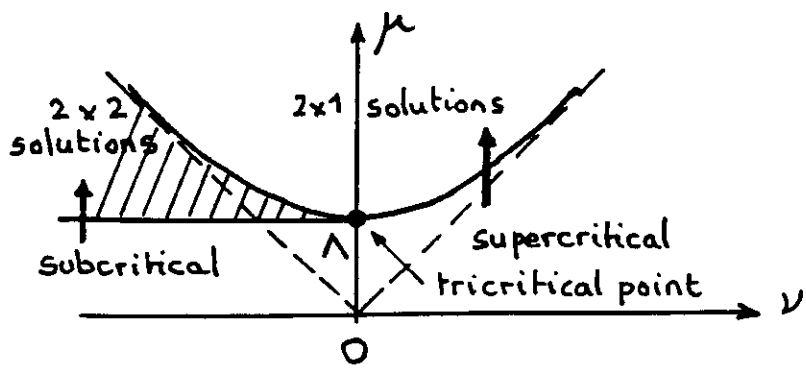

Figure 2.5. Bifurcation behaviour in parameter space

The behaviour is made clearer in the bifurcation diagrams. For $\nu > 0$ (Figure 2.6 a) we have a supercritical bifurcation at $\mu_c = \sqrt{\nu^2 + \Lambda^2}$. For $\nu < 0$ (Figure 2.6 b) we have a subcritical bifurcation which is why we have 2×2 non-zero solutions. The point $\nu = 0$, $\mu = \Lambda$ is a tricritical point (in the language of phase transitions). As usual in subcritical bifurcations one of the solutions is unstable (shown by the dashed branch in the diagram). The stability of the branches can be derived by perturbing the finite amplitude solutions. If we write $R = R_0 + r$ and $\theta = \theta_0 + \phi$, then the eigenvalue σ of the perturbation satisfies

$$\sigma^2 + 2\Lambda\sigma + 4\beta R_0^2(\nu + \beta R_0^2) = 0.$$

Thus, the bifurcated solutions are stable if $\nu + \beta R_0^2 > 0$.

Scaling behaviours above criticality display an interesting feature: for the tricritical point at $\nu = 0$, if one writes $\mu = \mu_c + \epsilon$, the amplitude scales as $R_0 \sim \epsilon^{\frac{1}{4}}$; for the supercritical

case $R_0 \sim \epsilon^{\frac{1}{2}}$ as for the Hopf bifurcation. For $\nu \simeq 0$, one expects a cross-over between the two behaviours. The bifurcation diagram of the parametric oscillator is richer than the one of the Hopf bifurcation. This is because parametric forcing involves two control-parameters, the forcing amplitude and its frequency, instead of one for the Hopf bifurcation.

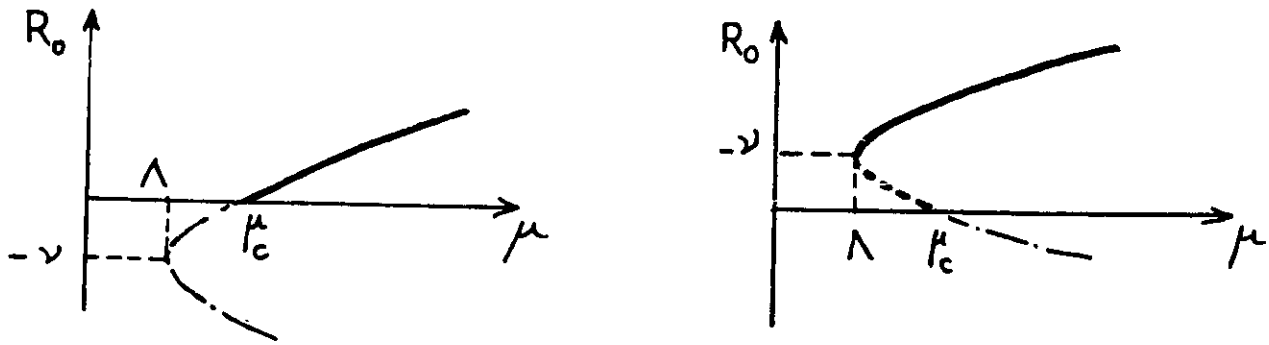

Figure 2.6. Bifurcation diagram for the parametric oscillator (a) $\nu > 0$, (b) $\nu < 0$.

2.3 Frequency locking

Two independent oscillators have generically incommensurate frequencies. In simple words, this means that if one sets-up two clocks, even as similar as possible, they oscillate at slightly different frequencies and thus finally indicate a different time if one waits long enough. It has been known since Huyghens that a coupling, even very small, can lock the phases of the oscillators i.e. force them to oscillate at the same frequency, or more generally with commensurate frequencies. In the phase-locking process, the system thus bifurcates from a quasiperiodic to a periodic regime. A similar situation exists in crystallography for spatial patterns, known as the commensurate-incommensurate transition.

Let us first show experimental results in Rayleigh-Benard convection. Convective rolls in a horizontal layer of mercury heated from below become unstable to an oscillatory motion as the temperature difference accross the layer is increased above a critical value. The mercury temperature thus oscillates at a "natural" frequency $\omega_0/2\pi$ (Figure 2.7 a). We apply an external periodic forcing by rotating the mercury layer about its vertical axis, with a sinusoidal angular velocity of frequency $\omega_e/2\pi$. Figure 2.7 displays the different flow regimes when the external frequency is about twice the natural one. One can observe locked (b) or quasiperiodic regimes (c, e). These regimes are located in the experimental parameter space displayed in Figure 2.8. At small forcing amplitude the locked regime is observed within a tongue (the "Arnold tongue") that begins at twice the natural frequency for vanishing external forcing amplitude. When the detuning is increased there is a transition from the locked to the quasiperiodic regime. For large forcing amplitude the natural oscillation is completely inhibited and the temperature oscillates at the forcing frequency ("forced" regime).

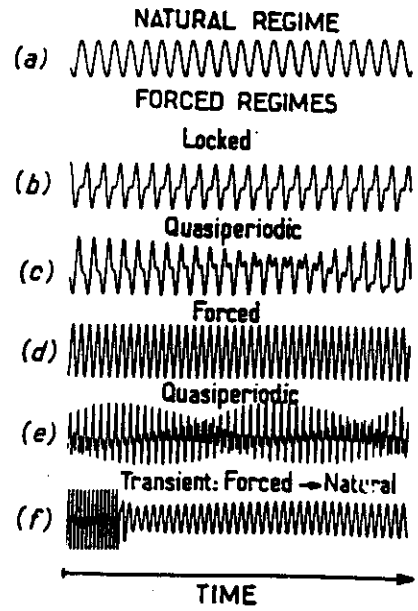

Figure 2.7. Temperature-time records of a layer of mercury heated from below, for different forcing amplitude and frequency, see Chiffaudel and Fauve (1987) for details.

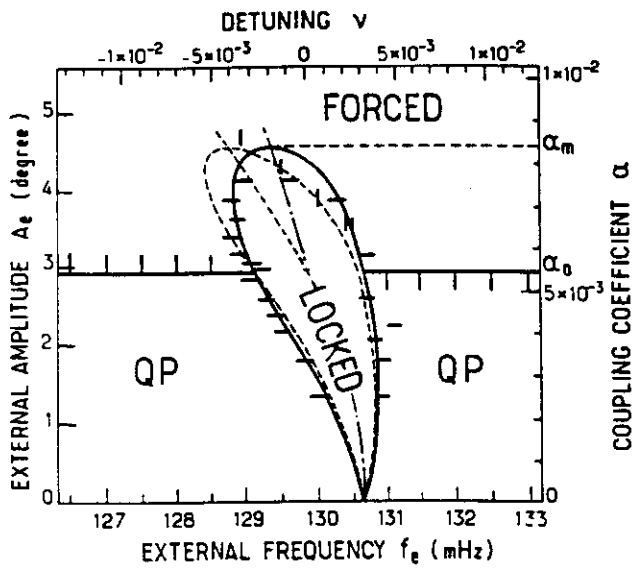

Figure 2.8. The locked, quasiperiodic and forced regimes as external forcing amplitude and frequency are varied. The bars correpond to experimentally measured transitions, the solid and dashed curves are calculated transition curves using an amplitude equation (the two theoretical curves correspond to different coefficients, see Chiffaudel and Fauve (1987) for details.

The transitions between these regimes can be modeled by considering the simpler system of a forced Van der Pol oscillator that is externally forced. The governing equation for this system is as considered in section 2, except for an additional forcing term $\sqrt{\epsilon} f \cos\omega_e t$. Assuming that the dissipation is small ($\lambda = \mu\epsilon$) and rescaling u by $\sqrt{\epsilon}$ we have

$$\ddot{u} + \omega_0^2 u = \epsilon(2\mu - u^2)\dot{u} + f\cos\omega_e t.$$

The method of multiple time scales is used to determine the amplitude equation for this system in precisely the same manner as for the previous systems.

We first consider non-resonant forcing (i.e. ω_e and ω_0 incommensurable). The leading order term in u is

$$u_0 = A(T)e^{i\omega_0 t} + \text{c.c.} + \frac{f}{\omega_0^2 - \omega_e^2}\cos\omega_e t,$$

where the last term is due to the external forcing. At the next order we have

$$\mathcal{L}u_1 = (2\mu - u_0^2)\frac{\partial u_0}{\partial t} - 2\frac{\partial^2 u_0}{\partial t \partial T}.$$

The solvability condition then gives

$$\frac{dA}{dT} = \xi A - \frac{1}{2}|A|^2 A,$$

where

$$\xi = \mu - \frac{1}{4}\left(\frac{f}{\omega_0^2 - \omega_e^2}\right)^2.$$

This amplitude equation is same as in the unforced case except for the form of the coefficients (when $f = 0$, $\xi = \mu$). The additional forcing term shifts the onset of instability to larger μ by reducing ξ, see Figure 2.9. One knows other examples of stabilization by applying a periodic forcing ; for instance, the unstable up-position of a pendulum can be stabilizated by vibrating the point of support.

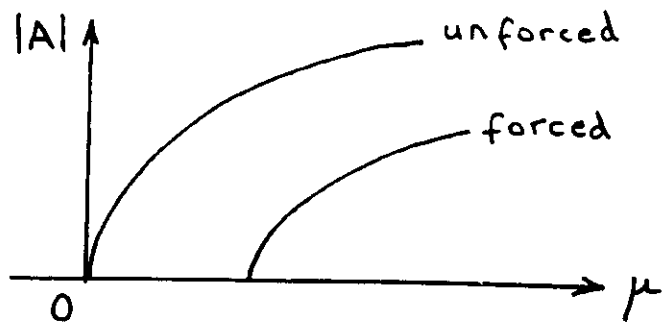

Figure 2.9. Variation of amplitude $|A|$ with μ for unforced (a) and forced (b) Van der Pol oscillators.

Note the symmetry, $t \to t + \frac{2\pi n}{\omega_e}$ (n is an integer), imposes the invariance $A \to Ae^{i2\pi n\frac{\omega_0}{\omega_e}}$, on the terms in the amplitude equation. For ω_0 and ω_e incommensurate, this is a constraint as strong as the rotation in the complex plane, $A \to Ae^{i\theta}$. Thus, the form of the amplitude equation is the same as in the unforced case, and phase-locking terms that break the $A \to Ae^{i\theta}$ invariance, cannot be found at any order in the amplitude equation. This is due to the form of the leading order solution, u_0.

Indeed, let us consider small amplitude forcing with $\omega_e = \omega_0 + \epsilon\sigma$ and $f = \epsilon F$. As the forcing is of order ϵ there is no term due to the forcing in u_0, and the leading order solution is

$$u_0 = A(T)\mathrm{e}^{i\omega_0 t} + \text{c.c.}.$$

However, the additional term $F\cos(\omega_0 t + \sigma t)$ at the next order changes the solvability condition so that

$$\frac{\mathrm{d}A}{\mathrm{d}T} = \mu A - \frac{1}{2}|A|^2 A - \frac{iF}{4\omega_0}\mathrm{e}^{i\sigma T}.$$

Writing $A = B\mathrm{e}^{i\sigma T}$, gives the amplitude equation

$$\frac{\mathrm{d}B}{\mathrm{d}T} = (\mu - i\sigma)B - \frac{1}{2}|B|^2 B - \frac{iF}{4\omega_0}.$$

This transformation amounts to writing

$$u_0 = B(T)\mathrm{e}^{i\omega_e t} + \text{c.c.},$$

and thus to looking for an amplitude equation in the "reference frame" of the external oscillator. For this new choice of u_0, the symmetry $t \to t + \frac{2\pi n}{\omega_e}$, only requires $B \to B$! There is no constraint on the amplitude equation, and indeed the rotation symmetry in the complex plane is broken to leading order by the forcing through the constant term $iF/4\omega_0$.

This simple example shows how important is the choice of the leading order solution, $u_0(t)$. The second choice is called "resonant forcing" although with a non-zero detuning σ one can describe a quasiperiodic regime. However, to leading order the response is assumed to be at the forcing frequency. It is the correct choice if one wants to describe frequency-locking phenomena.

Let us now generalize to the case : $\omega_e = n\omega_0/p$ (n, p are integers), where the system is invariant under discrete translation in time $t \to t + 2\pi/\omega_e$. The equation for the amplitude B of

$$u_0 = B(T)\mathrm{e}^{i\frac{p}{n}\omega_e t} + \text{c.c.},$$

must be invariant to the rotation $B \to B\mathrm{e}^{i2\pi p/n}$. Therefore an additional term $\bar{B}^{n-1}$ related to the forcing is allowed, and the amplitude equation is of the form

$$\frac{\mathrm{d}B}{\mathrm{d}T} = (\mu + i\nu)B - \beta|B|^2 B - \alpha\bar{B}^{n-1}.$$

The coefficient ν represents the detuning, while α is related to the forcing. When n=1, 2, 3 and 4 the forcing term is of at least the same order as the β term, and these are known as strong resonances.

The three different regimes correspond to :

1 $B = 0$, the forced regime,

2 B = const, the locked regime,

3 B time dependent, the quasiperiodic regime.

We consider the specific case $n/p = 2$. For simplicity we choose β to be real and equal to unity. The linear stability of the the forced regime $A = 0$ is exactly the same as that of the parametric oscillator considered earlier. It is stable when $\mu < 0$ and $\alpha^2 < \mu^2 + \nu^2$. The boundary at $\alpha^2 = \mu^2 + \nu^2$ corresponds to a stationary bifurcation (in the reference frame of the external oscillator), while the boundary at $\mu = 0$ is a Hopf bifurcation provided that $\nu^2 > \alpha^2$), and corresponds to the boundary between the forced and quasiperiodic regimes. Substituting $B = Re^{i\theta}$ into the amplitude equation we have that the locked regime ($d\theta/dt = 0$) occurs when $\sin 2\theta = \nu/\alpha$, hence when $|\nu| < |\alpha|$. When this inequality is not satisfied, there exists no constant non-zero solution for B and the system bifurcates to the quasiperiodic regime through a saddle-node bifurcation.

Figure 2.10 shows the three time-forced regimes on the (α, ν) plane.

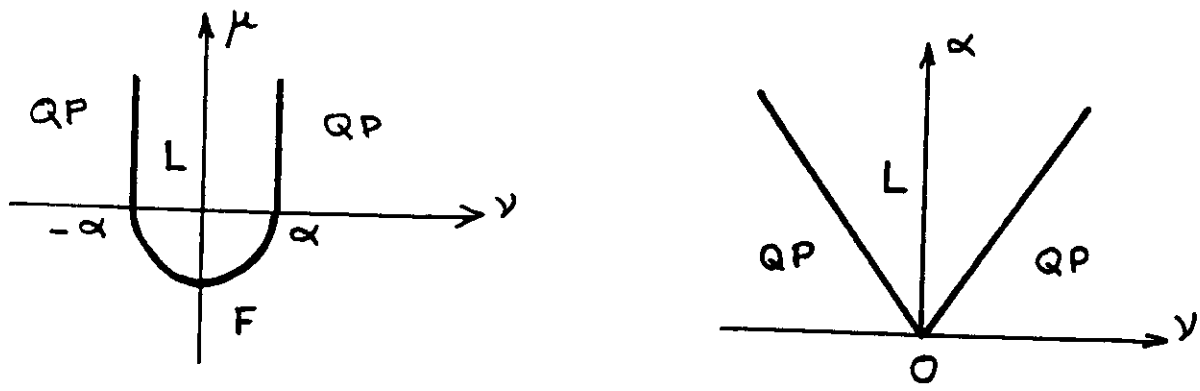

Figure 2.10. The three regimes for a forced Van der Pol oscillator. There is a stationary bifurcation between the forced (F) and locked (L) regimes, a Hopf bifurcation between the forced and quasiperiodic (QP) regimes, and a saddle-node bifurcation between the quasiperiodic and locked regimes. There are codimension-two points at ($\pm\alpha$, 0).

References

Arnold V. I. (1983) *Geometrical Methods in the Theory of Ordinary Differential Equations*, Springer Verlag.

Bender, C. M. and Orszag, S. A., (1978) *Advanced Mathematical Methods for Scientists and Engineers*, McGraw-Hill.

Chiffaudel, A. and Fauve, S., (1987) *Strong Resonance in Forced Oscillatory Convection*, Phys. Rev.**A 35**, 4004-4007.

Guckenheimer, J. and Holmes, P., (1984) *Nonlinear Oscillations, Dynamical Systems and Bifurcations of Vector Fields*, Springer Verlag.

Nayfeh A. H., (1973) *Perturbation Methods.*, Wiley-Interscience.

Van der Pol, B., (1934) Proc. I. R. E. **22**, 1051-1086.

3. Nonlinear Waves in Dispersive Media

In this section we consider the propagation of a quasi-monochromatic wave and study the dynamics of dispersion and nonlinearity. To wit, the objective is to find an evolution equation for the slowly varying amplitude and phase of the wave. Using this amplitude equation we can then study the long wavelength stability of periodic waves, and look for solitary wave-trains.

We begin with a simple example, namely the array of pendula shown in figure (3.1). Each pendulum oscillates in the plane perpendicular to the axis of the array and is coupled to its neighbours by torsion springs.

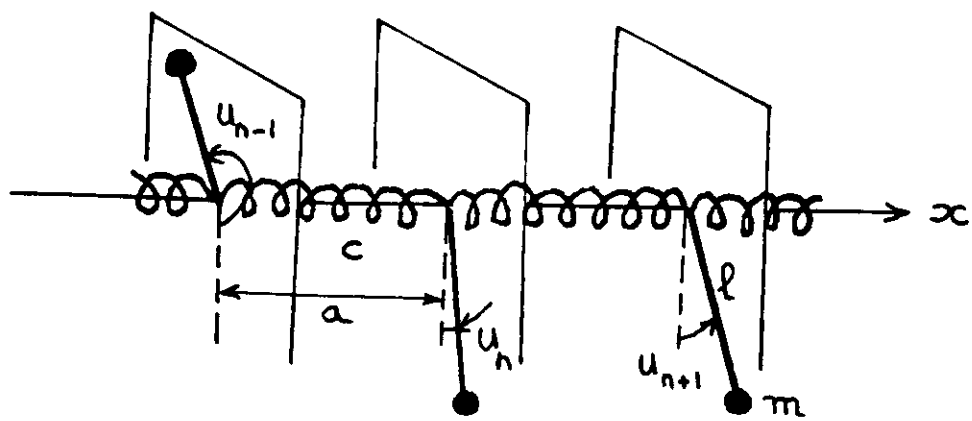

Figure 3.1. The array of coupled pendula

The equation governing the angle from the vertical, $u_n(t)$, of the n^{th} pendulum is,

$$m\,l^2\,\frac{d^2u_n}{dt^2} = -m\,g\,l\,\sin u_n + c\,(u_{n-1} - 2u_n + u_{n+1}),$$

where m is the mass of a pendulum, L is its length and c is the spring torsion constant. We want to investigate phenomena on a lengthscale $\lambda >> a$, where a is the distance between two pendula. In this case we can take the continuous limit of the above equation, and after rescaling time and space we obtain:

$$\frac{\partial^2 u}{\partial t^2} = -\sin u + \frac{\partial^2 u}{\partial x^2}. \tag{3.1}$$

This is the Sine-Gordon equation, which is also found in nonlinear optics, where it models the propagation of pulses in resonant media, in condensed-matter physics where it describes charge-density waves in periodic pinning potentials or propagation along Josephson transmission lines, and in field theory where it was used to describe elementary particles. However, it is also a long wavelength approximation of our array of pendula and it will be helpful to keep this example in mind to understand the results of this section and the different approximation levels.

3.1 Evolution of a wave packet

Consider a wave packet which is peaked around $k = k_0$, and can be written

$$u(x,t) = \int_{-\infty}^{\infty} F(k)\, e^{i(\omega(k)t - kx)} dk. \tag{3.2}$$

Linearising (3.1) about $u = 0$ and substituting for u using (3.2) gives the dispersion relation,

$$\omega^2 = 1 + k^2.$$

The group velocity, $U(k)$, is given by

$$U = \frac{d\omega}{dk} = \frac{k}{\omega}.$$

Notice that

$$\frac{d^2\omega}{dk^2} = \frac{\omega - U\,k}{\omega^2} = \frac{1 - U^2}{\omega} \neq 0,$$

so that the medium is dispersive.

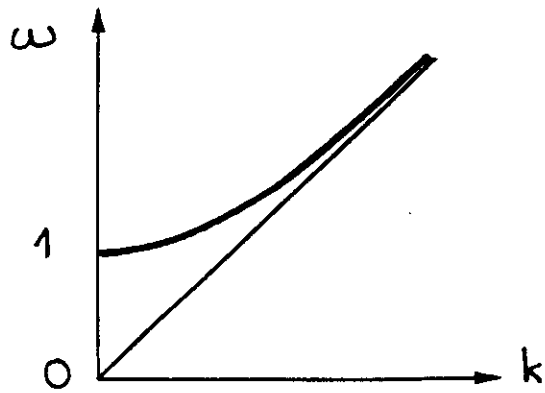

Figure 3.2. The dispersion relation for the wave packet described by equation (3.2).

The largest contribution to the integral in equation (3.2) will come from k in the neighbourhood of k_0 and we make the approximation

$$u(x,t) \simeq e^{i(\omega(k_0)-k_0 x)} \int_{-\infty}^{\infty} F(k_0+K) e^{i(\Omega(K)-Kx)} dK$$

where

$$\Omega(K) = U_0 K + \frac{\omega_0'' K^2}{2} + \cdots \tag{3.3}$$

$$U_0 = U(k_0),$$

$$\omega_0'' = \frac{d^2\omega}{dk^2}(k_0).$$

This gives us

$$u(x,t) \simeq A(x,t) e^{i(\omega_0 t - k_0 x)} + c.c. \tag{3.4}$$

where the envelope is

$$A(x,t) = \int_{-\infty}^{\infty} \hat{A}(K,t) e^{-iKx} dK,$$

and

$$\hat{A}(K,t) = F(k_0+K) e^{i\Omega(K)t}.$$

Now using (3.3) gives

$$i\Omega\hat{A} = iU_0 K\hat{A} + \frac{i\omega_0'' K^2 \hat{A}}{2} + \cdots$$

Taking the inverse Fourier transform we see that this corresponds to

$$\frac{\partial A}{\partial t} = -U_0 \frac{\partial A}{\partial x} - \frac{i\omega_0''}{2} \frac{\partial^2 A}{\partial x^2}. \tag{3.5}$$

Note that A is slowly varying in space compared to $2\pi/k_0$ since the wave packet is peaked around k_0. Thus it is clear from (3.5) that A is also slowly varying in time compared to $2\pi/\omega_0$ (where $\omega_0 = \omega(k_0)$). Equation (3.5) describes the amplitude of a slowly varying wave. The first term on the right hand side represents the propagation of amplitude perturbations at the group velocity, and can be removed if we transform to a reference frame moving at U_0. We then get a Schrödinger equation

$$\frac{\partial A}{\partial t} = i\alpha \frac{\partial^2 A}{\partial x^2},$$

where $\alpha = -\omega_0''/2$ represents dispersion. It is easily seen that $\xi = x^2/4i\alpha t$ is a similarity variable and that $\int |A|^2 dx$ is conserved. Thus, a self-similar solution is,

$$A \propto (4i\alpha t)^{-1/2} f(\xi)$$

In particular, with an initial condition of the form

$$A(x,0) \propto \exp(-x^2/x_0^2),$$

we have

$$A(x,t) \propto (x_0^2 + 4i\alpha t)^{-1/2} \exp[-x^2/(x_0^2 + 4i\alpha t)],$$

and we get a well-known result : dispersion causes the amplitude of the wave-packet to decrease like $t^{-1/2}$. This is valid for large t and x_0, since A is assumed to vary slowly in time and space. Notice that here the approximation is included at the stage of formulating the amplitude equation.

The next step is to include nonlinear terms in the evolution equation of the amplitude A. Assuming that these terms are monomials in A and $\bar{A}$, we proceed using symmetry arguments in a similar way as we did for nonlinear oscillators. The Sine-Gordon equation (3.1) is invariant to translations in both time and space,

$$t \to t + \theta, \quad x \to x + \phi,$$

and from (3.4) we see that this corresponds to

$$A \to Ae^{i\psi},$$

where ψ can vary through all reals. Considering all possible nonlinear terms, we find that the lowest order term with the right transformation property is $|A|^2 A$. So we can write

$$\frac{\partial A}{\partial t} = -U_0 \frac{\partial A}{\partial x} - i\frac{\omega_0''}{2}\frac{\partial^2 A}{\partial x^2} + \beta |A|^2 A. \tag{3.6}$$

There are two further symmetries: time reversal and space reflection. In the general case these can be applied separately, but we have taken the particular form of u given by (3.4) that consists only of waves propagating to the right, and this constrains us to applying both transformations together (see below for the general case).

Applying the symmetries together implies the invariance of the amplitude equation under the transformation

$$t \to -t, \quad x \to -x \quad A \to \bar{A},$$

and applying this to (3.6) gives

$$-\frac{\partial \bar{A}}{\partial t} = U_0 \frac{\partial \bar{A}}{\partial x} + i\alpha \frac{\partial^2 \bar{A}}{\partial x^2} + \beta |A|^2 \bar{A}$$

However the complex conjugate of (3.6) is

$$\frac{\partial \bar{A}}{\partial t} = -U_0 \frac{\partial \bar{A}}{\partial x} + i\alpha \frac{\partial^2 \bar{A}}{\partial x^2} + \bar{\beta} |A|^2 \bar{A}$$

Hence $\bar{\beta} = -\beta$, and β is pure imaginary, so we can replace β with $-i\beta$ in (3.6). If we also transform to a frame moving with the group velocity, U_0, we obtain

$$\frac{\partial A}{\partial t} = i\alpha \frac{\partial^2 A}{\partial x^2} - i\beta |A|^2 A \tag{3.7}$$

This is the nonlinear Schrödinger equation. It shows that the dynamics of the wave-packet consists of a balance between dispersion, $i\alpha A_{xx}$, and nonlinearity, $-i\beta|A|^2A$, that traces back in this problem to the amplitude dependence of the frequency of each oscillator. These points are illustrated by the particular solution

$$A = Qe^{i(\Omega t - qx)}$$

$$\Omega = -\alpha q^2 - \beta Q^2$$

which corresponds to shifting $\omega_0 \rightarrow \omega_0 + \Omega$, $k_0 \rightarrow k_0 + q$. Thus, nonlinearity and dispersion act in antagonistic ways if $\alpha\beta < 0$.

We now derive the nonlinear Schrödinger equation from the Sine-Gordon equation using a multiple-scale expansion. Considering an initial condition which is a slowly modulated wave in space, we take as a small parameter the typical modulation wavenumber compared to the wavenumber of the carrier wave, thus

$$\frac{\partial}{\partial x} \rightarrow \frac{\partial}{\partial x} + \epsilon \frac{\partial}{\partial X}.$$

As discussed above, we expect two characteristic timescales, one corresponding to the propagation of the wave envelope at the group velocity, and the other to the dispersion of the wave-packet, thus

$$\frac{\partial}{\partial t} \rightarrow \frac{\partial}{\partial t} + \epsilon \frac{\partial}{\partial T_1} + \epsilon^2 \frac{\partial}{\partial T_2}.$$

We need now to scale the oscillation amplitude $u(x, t, X, T_1, T_2)$ to be able to handle the nonlinear term of (3.1) perturbatively. There does not exist a correct scaling versus a wrong one. If the amplitude is scaled too small, we get to leading orders an amplitude equation with only linear terms, which is correct ; if it is scaled too large, we get nonlinear terms at a lower order than dispersion, which is also true is the amplitude is large. One generally considers that the most interesting situation consists of having both effects, nonlinearity and dispersion, at the same order in the amplitude equation; this fixes the scale for the amplitude, and

$$u(x,t) = \epsilon[A(X, T_1, T_2)e^{i(\omega_0 t - k_0 x)} + c.c.] + \epsilon u_1(x, t, X, T_1, T_2) + \epsilon^2 u_2(x, t, X, T_1, T_2) + \ldots$$

At $O(\epsilon^2)$, the solvability condition is

$$\frac{\partial A}{\partial T_1} = -U_0 \frac{\partial A}{\partial X}$$

which leads us to take $A \equiv A(X - U_0 T_1, T_2)$. Then at $O(\epsilon^3)$, the solvability condition gives

$$\frac{\partial A}{\partial T_2} = i\alpha \frac{\partial^2 A}{\partial X^2} - i\beta |A|^2 A$$

with $\alpha = -\omega_0''/2$ and $\beta = 1/4\omega_0$. Note that $\alpha\beta < 0$ so that dispersion and nonlinearity are antagonistic. We have recovered the nonlinear Schrödinger equation (3.7). We could have taken two slow lengthscales and one slow timescale, and this would have resulted in a different form of the nonlinear Schrödinger equation which is widely used in nonlinear optics.

To deal with the general case we must consider both left and right-propagating waves, and begin the expansion with

$$u = Ae^{i(\omega_0 t - k_0 x)} + Be^{i(\omega_0 t + k_0 x)} + c.c.$$

This leads to the two coupled amplitude equations

$$\frac{\partial A}{\partial t} = -U_0 \frac{\partial A}{\partial x} - i\frac{\omega_0''}{2}\frac{\partial^2 A}{\partial x^2} - i\beta |A|^2 A - i\gamma |B|^2 A,$$

$$\frac{\partial B}{\partial t} = U_0 \frac{\partial B}{\partial x} - i\frac{\omega_0''}{2}\frac{\partial^2 B}{\partial x^2} - i\gamma |A|^2 B - i\beta |B|^2 B.$$

Translational invariances in time and space constrain the form of the leading order nonlinear terms. Space reflection symmetry implies the invariance under the transformation

$$x \to -x, \quad A \to B, \quad B \to A,$$

and shows that the coefficients of the similar nonlinear terms should be the same in both equation. Time reversal symmetry implies

$$t \to -t, \quad A \to \bar{B}, \quad B \to \bar{A},$$

so that the coefficients of the nonlinear terms are pure imaginary. Note that one can check that the coefficient of the propagative term is real whereas the one of the dispersive term is pure imaginary.

A slight problem arises if one tries to get these coupled equations with a multiple-scale expansion. Indeed, one cannot remove both propagative terms by transforming to a frame moving at the group velocity. It is straightforward to change the scaling of the amplitude in order to bring nonlinear terms at the same order as propagative ones, but dispersive terms are smaller, and one should not in principle keep them. This is obviously a bad choice since one does not expect dispersion to become negligible because of the presence of counter-propagating waves. The problem here is that one small adjustable parameter is not enough to balance all the relevant terms allowed by symmetries. One way out is to look for another small parameter, here obviously the group velocity, however this restricts our study to the

case of small carrier wave frequency. Another way is to keep the dispersive terms; but should we scale amplitude as for the nonlinear Schrödinger equation or in order to bring leading order nonlinear terms with propagative terms, and then keep higher order nonlinearities at the order of dispersive terms ? The two different scalings might be relevant, one when the counter-propagating wave-packets are far apart, the other when they collide. There is perhaps no rigorous way to describe that situation with amplitude equations.

The nonlinear Schrödinger equation is the generic evolution equation that governs the complex amplitude of a nonlinear wave in dispersive media. It has been widely used to describe surface waves and light propagation in optical fibers. It should be modified in the vicinity of a caustic where the group velocity is stationary and correspondingly dispersive effects are small. It also occurs that the wave amplitude is coupled to a mean field. This is a general situation when there exists a neutral mode at zero wave number and we will discuss that later; as a simple example derive the nonlinear Schrödinger equation for the envelope of a quasi-monochromatic wave governed by the Korteweg-de Vries equation. Note also that when a conservative system undergoes a dispersive instability, such as the Kelvin-Helmholtz instability, the amplitude of the unstable waves is not governed by the nonlinear Schrödinger equation (see section 4).

3.2 The side-band or Benjamin-Feir instability

We now use the nonlinear Schrödinger equation to study the stability of a quasi-monochromatic wave. The original motivation was to understand the instability of Stokes waves. When a wave train of surface gravity waves is generated with a paddle oscillating at constant frequency, one observes that if the fluid layer is deep enough compared to the wavelength, the quasi-monochromatic wave is unstable and breaks into a series of pulses.

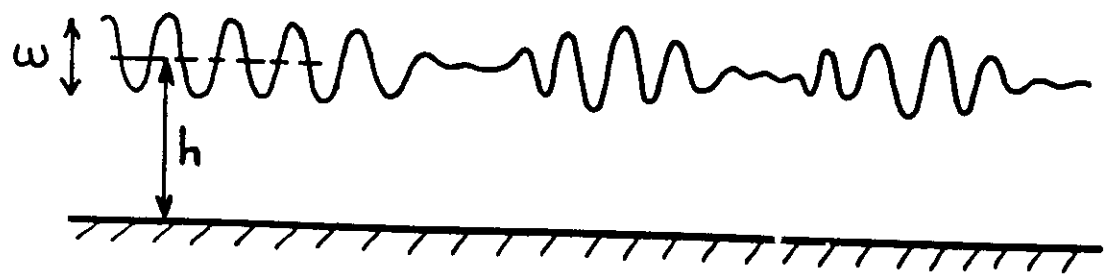

Figure 3.3. A deep layer of water, forced by an oscillating paddle, exhibits the side-band instability. Benjamin-Feir (1967), Lake *et al.* (1977), Melville (1982).

Return to the nonlinear Schrödinger equation (3.7),

$$\frac{\partial A}{\partial t} = -i\alpha\frac{\partial^2 A}{\partial x^2} - i\beta|A|^2 A$$

and consider the particular solution

$$A_0 = Qe^{i\Omega t}, \quad \Omega = -\beta Q^2,$$

that represents a quasi-monochromatic wave of amplitude Q, wavenumber k_0 and frequency $\omega_0 + \Omega$. If we perturb A_0 slightly, so that

$$A = [Q + r(x,t)]e^{i[\Omega t + \theta(x,t)]},$$

we obtain

$$\frac{\partial r}{\partial t} + i\Omega(Q+r) + i(Q+r)\frac{\partial \theta}{\partial t} = -i\beta(Q+r)^3 + i\alpha\left[\frac{\partial^2 r}{\partial x^2} + 2i\frac{\partial r}{\partial x}\frac{\partial \theta}{\partial x} + i(Q+r)\frac{\partial^2 \theta}{\partial x^2} - (Q+r)\frac{\partial \theta}{\partial x}^2\right].$$

Linearising, and separating real and imaginary parts, gives

$$\frac{\partial r}{\partial t} = -\alpha Q\frac{\partial^2 \theta}{\partial x^2}, \tag{3.8}$$

$$\frac{\partial \theta}{\partial t} = -2\beta Q r + \frac{\alpha}{Q}\frac{\partial^2 r}{\partial x^2}. \tag{3.9}$$

Taking $\begin{pmatrix} r \\ \theta \end{pmatrix} \propto e^{\eta t - iKx}$, one finds for the dispersion relation

$$\begin{vmatrix} -\eta & \alpha Q K^2 \\ -2\beta Q - \frac{\alpha}{Q}K^2 & -\eta \end{vmatrix} = 0,$$

or

$$\eta^2 = -[2\alpha\beta Q^2 K^2 + \alpha^2 K^4],$$

which is always negative for $\alpha\beta > 0$, but has a positive region for $\alpha\beta < 0$ as shown in figure (3.4). Thus if $\alpha\beta > 0$ then η is pure imaginary and the quasi-monochromatic wave (3.4) is a stable solution.

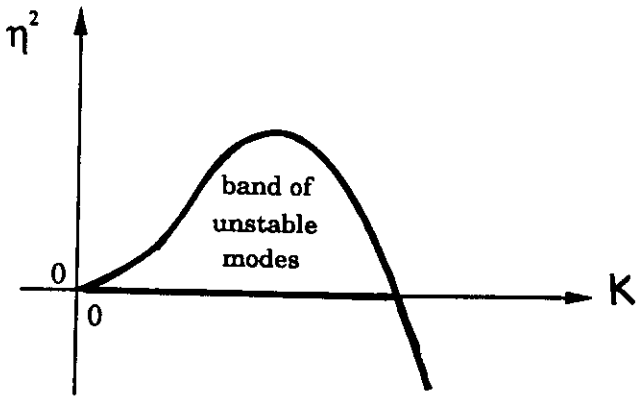

Figure 3.4. The dispersion relation for the perturbation to A_0

On the other hand if $\alpha\beta < 0$ then in the long wavelength region, η has both a negative and a positive root. When η is positive, there is an instability, the Benjamin-Feir or side-band instability. It has the name "side-band" because if one takes a band of frequencies centred on ω_0 as shown in figure (3.5), the interaction of one side-mode with the second harmonic is resonant with the other side-mode, causing it to be amplified, *i.e.* $2\omega_0 - (\omega_0 - \Omega) = \omega_0 + \Omega$. As an exercise, write the perturbation to A_0 as the sum of two side-band modes and see how their coupling generates the instability.

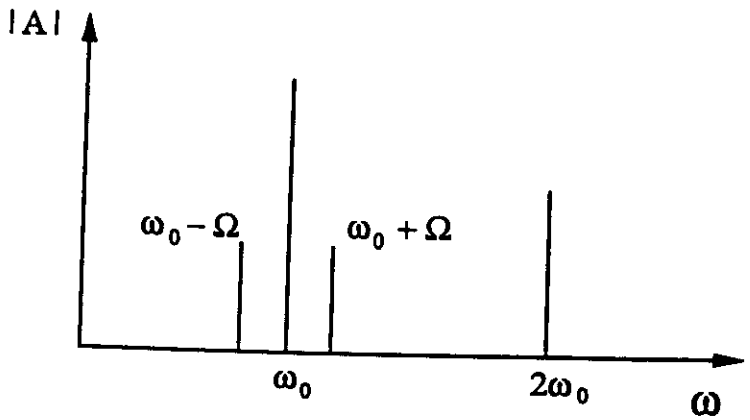

Figure 3.5. The mode at $\omega = \omega_0 - \Omega$ is resonant with the interaction of the modes at $\omega_0 + \Omega$ and $2\omega_0$

Another way to understand this instability is to combine (3.8) and (3.9) and find

$$\frac{\partial^2\theta}{\partial t^2} = 2\alpha\beta Q^2 \frac{\partial^2\theta}{\partial x^2} - \alpha^2 \frac{\partial^4\theta}{\partial x^4}.$$

So if $\alpha\beta < 0$,the phase of the wave obeys an unstable propagation equation (the propagation velocity is imaginary).

Time reversal and space-reflection symmetries imply,

$$t \to -t, x \to -x, \theta \to -\theta$$

and thus determine the lowest order nonlinear term in the equation for the phase, resulting in

$$\frac{\partial^2\theta}{\partial t^2} = 2\alpha\beta Q^2 \frac{\partial^2\theta}{\partial x^2} - \alpha^2 \frac{\partial^4\theta}{\partial x^4} + g\frac{\partial\theta}{\partial x}\frac{\partial^2\theta}{\partial x^2}$$

This is the Boussinesq equation. It has well-known solitary wave solutions consisting of a localized region with a non zero phase-gradient, thus a localized region with a different local wavenumber for the wave train. We consider in the next section these localized structures as solitary waves solutions of the nonlinear Schrödinger equation.

Before, try this exercise. If we were now to set $\theta = A_1(x,t)e^{i(\omega_1 t - k_1 x)} + c.c.$, in the Boussinesq equation, we would find that A_1 satisfies the nonlinear Schrödinger equation with coefficients depending on the ones of the nonlinear Schrödinger equation we start from at the beginning of this section. Derive the mapping between the old and new coefficients. Is there a fixed point? If yes, what does this would mean? Find other similar examples using symmetry arguments to guess the form of the successive equations.

3.3 Solitary waves

Nonlinear wave equations sometimes have solitary wave solutions, which have locally distributed amplitudes and propagate without changing their profiles, because of the balance between nonlinearity and dispersion. In this section, we look for solitary wave solutions of the nonlinear Schrödinger equation.

3.3.1 Solitary wave solutions in the Benjamin-Feir unstable regime

Firstly, we solve the nonlinear Schrödinger equation to get solitary wave solutions in the Benjamin-Feir unstable case, *i.e.* $\alpha\beta < 0$. For simplicity, we select the parameters to be $\alpha = 1$ and $\beta = -2$ with appropriate scalings of space and amplitude. Then the nonlinear Schrödinger equation is

$$\frac{\partial A}{\partial t} = i\frac{\partial^2 A}{\partial x^2} + 2i|A|^2 A, \tag{3.10}$$

We assume the form of the solution is $A_s(x,t) = R(x)\exp(i\Omega t)$. Substituing this into (3.10), we get

$$R_{xx} = -\frac{\partial V}{\partial R} \tag{3.11}$$

where the potential $V(R)$ is

$$V(R) \equiv -\frac{1}{2}\Omega R^2 + \frac{1}{2}R^4.$$

Figure 3.6 shows the profile of the potential $V(R)$. Equation (3.11) corresponds to the equation of motion of a particle in the potential $V(R)$ by considering x as time and R as the position of the particle. Multiplying by R_x and integrating, we have

$$\frac{1}{2}R_x^2 + V(R) = E, \tag{3.12}$$

where E is a constant. In the case of $E < 0$, the solution of (3.12) corresponds to the periodic motion between $R_1 < R < R_2$ in figure 3.6. Thus, we get periodic solutions with respect to x as shown in figure 3.7. These solutions are called cnoidal waves. In the case of $E = 0$, the solution corresponds to the motion of the particle which starts with $R = 0$ at $t \to -\infty$, reaches $R = R_0$ and returns to $R = 0$ as $t \to \infty$. Therefore, we get a solitary wave solution whose profile tends to zero as $x \longrightarrow \pm\infty$. There is a simple analytic form for this special case:

$$A_s = \sqrt{\Omega}\,\mathrm{sech}(\sqrt{\Omega}x)\exp(i\Omega t).$$

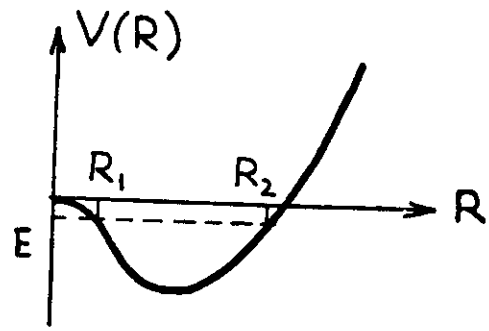

Figure 3.6. The potential $V(R)$

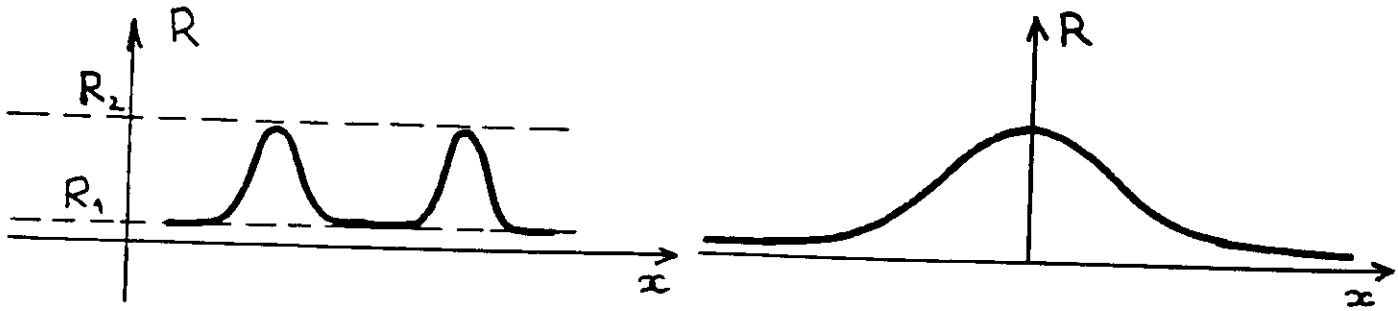

Figure 3.7. (a) Cnoidal wave ($E < 0$), (b) Solitary wave ($E = 0$)

3.3.2 Symmetries and other solitary wave solutions

By symmetry argument, we can derive other solitary waves from one simple solitary wave. The nonlinear Schrödinger equation has the following symmetry properties,

$$\begin{cases} x \longrightarrow \lambda x, \\ t \longrightarrow \lambda^2 t, \\ A \longrightarrow \lambda^{-1} A \end{cases}$$

Applying this symmetry to the simple solitary wave solution $A_{s1} = \mathrm{sech}x \exp(it)$, we have

$$A_{s2} = \sqrt{\Omega}\mathrm{sech}(\sqrt{\Omega}x)\exp(i\Omega t).$$

Further, using another symmetry

$$\begin{cases} x \longrightarrow x + vt, \\ A \longrightarrow A\exp(-i\frac{v}{2}x + i\frac{v^2}{4})t, \end{cases}$$

we get a further solitary wave solution,

$$A_{s3} = \sqrt{\Omega}\mathrm{sech}[\sqrt{\Omega}(x - vt)]\exp i\left[\frac{1}{2}vx + (\Omega - \frac{v^2}{4}t)\right].$$

One can also consider translational invariance in space, thus replacing x by $x - x_0$, and rotational invariance in the complex plane that leads to an arbitrary phase factor in A. The important point to notice is that continuous families of solutions are associated with the invariance properties of the evolution equation. We will use this later to study the dynamics of localized structures.

3.3.3 Solitary wave solutions in the Benjamin-Feir stable regime

Next we consider solitary wave solutions in the Benjamin-Feir stable case, *i.e.* $\alpha\beta > 0$. For simplicity, we select the parameters to be $\alpha = 1$ and $\beta = 2$.

$$\frac{\partial A}{\partial t} = i\frac{\partial^2 A}{\partial x^2} - 2i|A|^2 A. \tag{3.13}$$

We assume the form of the solution is $A_s = R(x)\exp(i\Omega t + \theta(x))$. Substituing it into (3.13), we get

$$\Omega R = -2R^3 + R_{xx} - R\theta_x^2, \tag{3.14}$$

$$0 = -2R_x\theta_x - \theta_{xx}R = -(R^2\theta_x)_x, \tag{3.15}$$

We can eliminate θ by integrating (3.15) and substituting into (3.16),

$$R_{xx} = -\frac{\partial V}{\partial R},$$

$$V(R) = \frac{1}{2}\left(-\Omega R^2 - R^4 + \frac{h^2}{R^2}\right),$$

where $h \equiv R^2\theta_x$ is constant.

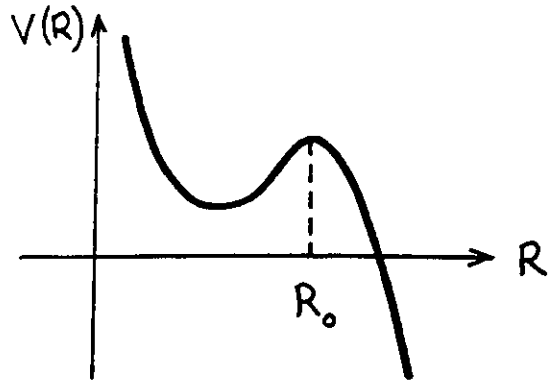

Figure 3.8. The potential $V(R)$

In the same manner as for the Benjamin-Feir unstable case, we can find the solution by selecting the maximum value of the potential (figure 3.9),

$$R^2 = R_0^2 - \frac{a^2}{\cosh^2 ax},$$

where $R = R_0$ gives the maximum of $V(R)$, and the parameters are

$$\begin{cases} \Omega = -3R_0^2 + a^2, \\ h^2 = R_0^4(R_0^2 - a^2). \end{cases}$$

This solution is called an "envelope hole soliton", or a "dark soliton" in optics since it consists of a region with a smaller oscillation amplitude. Note that the local wavenumber is changed according to the relation $R^2\theta_x = \text{constant}$.

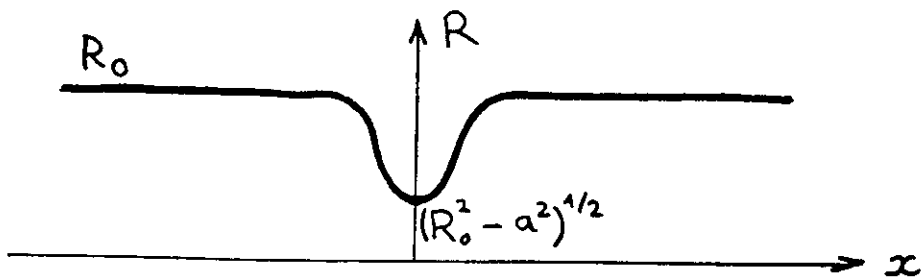

Figure 3.9. A envelope hole soliton or dark soliton

In particular, when we choose $h = 0, a = R_0$, we have

$$R^2 = R_0^2 \tanh^2 R_0 x.$$

In the pendula model, this represents a non-oscillating location that separates two regions that oscillate out of phase.

References

Benjamin, T. B. and Feir, J. E. (1967) *The disintegration of wave trains on deep water*, J. Fluid Mech. **27**, 417-430.

Lake, B.M., Yuen, M.C., Rungaldier, M., and Ferguson, W.E. (1977) *Nonlinear deep-water waves: theory and experiment. Part 2. Evolution of a continuous wave train*, J. Fluid Mech. **83**, 49-74.

Melville, W.K. (1982) *The instability and breaking down of deep-water waves*, J. Fluid Mech. **115**, 165-185.

Newell, A. C. (1985) *Solitons in Mathematics and Physics*, SIAM

Stuart, J. T. and Di Prima, R. C. (1978) *The Eckhaus and Benjamin-Feir resonance mechanisms*, Proc. Roy. Soc. London **A 362**, 27-41.

Whitham, G.B.(1974) *Linear and Nonlinear Waves Wiley*

4. Cellular Instabilities: A canonical example, Rayleigh-Bénard convection

Various fluid flows display instabilities that generate cellular structures. Examples are the Couette-Taylor flow, Rayleigh-Bénard convection, the Faraday instability and many shear flow experiments. The fluid can sometimes assumed to be inviscid but we will first consider situations where dissipation cannot be neglected. These "dissipative instabilities" are described by simpler amplitude equations, in particular when they generate stationary patterns, such as convective rolls for instance. A canonical example of stationary cellular instability is Rayleigh-Bénard convection that we will study in this section.

4.1 Rayleigh-Bénard convection

4.1.1 Convection in the Rayleigh-Bénard geometry

Thermal convection widely occurs in geophysical and astrophysical flows: in the earth mantle, it is responsible for the motion of tectonic plates, in the earth core, it generates the earth magnetic field by dynamo effect, in the sun or other stars, it is the advection mechanism for the energy generated in the core. Thermal convection has been also studied extensively in laboratory experiments, both for engineering purposes and also as one of the simplest example of hydrodynamic instability that displays pattern formation and transition to turbulence. There exist many reviews about thermal convection, for instance, Spiegel (1971, 1972), Palm (1975), Normand et al. (1977), Busse (1978, 1981); the reader may also look at the book by Gershuni and Zhukovitskii (1976).

Convection in the Rayleigh-Bénard geometry is achieved by uniformly heating from below a horizontal layer of fluid (Figure 4.1).For small temperature gradients, the fluid remains in a stable heat-conducting state, with a linear temperature profile and no fluid motion. However, if the fluid has a negative thermal expansion coefficient, $-\alpha$, the thermal gradient generates a density stratification with cold heavy fluid above warm light fluid. For sufficiently large temperature differences, the resulting buoyancy force overcomes dissipative effects due to viscosity and heat diffusivity, causing less dense warmer fluid to rise and cooler fluid to

sink. With appropriate boundary conditions, periodic parallel convection rolls result from the circulation of the fluid.

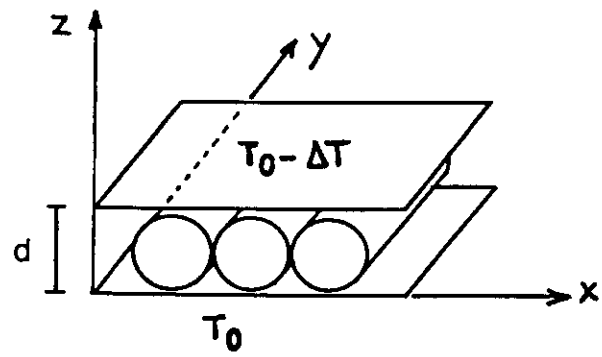

Figure 4.1. Sketch of a Rayleigh-Bénard experiment

At the onset of convection, any field $u(x, y, z, t)$ representing the state of the system, i. e. one of the velocity components, the temperature fluctuation from the heat-conduction profile or the pressure fluctuation from hydrostatic equilibrium, takes the form

$$u(x, y, z, t) = [A(X, Y, T) \exp(ik_c x) + \text{c.c.}] f(z) + \cdots$$

This represents periodic convection rolls perpendicular to the x-axis with a slowly varying complex amplitude $A(X, Y, T)$. The modulus of A accounts for the convection amplitude whereas the phase of A is related to the local wavenumber difference from its critical value, k_c. The vertical structure of the convection mode is described by $f(z)$ and depends on the boundary conditions at the lower and upper plates (see below).

Our objective is to find the amplitude equation, i. e. the evolution equation for A, and to use it to describe patterns dynamics in the vicinity of convection onset.

4.1.2 The Boussinesq approximation

The Boussinesq approximation is reasonably valid in usual experimental situations. In this approximation, the fluid behaves as though it were incompressible, the density varying only as a consequence of changes in temperature; the density variation about its mean value is taken into account only in the buoyancy force term; the mechanical dissipation rate is neglected in the heat equation, and the fluid parameters, viscosity, heat diffusivity and heat capacity are assumed to be constant. These a priori physical assumptions can be replaced by a rigorous asymptotic expansion of the conservation equations of mass, momentum and energy (see the review by Malkus, 1964); the resulting Boussinesq equations are ,

$$\nabla \cdot \mathbf{v} = 0 \tag{4.1}$$

$$\rho_0 \left[\frac{\partial \mathbf{v}}{\partial t} + (\mathbf{v} \cdot \nabla)\mathbf{v} \right] = -\nabla p + \rho_0 \nu \nabla^2 \mathbf{v} - \rho(T) g \hat{\mathbf{z}} \tag{4.2}$$

$$\frac{\partial T}{\partial t} + \mathbf{v} \cdot \nabla T = \kappa \nabla^2 T, \tag{4.3}$$

where ν is the fluid kinematic viscosity and κ is the heat diffusivity; ρ_0 is the fluid density at a reference temperature and T is the temperature difference from that reference. Thus,

$$\rho(T) \simeq \rho_0 (1 - \alpha T). \tag{4.4}$$

Defining θ as the temperature fluctuation from the heat-conducting profile,

$$T = T_0 - \frac{\Delta T}{d} z + \theta, \tag{4.5}$$

where ΔT is the temperature difference across the layer of height d, and using d, d^2/κ and ΔT as scales for length, time and temperature, one get

$$\nabla \cdot \mathbf{v} = 0 \tag{4.6}$$

$$\frac{\partial \mathbf{v}}{\partial t} + (\mathbf{v} \cdot \nabla)\mathbf{v} = -\nabla \pi + P \nabla^2 \mathbf{v} + RP\theta \hat{\mathbf{z}} \tag{4.7}$$

$$\frac{\partial \theta}{\partial t} + \mathbf{v} \cdot \nabla \theta = \mathbf{v} \cdot \hat{\mathbf{z}} + \nabla^2 \theta, \tag{4.8}$$

where $P = \nu/\kappa$ is the Prandtl number, and $R = g\alpha \Delta T d^3/\nu\kappa$ is the Rayleigh number. These two dimensionless numbers, together with the boundary conditions, characterize the convection problem in the Boussinesq approximation. Let us mention that the small or large Prandtl number or large Rayleigh number limits of equations (4.6, 4.7., 4.8) are usually considered without any caution in the litterature, although these limits might invalidate the Boussinesq approximation.

The Prandtl number is the ratio of the timescales of the two diffusive processes involved in convection, heat diffusion and momentum diffusion. Depending on the microscopic mechanisms of transport, the Prandtl number varies on many orders of magnitude in different convective flows of interest.

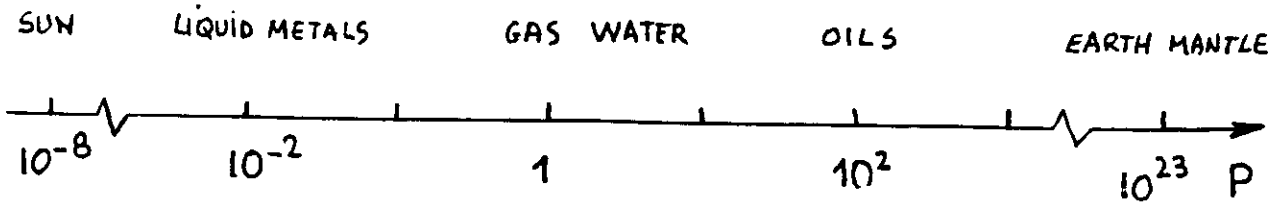

Figure 4.2. Typical values of the Prandtl number

The Rayleigh number is proportional to the temperature difference across the fluid layer, and relates the strength of the driving mechanism to dissipative processes. It is the control parameter in a convection experiment.

4.1.3 Boundary Conditions

We need now to specify the boundary conditions. We consider a fluid layer of infinite horizontal extent or periodic lateral boundary conditions. At the upper and lower boundaries, the temperature and the heat flux are assumed to be continuous. There exist two simple limit situations:

- boundaries with high heat conductivity

$$\theta|_B = 0, \tag{4.9}$$

- insulating boundaries

$$\frac{\partial \theta}{\partial z}|_B = 0. \tag{4.10}$$

Depending on the nature of the boundaries, the boundary condition for velocity can be either "no-slip" or "stress-free". If the boundary is a rigid plate, the "no-slip" boundary condition is applicable for viscous fluids, i.e.

$$\mathbf{v}|_B = 0.$$

We separate the velocity into horizontal and vertical components, $\mathbf{v} = \mathbf{v}_h + w\hat{\mathbf{z}}$, where $\mathbf{v}_h$ is the horizontal velocity, and w is the z component. Since $\mathbf{v}_h$ must vanish identically at $z = z_B$, it's horizontal derivatives also must vanish at $z = z_B$. Using $\nabla \cdot \mathbf{v} = 0$, we have

$$\begin{aligned} w|_B &= 0, \\ \frac{\partial w}{\partial z}|_B &= 0. \end{aligned} \tag{4.11}$$

If the boundary is an interface with another fluid or a free surface open to the air, boundary conditions have to account for the continuity of both the normal velocity w and of the tangential stress in the plane of the interface. Assuming that surface tension effects are not involved and that the interface remains flat, then we have the following "stress-free" boundary conditions:

$$w|_B = 0, \quad \frac{\partial \mathbf{v}_h}{\partial z}|_B = 0.$$

Again using the incompressibility condition $\nabla \cdot \mathbf{v} = 0$, we get

$$\begin{aligned} w|_B &= 0, \\ \frac{\partial^2 w}{\partial z^2}|_B &= 0. \end{aligned} \tag{4.12}$$

One example of a "stress-free" experimental boundary condition consists of a convection layer of oil sandwiched between layers of mercury and gazeous helium (Goldstein and Graham, 1969). The "stress-free" boundary conditions can be applied since the viscosity of oil is much larger than the one of mercury or helium, and the temperature fluctuation should be zero at the oil-mercury interface, while the fluctuation heat flux should be zero at the oil-helium interface.

Finally, let us mention the crucial effect of temperature boundary conditions on the convective regime observed at onset. As buoyancy is the driving mechanism, the length-scale of the convection pattern is primarily fixed by the charateristic scale for the temperature disturbances. In the case of boundaries with a high heat-conductivity compared to the one of the fluid, the temperature disturbances should vanish on the boundaries and the relevant length-scale is the height of the layer d.

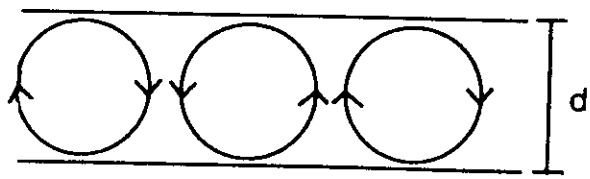

Figure 4.3. Convective regime at onset with boundaries of high heat conductivity

For insulating boundaries, the isotherms can penetrate into the boundaries and the temperature can vary on a very large length-scale compared to d. The pattern wavelength goes to infinity in the insulating limit, i. e. there is only one roll in the fluid container (Figure 4.4).

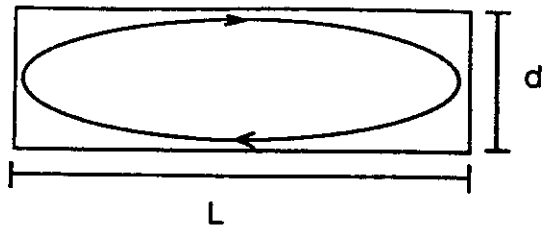

Figure 4.4. Convective regime at onset with insulating boundaries

4.2 Linear Stability Analysis

The linear stability of the motionless heat-conducting state can be studied analitycally using the Boussinesq equations (4.6, 4.7, 4.8) with stress-free (4.12) and perfectly conducting (4.9) boundary conditions.

We first eliminate the pressure field by applying the operators curl and curl curl to the momentum equation (4.7) and we get the evolution equations for the vertical vorticity, ζ, and the vertical velocity, w, by projecting on the vertical axis:

$$\frac{\partial \zeta}{\partial t} + \hat{\mathbf{z}} \cdot \nabla \times [(\mathbf{v} \cdot \nabla)\mathbf{v}] = P\nabla^2 \zeta \tag{4.13}$$

$$\frac{\partial}{\partial t}\nabla^2 w - \hat{\mathbf{z}} \cdot \nabla \times \nabla \times [(\mathbf{v} \cdot \nabla)\mathbf{v}] = P\nabla^4 w + RP\nabla_h^2 \theta, \tag{4.14}$$

where ∇_h^2 stands for the Laplacian operator in the horizontal plane. Note that, at the linear stage, the vertical vorticity decouples and obeys a diffusion equation. Thus, the vertical vorticity modes can be ignored in the linear stability analysis; however, they should be kept in the study of finite amplitude convection since they are nonlinearly coupled to the linear convection modes. Neglecting the nonlinear terms in equations (4.14) and (4.8) yields the coupled linearized system for w and θ.

$$\begin{aligned} \frac{\partial}{\partial t}\nabla^2 w &= P\nabla^4 w + RP\nabla_h^2 \theta, \\ \frac{\partial \theta}{\partial t} &= w + \nabla^2 \theta. \end{aligned} \tag{4.15}$$

From the requirement of spatial periodicity in the horizontal plane, we consider a normal mode of the disturbances (w, θ) under the form

$$\begin{aligned} w(x, y, z, t) &= W(z) \exp[i\mathbf{k} \cdot \mathbf{r} + \sigma t], \\ \theta(x, y, z, t) &= \Theta(z) \exp[i\mathbf{k} \cdot \mathbf{r} + \sigma t], \end{aligned} \tag{4.16}$$

where $\mathbf{r}$ is the position vector in the horizontal plane, and $\mathbf{k}$ is the pattern (horizontal) wavevector. Boundary conditions (4.9, 4.12) together with equations (4.15) require that W and all its even derivatives vanish for $z = 0$ and $z = 1$. It follows that

$$W(z) = W_0 \sin n\pi z \quad \text{with } n = 0, 1, \ldots \tag{4.17}$$

Using (4.15), (4.16) and (4.17) we obtain the dispersion relation for the growthrate σ of the normal mode k

$$\sigma^2 + q_n^2(1 + P)\sigma + \left(Pq_n^4 - \frac{RPk^2}{q_n^2}\right) = 0, \tag{4.18}$$

where $q_n^2 = k^2 + n^2\pi^2$.

A stationary instability occurs when the constant term in σ of the dispersion relation vanishes and becomes negative. Thus, as the Rayleigh number is increased, a mode with $n = 1$ bifurcates first for $R = R_c(k)$ with

$$R_c(k) = \frac{(\pi^2 + k^2)^3}{k^2}. \tag{4.19}$$

This defines the marginal stability curve on which a mode with $n = 1$ and horizontal wavenumber k has a zero growth rate (Figure 4.5).

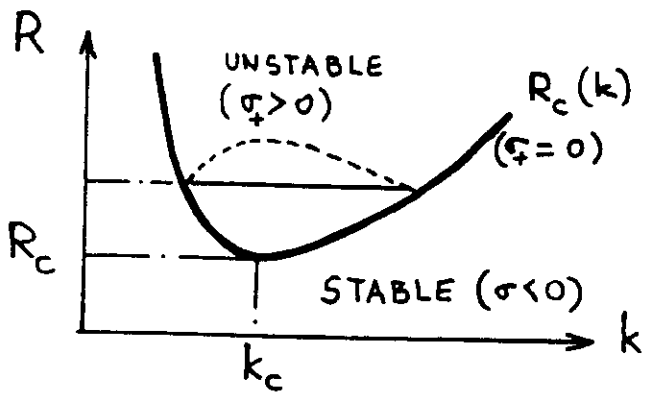

Figure 4.5. The marginal stability curve $R_c(k)$; the dashed curve represents the growth rate of the unstable modes for $R > R_c$.

The critical Rayleigh number R_c and the critical vawenumber k_c at convection onset correspond to the minimun of the marginal stability curve (4.19),

$$R_c = \frac{27\pi^4}{4}, \quad k_c = \frac{\pi}{\sqrt{2}}.$$

These critical values depend on the boundary conditions; in particular, as said above, k_c vanishes in the limit of thermally insulating upper and lower boundaries.

Slightly above criticality we expand the positive solution σ_+ of the dispersion relation (4.18) and get the growth rate of the unstable modes

$$\sigma_+(R,k) \simeq (\pi^2 + k_c^2)\frac{P}{1+P}\frac{R - R_c(k)}{R_c(k)},$$

which is proportional to the distance to critcality. Using

$$R_c(k) = R_c + \frac{(k-k_c)^2}{2}\left(\frac{\partial^2 R_c}{\partial k^2}\right)_c + \cdots,$$

we get to leading order in $R - R_c$ and $k - k_c$,

$$\sigma_+(k,R) = (\pi^2 + k_c^2)\,\frac{P}{1+P}\,\frac{(R-R_c)}{R_c} - \alpha(k-k_c)^2 + \cdots, \tag{4.20}$$

with

$$\alpha = (\pi^2 + k_c^2)\,\frac{P}{1+P}\,\frac{1}{2R_c}\left(\frac{\partial^2 R_c}{\partial k^2}\right)_c. \tag{4.21}$$

Note that $\sigma_+(R,k)$ involves a term proportional to $(R-R_c)\,(k-k_c)$; as the marginal stability curve is locally a parabola close to its minimum, we have, $(k-k_c) \leq (R-R_c)^{1/2}$, and this term is of higher order in (4.20). Thus, for R larger than R_c, there exists a band of unstable modes with growth rates determined by equation(4.20) (Figure 4.5).

Linear analysis gives the critical Rayleigh number R_c for instability onset and determines the modulus k_c of the critical wavevector $\mathbf{k}$ of the unstable modes. The direction of $\mathbf{k}$ is arbitrary; this orientational degenaracy is obviously related to the isotropy in the horizontal plane. There is also a translational degeneracy which is related to the translational invariance of the layer of infinite horizontal extent. These degeneracies do not result from the linear approximation but from the symmetries of the Rayleigh-Bénard geometry; thus, they will subsist in the nonlinear analysis. On the other hand, there is a pattern degeneracy that results from the linear approximation; indeed, any superposition of normal modes

$$w(\mathbf{r},z) = \sum_p c_p \exp(i\mathbf{k}_p \cdot \mathbf{r}), \tag{4.22}$$

with $|\mathbf{k}_p| = k_c$ and where the c_p's are constant coefficients, is a solution of the linear problem with a zero growth rate at criticality. In order to represent a real field w, we must impose the conditions, $c_{-p} = \bar{c}_p$ and $\mathbf{k}_{-p} = -\mathbf{k}_p$, but the number of non zero c_p's, i. e. the shape of the pattern, and their modulus, i. e. the amplitude of the convection velocity, remain undeterminate. Three basic examples of cellular pattern described by (4.22), that involve respectively one, two and three wavevectors, are sketched in Figure 4.6.

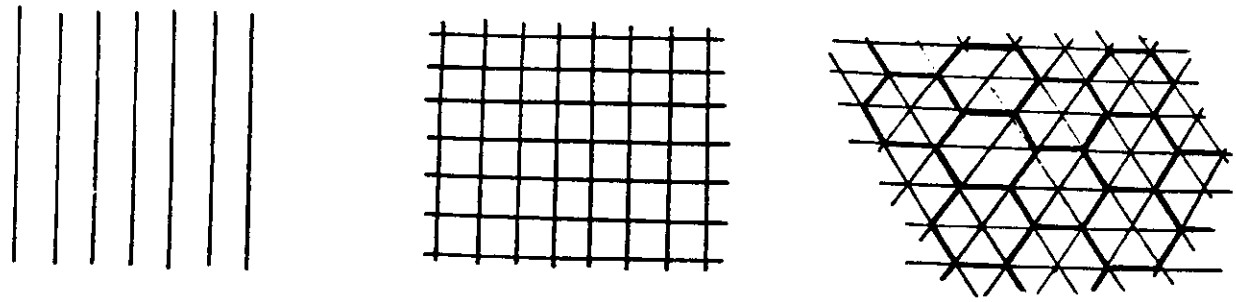

Figure 4.6. Rolls, squares and hexagons

Nonlinear interactions between the modes with different wave vectors generally select one pattern at instability onset and determine the amplitude above criticality. However, it happens sometimes that no stationary pattern exists even immediately above a stationary instability onset; the nonlinear regime is then time-periodic or chaotic.

Another problem results from the existence of a continuous band of unstable modes above criticality as described by equation (4.20). Linear analysis only determines the one with the highest growth rate, but the wavenumber selected by nonlinear interactions may correspond to a different one. The interaction of two (or several) modes within the unstable band gives rise to a spatial modulation of the periodic pattern on a large length-scale compared to the pattern wavelength. The inverse of this length-scale is of order $(k - k_c)$, thus within a multiple-scale expansion procedure, it corresponds to a "slow scale" X such that

$$X = (R - R_c)^{1/2} x. \tag{4.23}$$

Let us recall, that close to the instability onset, the slow time scale T that corresponds to the vanishing growth rate of the unstable mode (4.20) is

$$T = (R - R_c)t. \tag{4.24}$$

4.3 Nonlinear saturation of the critical modes

4.3.4 Nonlinear saturation of a roll pattern: the Landau equation

We first show how nonlinear terms saturate the amplitude of the convection velocity of a roll pattern above R_c. We use a stream function, $\psi(x, z, t)$, and write the velocity field

$$\mathbf{v} = (-\partial_z \psi, 0, \partial_x \psi).$$

Equations (4.6, 4.7, 4.8) become

$$\frac{\partial}{\partial t}\nabla^2\psi + J(\psi, \nabla^2\psi) = P\nabla^4\psi + RP\frac{\partial\theta}{\partial x}, \tag{4.25}$$

$$\frac{\partial\theta}{\partial t} + J(\psi,\theta) = \frac{\partial\psi}{\partial x} + \nabla^2\theta, \tag{4.26}$$

where J is the Jacobian,

$$J(f,g) \equiv \frac{\partial f}{\partial x}\frac{\partial g}{\partial z} - \frac{\partial f}{\partial z}\frac{\partial g}{\partial x}.$$

Assuming stress-free perfectly conducting boundary conditions at $z = 0, 1$, the marginal mode that describes rolls perpendicular to the x-axis for $R = R_c$ reads

$$\begin{aligned} \psi(x,z) &= [A\exp(ik_c x) + c.c.]\ \sin\pi z, \\ \theta(x,z) &= \frac{ik_c}{{k_c}^2 + \pi^2}[A\exp(ik_c x) - c.c.]\ \sin\pi z. \end{aligned} \tag{4.27}$$

The problem is to determine how the convection amplitude, $|A|$, saturates above criticality because of nonlinear interactions. This has been shown by Gorkov (1957) and Malkus and Veronis (1958) with a Poincaré-Lindstedt expansion. We will use a multiple-scale expansion, which is only slightly different, in order to keep the time-dependence of A. We don't consider in this section a possible modulation of A on a slow length-scale (see section 4.3.3).

We expand ψ and θ

$$\psi = \sum_{n=1}\epsilon^n\psi_n, \quad \theta = \sum_{n=1}\epsilon^n\theta_n,$$

where ϵ is a small parameter related to the distance to criticality by

$$R = R_c + \sum_{n=1}\epsilon^n R_n.$$

The Boussinesq equations are symmetric under a mid-plane reflection, $z \to -z$, coupled with a temperature inversion, $\theta \to -\theta$, which corresponds to $\psi \to -\psi$ and $\theta \to -\theta$; thus to leading order, $R_1 = 0$, and

$$R - R_c \simeq \epsilon^2 R_2.$$

Using the result of the linear theory for the growth rate of the unstable mode, we obtain for the convection mode time scale

$$\partial_t = \epsilon^2\partial_T.$$

To leading order in ϵ, equations (4.25, 4.26) give the linear problem, and the solutions for ψ_1 and θ_1 are given by the linear modes (4.27). To the next order we get,

$$\psi_2 = 0,$$

$$\theta_2 = -\frac{k_c^2}{2\pi(k_c^2 + \pi^2)}\sin 2\pi z,$$

that describes how the temperature advection nonlinear term deforms the vertical temperature profile. The solvability condition at the next order gives the evolution equation for A.

$$\frac{dA}{dT} = \mu A - \beta |A|^2 A, \tag{4.28}$$

with

$$\mu = (\pi^2 + k_c^2)\,\frac{P}{1+P}\,\frac{(R-R_c)}{\epsilon^2 R_c}, \qquad \beta = \frac{k_c^2}{2}\frac{P}{1+P}. \tag{4.29}$$

Note that, since $R - R_c$ is of order ϵ^2, all the terms of the amplitude equation (4.28) are of order one. However, we can easily write this equation using original unscaled variables for time, amplitude and distance to criticality, $R - R_c$; we can check on the unscaled form that all terms are of order $(R - R_c)^{3/2}$.

As previously shown for nonlinear oscillators, the form of the amplitude equation is here also determined by symmetry constraints. Translational invariance in the horizontal plane implies that, if $(\psi_0(x,z), \theta_0(x,z))$ represents a roll solution, $(\psi_0(x+x_0,z), \theta_0(x+x_0,z))$ is another solution; this amounts to shift the rolls in the horizontal plane, or to change the origin of the x-axis. From equation (4.27) this transformation corresponds to a rotation in the complex plane for A, and the amplitude equation should be invariant under the transformation

$$A \rightarrow A \exp i\phi, \quad \text{for any real } \phi.$$

As shown for nonlinear oscillators, the only allowed nonlinear term up to third order in amplitude is thus $|A|^2 A$, and the amplitude equation reads

$$\frac{dA}{dT} = \mu A - \beta |A|^2 A,$$

where β is a priori a complex number.

However, there is here an additional symmetry, space-reflection: $x \rightarrow -x$. From equation (4.27) this transformation corresponds to

$$A \rightarrow \overline{A}$$

for the complex amplitude. Taking the complex conjugate of the amplitude equation, applying the reflection transformation and comparing to the original amplitude equation, gives $\beta = \overline{\beta}$, thus β real. The form of the amplitude equation (4.28) is determined by symmetry constraints. The perturbative calculation starting from the Boussinesq equations is only useful to get the sign of β and shows that the bifurcation is supercritical. This can be also shown using variational methods (Sorokin, 1953), and for a large variety of boundary conditions, the motionless state is globally stable below R_c in the Boussinesq approximation.

Above R_c, the convection velocity amplitude increases continuously from zero and scales as $(R - R_c)^{1/2}$. It is the order parameter of the transition, the corresponding broken symmetry being translational invariance in space. Note finally that equation (4.28) can be writen in a variational form

$$\frac{dA}{dT} = -\frac{\partial V}{\partial \overline{A}},$$

where

$$V(A, \overline{A}) = -\mu A\overline{A} + \frac{1}{2}\beta A^2\overline{A}^2,$$

is the "Landau free-energy" in the vicinity of the transition.

4.3.5 Pattern selection

We now consider the problem of pattern selection via nonlinear interactions. As said above, in the slightly supercritical range, any superposition (4.22) of marginal modes has the same growth rate. Let us consider two examples, squares and hexagons.

For squares, we have

$$\psi(x, y, t) = \epsilon([A_1 \exp(ik_c x) + c.c.] + [A_2 \exp(ik_c y) + c.c.]) \sin\pi z + \cdots, \tag{4.30}$$

where $A_1(T)$ and $A_2(T)$ are the complex amplitudes of the two sets of perpendicular rolls. Using symmetry considerations, the amplitude equations read

$$\begin{aligned} \frac{dA_1}{dT} &= \mu A_1 - \left[\beta|A_1|^2 + \gamma|A_2|^2\right] A_1, \\ \frac{dA_2}{dT} &= \mu A_2 - \left[\gamma|A_1|^2 + \beta|A_2|^2\right] A_2. \end{aligned} \tag{4.31}$$

It is an easy exercise to show that for $\mu > 0$, stationary squares ($|A_1| = |A_2|$) are stable when $|\gamma| < \beta$, i.e when the cross-coupling nonlinear term is small enough so that the two sets of rolls weakly interact; when their interaction is too strong, more precisely when, $\gamma > \beta$, one of the two sets of rolls nonlinearly damps out the other, and rolls are the stable nonlinear state. This is the situation for Boussinesq convection with stress-free perfectly heat-conducting boundary conditions. On the contrary, with insulating boundaries, squares are observed.

For hexagons, we have

$$\psi(x, y, t) = \epsilon \sum_{p=1}^{3} [A_p \exp(i\mathbf{k}_p \cdot \mathbf{r}) + c.c.] \sin\pi z + \cdots, \tag{4.32}$$

with $|\mathbf{k}_p| = k_c$ and $\mathbf{k}_1 + \mathbf{k}_2 + \mathbf{k}_3 = 0$, and where the $A_p(T)$'s are the complex amplitudes of the three sets of rolls. Using symmetry considerations, the amplitude equations read

$$\frac{dA_l}{dT} = \mu A_l - \left[\beta|A_l|^2 + \delta(|A_m|^2 + |A_n|^2)\right] A_l, \quad \text{cyclic permutations of (l, m, n).} \tag{4.33}$$

Note that a term proportional to $\overline{A}_m \overline{A}_n$ in the evolution equation for A_l respects the translational and reflection ($x \to -x$) symmetries, but is forbidden here because of the additional Boussinesq symmetry ($z \to -z$, $\theta \to -\theta$). A possible exercise at this stage is to determine the stability domains of rolls, squares and hexagons as a fonction of the real coupling constants β, γ, δ and μ. Show also that the square-hexagons transition is "first order" and relate that to a symmetry argument.

The general problem of pattern selection is much more difficult to solve and has been studied by Schlüter et al. (1965) for the case of rigid perfectly conducting boundary conditions. They have found that rolls are the only stable stationary pattern just above the onset of convection. Using a similar analysis, Riahi (1983) has found stationary squares in the case of thermally insulating rigid boundaries.

4.3.6 Slowly varying amplitude of a roll pattern: the Ginzburg-Landau equation

We now consider the problem of the existence of a band of unstable modes above R_c. For simplicity we assume stress-free perfectly heat conducting boundaries, so that the pattern consists of parallel rolls. To take into account the modes around k_c, we consider a wave packet

$$\psi(x, z) = [A(X, Y, T) \exp(ik_c x) + c.c.] \sin \pi z + \cdots, \tag{4.34}$$

where $A(X, Y, T)$ represents the slowly varying envelope of the roll pattern. We first consider modulations only along the x-axis, thus $A = A(X, T)$. We have

$$A(X, T) = \int \hat{A}(K, \Sigma) \exp(\Sigma T + iKX)\, \delta(\Sigma - \Sigma(\mu, K)\, dK d\Sigma, \tag{4.35}$$

where

$$\Sigma(\mu, K) = \mu - \alpha K^2 + \cdots, \tag{4.36}$$

is the dispersion relation (4.20) in terms of scaled (order one) variables, i. e. $K = (k - k_c)/\epsilon$. The Fourier-Laplace transform of the dispersion relation (4.36) gives the linear part of the evolution equation for the ampliude $A(X, T)$

$$\frac{\partial A}{\partial T} = \mu A + \alpha \frac{\partial^2 A}{\partial X^2}$$

Taking into account the leading order nonlinear term, we get

$$\frac{\partial A}{\partial T} = \mu A + \alpha \frac{\partial^2 A}{\partial X^2} - \beta |A|^2 A. \tag{4.37}$$

We now consider modulations also along the rolls axis, thus $A = A(X, Y, T)$. We have

$$\mathbf{k} = (k_c + \delta k_x)\,\hat{\mathbf{x}} + (\delta k_y)\,\hat{\mathbf{y}},$$

and the generalisation of the dispersion relation (4.20) that respects rotational invariance in the horizontal plane, is

$$\sigma(k, R) = (\pi^2 + k_c^2)\,\frac{P}{1+P}\,\frac{(R - R_c)}{R_c} - \xi_0^2(\mathbf{k}^2 - k_c^2)^2 + \cdots$$

with $4k_c^2\xi_0^2 = \alpha$. We have

$$(\mathbf{k}^2 - k_c^2)^2 = \left(2k_c\delta k_x + (\delta k_x)^2 + (\delta k_y)^2\right).$$

Thus, the relevant scalings are

$$\delta k_x = \epsilon K_x, \quad \delta k_y = \epsilon^{1/2} K_y.$$

Slower y-modulations do not affect the amplitude equation to leading order, whereas modes corresponding to modulations on shorter scales are too strongly damped to be marginal. In terms of scaled variables, the dispersion relation reads

$$\Sigma = \mu - \alpha\left[K_x + \frac{1}{2k_c}K_y^2\right]^2 + \cdots$$

Taking its Fourier-Laplace transform and adding the leading order nonlinear term, gives

$$\frac{\partial A}{\partial T} = \mu A + \alpha\left(\frac{\partial}{\partial X} - \frac{i}{2k_c}\frac{\partial^2}{\partial Y^2}\right)^2 A - \beta|A|^2 A. \tag{4.38}$$

In terms of unscaled variables, all the terms of (4.38) are of order ϵ^3. This equation has been obtained by Newell and Whitehead (1969) and Segel (1969), using a multiple-scale expansion both in space and time. Note that partial derivatives in X and Y are not involved similarly because the roll pattern breaks the rotational invariance in the horizontal plane.

We can write the amplitude equation (4.38) in variational form,

$$\frac{\partial A}{\partial T} = -\frac{\delta \mathcal{L}}{\delta \overline{A}} \tag{4.39}$$

where

$$\mathcal{L}[A] = \int \left[-\mu |A|^2 + \frac{\beta}{2}|A|^4 + \alpha \left| \left(\frac{\partial}{\partial X} - \frac{i}{2k_c} \frac{\partial^2}{\partial Y^2} \right) A \right|^2 \right] dX dY, \qquad (4.40)$$

is analogous to a "Ginzburg-Landau" free-energy.

In the following lectures we will study pattern dynamics governed by this "Ginzburg-Landau" equation, also named in the context of convection, the Newell-Whitehead-Segel equation. In the case of stress-free boundary conditions, this equation is incorrect because it does not take into account the nonlinear interaction with vertical vorticity modes. We will discuss this effect later. With different coefficients than the ones derived above, the Ginzburg-Landau equation is correct to leading order for the description of slowly modulated roll-patterns in convection with rigid thermally conducting boundaries. More generally, it describes slowly modulated one-dimensional patterns that occur via a stationary bifurcation in a dissipative system, invariant under translations, rotations and space reflections in the horizontal plane, when no other marginal mode than the roll-mode at wavenumber k_c is involved.

References

Busse, F. H. (1978) *Nonlinear Properties of Convection*, Rep. Prog. Phys. **41**, 1929-1967.

Busse, F. H. (1981) *Transition to Turbulence in Rayleigh-Bénard Convection, Hydrodynamic Instabilities and the Transition to Turbulence*, Swinney, H. L. and Gollub, J. P. Editors, Topics in Applied Physics **45**, 97-137, Springer Verlag.

Gershuni, G. Z., Zhukovitskii, E. M., (1976) *Convection Stability of Incompressible Fluids*, Ketter Publications.

Goldstein, R. J., Graham, D. J. (1969) *Stability of a Horizontal Fluid Layer with Zero Shear Boundaries*, Phys. Fluids **12**, 1133-1137.

Gorkov, L. P., (1957) *Stationary Convection in a Plane Liquid Layer Near the Critical Heat Transfer Point*, Soviet. Phys. JETP **6**, 311-315.

Malkus, W. V. R., (1964) *Boussinesq Equations and Convection Energetics*, W. H. O. I. Tech. Rep., 11-37.

Malkus, W. V. R., Veronis, G. (1958) *Finite amplitude cellular convection*, J. Fluid Mech. **4**, 225-260.

Newell, A.C., Whitehead, J.A. (1969) *Finite bandwidth, finite amplitude convection*, J. Fluid Mech. **38**,279–303.

Normand, C., Pomeau, Y. Velarde, M. G. (1977) *Convective Instability: a Physicist Approach*, Rev. Mod. Phys. **49**, 581-624.

Palm, E. (1975) *Nonlinear Thermal Convection*, Ann. Rev. Fluid Mech. **7**, 39-61.

Riahi, N. (1983) *Nonlinear Convection in a Porous Layer with Finite conducting Boundaries*, J. Fluid Mech. **129**, 153-171.

Schlüter, A., Lortz, D., Busse, F. (1965) *On the Stability of Steady Finite Amplitude Convection*, J. Fluid Mech. **23**, 129-144.

Segel, L. A., (1969) J. Fluid Mech. **38**, 203-224.

Sorokin, V. S. (1953) *Variational Method in the Theory of Convection*, Prikl. Mat. Mekh. **17**, 39.

Spiegel, E. A. (1971) *Convection in Stars*, Ann. Rev. Astron. Astrophys. **9**, 323-352.

Spiegel, E. A. (1972) *Convection in Stars*, Ann. Rev. Astron. Astrophys. **10**, 261-304.

5. Amplitude Equations in Dissipative Systems

We consider a dissipative system governed by a nonlinear partial differential equation

$$\frac{\partial U}{\partial t} = L_\mu(\nabla) \cdot U + N(\nabla, U), \tag{5.1}$$

where $U(\mathbf{r}, t)$ represents a set of scalar or pseudo-scalar fields. The system is driven externally by a control parameter μ constant in space and time (except in section 5.3 where we consider parametric instabilities). Its basic state is thus homogeneous in space and constant in time, and corresponds to $U = 0$, say. $L_\mu(\nabla)$ is a linear operator which involves spatial-derivatives, and $N(\nabla, U)$ represents nonlinear terms. We assume that equation (5.1) is invariant under continuous translations in space and time (except in section 5.3 where it is invariant under continuous translations in space and discrete translations in time). We also assume in some cases, space-reflection symmetry or invariance under galilean transformations.

For a critical value of μ, the basic state, $U = 0$, loses its stability. The linear stability analysis consists of solving the eigenvalue problem

$$L_\mu(\nabla) \cdot U = \eta U. \tag{5.2}$$

The basic state is stable when all the eigenvalues η have a negative real part. The instability onset, or the bifurcation of $U = 0$, is characterized by one or several eigenvalues with a zero real part. The corresponding eigenfunctions, $U_{i,\mathbf{k}}(\mathbf{r}, t)$, are the critical modes, and characterize the temporal or spatial pattern that sets in at the instability onset, and breaks spontaneously some of the invariances listed above. In the vicinity of the instability onset, the amplitudes A_i of the critical modes vary on a time-scale much slower than the one of the other modes, and thus contain all the information about the asymptotic time-dependence of U. More precisely, the non-critical (damped) modes don't vanish only because they are forced by the critical (slightly unstable) modes through nonlinear interactions; thus, they follow adiabatically critical modes; adiabatic elimination of fast modes leads to amplitude equations. We observed in the previous lectures that symmetry constraints determine their form. We give now a catalogue of the most frequent situations.

5.1 Stationary instability

In the previous lecture we studied the example of Rayleigh- Bénard convection. A stationary instability corresponds to a marginal mode with a real growth-rate. We shall discuss the case when the critical wave number, k_c, is non-zero; situations where the critical wave number is vanishingly small will be considered in section 5.5.

5.1.1 One-dimensional pattern

Let us first consider the situation where the nonlinear terms select a one-dimensional "roll-pattern". In the vicility of the instability onset, $r \simeq r_c$, the growth-rate is a real function of k with a maximum around k_c (Figure 5.1)

$$\sigma = r - r_c + \frac{1}{2}\left(\frac{\partial^2 \sigma}{\partial k^2}\right)_c (k - k_c)^2 + \cdots \tag{5.3}$$

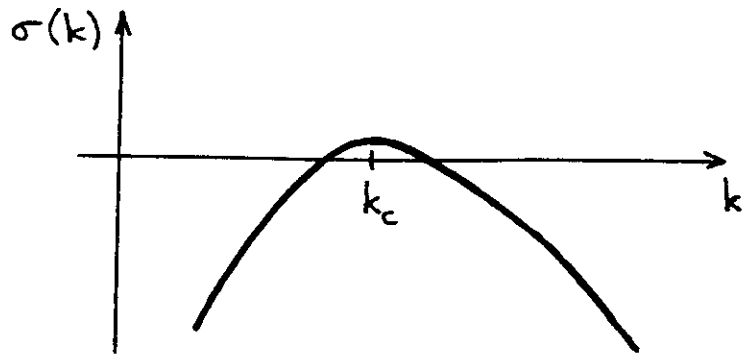

Figure 5.1. Growth-rate versus wave number for a stationary instability at $k = k_c$

We take the distance to criticality, $r - r_c$, of order ϵ^2 ($\epsilon \ll 1$), accordingly the instability growth-rate is of order ϵ^2; this is the time-scale for the slow critical modes. Correspondingly, there is a large spatial scale generated by modes interaction in the unstable wavenumber band; as $\sigma(k)$ is locally a parabola, $k - k_c \leq O(\epsilon)$, and the large spatial scale corresponds to $k - k_c = \epsilon K$. Thus, the scaled dispersion relation is

$$\Sigma(K) = \mu - \alpha K^2 + \cdots, \tag{5.4}$$

where $\Sigma = \sigma/\epsilon^2$, $\mu = (r - r_c)/\epsilon^2$, $\alpha = -\frac{1}{2}\left(\frac{\partial \sigma}{\partial k}\right)_c$, and K, are all of order one.

We first consider modulations of the pattern only along the x-axis, and write

$$\mathbf{U}(x,t) = \epsilon\,[A(X,T)\exp(\mathrm{i}k_c x) + c.c.]\,\tilde{\mathbf{U}}_{k_c} + \cdots, \tag{5.5}$$

where $\tilde{\mathbf{U}}_{k_c}\exp(ik_c x)$ is the critical mode. As shown in previous lectures, the linear evolution equation for A is the Fourier-Laplace transform of (5.4), and the leading order nonlinear term compatible with translational invariance in space is $|A|^2 A$. Moreover, its coefficient β is real if the system is invariant under spase-reflection symmetry, $x \to -x$. Thus, to leading order, A obeys the Ginzburg-Landau equation

$$\frac{\partial A}{\partial T} = \mu A + \alpha \frac{\partial^2 A}{\partial X^2} - \beta |A|^2 A. \tag{5.6}$$

The nonlinear term saturates the instability growth if $\beta > 0$, and the bifurcation is supercritical. In terms of the original scaled variables, the critical mode amplitude scales like ϵ i. e. like $(r - r_c)^{1/2}$. The slow spatial scale can be understood as a coherence length and diverges at criticality like $(r - r_c)^{-1/2}$.

If $\beta < 0$, higher order nonlinear terms should be taken into account, and a simple model for a subcritical bifurcation is

$$\frac{\partial A}{\partial T} = \mu A + \alpha \frac{\partial^2 A}{\partial X^2} - \beta |A|^2 A - \gamma |A|^4 A, \tag{5.7}$$

with $\gamma > 0$. However, in terms of scaled variables, β should be small in order to get the two nonlinear terms at the same order; thus (5.7) is asymptotically correct only in the vicinity of a tricritical point.

Like the Ginzburg-Landau equation, (5.7) can be put in variational form

$$\frac{\partial A}{\partial T} = -\frac{\delta \mathcal{L}}{\delta \overline{A}} \tag{5.8}$$

where

$$\begin{aligned} \mathcal{L}[A] &= \int \left[\alpha \left| \frac{\partial A}{\partial X} \right|^2 - V(A, \overline{A}) \right] dX, \\ V(A, \overline{A}) &= \mu |A|^2 - \frac{\beta}{2} |A|^4 - \frac{\gamma}{3} |A|^6. \end{aligned} \tag{5.9}$$

$\mathcal{L}[A]$ is a Lyapunov functional; indeed, multiplying (5.7) by $\partial \overline{A}/\partial T$, and adding to the complex conjugate expression, yields

$$\frac{d}{dt}\mathcal{L}[A] = -2 \int \left| \frac{\partial A}{\partial T} \right|^2 dX < 0. \tag{5.10}$$

Thus $\mathcal{L}[A]$ is a decreasing function, bounded from below for the constant A's that are the maxima of $V(A, \overline{A})$. For a supercritical bifurcation ($\beta > 0$, fifth order term neglected), the uniform state $A = 0$ is globally stable for $\mu < 0$, whereas perfectly periodic patterns corresponding to $A = \sqrt{\mu/\beta}\, \exp(i\phi)$, with constant ϕ, are globally stable for $\mu > 0$. The degenaracy in ϕ is obviously related to translational invariance in space, but a more subbtle

effect that involves the phase might happen when the system is not invariant under reflection symmetry, $x \to -x$.

When the system is not invariant under reflection symmetry, $x \to -x$, the coefficient β is in general a complex number. Writing $A(X,T) = R(X,T)\exp i\phi(X,T)$, equation (5.6) yields

$$\begin{aligned} \frac{\partial R}{\partial T} &= \left[\mu - \alpha\left(\frac{\partial \phi}{\partial X}\right)^2\right] R + \alpha\frac{\partial^2 R}{\partial X^2} - \beta_r R^3 \\ R\frac{\partial \phi}{\partial T} &= 2\frac{\partial R}{\partial X}\frac{\partial \phi}{\partial X} + R\frac{\partial^2 \phi}{\partial X^2} - \beta_i R^3. \end{aligned} \tag{5.11}$$

Consequently, a homogeneous roll-pattern of amplitude R_0 has its phase that linearly increases in time

$$\phi_0 = -\beta_i R_0^2 T.$$

Thus, from (5.5), one observes that this "stationary" instability gives rise to a travelling pattern

$$\mathbf{U}_0(x,t) = \epsilon\left[R_0 \exp\, i(k_c x - \epsilon^2 \beta_i R_0^2 t) + cc\right] \tilde{\mathbf{U}}_{k_c} + \cdots$$

due to the externally broken reflection symmetry. We will study a similar effect when the reflection symmetry is spontaneously broken; a secondary instability then generates a drifting pattern from a stationary one (see lecture 7).

Note that the absence of a term proportional to $\partial A/\partial X$ in (5.6) is not related to reflection symmetry. Indeed, a term of the form $i\partial A/\partial X$ is compatible with the $x \to -x$ symmetry, and is present as soon as one expands $\mathbf{U}$ in (5.5) at $k \neq k_c$. This corresponds to the change of variable

$$A = B\,\exp(iqX)$$

that gives

$$\frac{\partial B}{\partial T} = (\mu - \alpha q^2)B + 2iq\alpha\frac{\partial B}{\partial X} + \alpha\frac{\partial^2 B}{\partial X^2} - \beta|B|^2 B, \tag{5.10}$$

thus showing that the growth-rate of the mode $k = k_c + \epsilon q$ is $\mu - \alpha q^2$, i. e. in scaled terms, $r - r_c - \alpha(k - k_c)^2$, in agreement with the dispersion relation. The absence of a term in $i\partial A/\partial X$ in (5.6) is thus only related to the fact that the first unstable mode k_c is the one with the maximum growth-rate $\sigma(k)$.

A simple model, that mimics the formation of a one-dimensional pattern is the Swift-Hohenberg equation for a field $u(x,y,t)$

$$\frac{\partial u}{\partial t} = \left[r - r_c - (k_c{}^2 + \Delta)^2\right] u - u^3. \tag{5.13}$$

Consider a one-dimensional field in space, $u(x,t)$, and using a multiple-scale expansion technique, derive the Ginzburg-Landau equation in the vicinity of the instability onset, $r - r_c \simeq \mu\epsilon^2$. Try the same exercise with the model

$$\frac{\partial u}{\partial t} = \left[r - r_c - ({k_c}^2 + \Delta)^2\right] u - au^2 - u\frac{\partial u}{\partial x}, \tag{5.14}$$

which is not invariant under the $x \to -x$ reflection symmetry, and show that β is complex. Find the nature of the bifurcation as a function of a, and derive (5.7) in the vicinity of the tricritical point.

Finally, let us consider a situation where the spatial phase is quenched. This occurs in the convection problem for instance, if one takes stress-free boundary conditions also at the lateral boundaries, $x = 0$ and $x = 2n\pi/k_c$, where n is an integer. Then, the phase of the pattern is fixed,

$$\mathrm{U}(x,t) = \epsilon R(X,T)\,\sin(k_c x)\,\tilde{\mathbf{U}}_{k_c} + \cdots, \tag{5.15}$$

and its amplitude is governed by a real Ginzburg-Landau equation

$$\frac{\partial R}{\partial T} = \mu R + \alpha\frac{\partial^2 R}{\partial X^2} - \beta R^3. \tag{5.16}$$

The broken symmetry at the instability onset is not translational invariance, which is here externally broken because of the lateral boundary conditions, but the $R \to -R$ symmetry of Boussinesq convection.

5.1.2 Two-dimensional modulations of a one-dimensional cellular pattern

We now consider the dynamics of two-dimensional modulations of a one-dimensional roll-pattern, parallel to the x-axis. In isotropic systems, the growth-rate depends on $\mathbf{k}^2$ and is maximum for $\mathbf{k}^2 = {k_c}^2$; thus, for $|\mathbf{k}| \simeq k_c$

$$\sigma(\mathbf{k}) = r - r_c - {\xi_0}^2(\mathbf{k}^2 - {k_c}^2)^2 + \cdots, \tag{5.17}$$

and as shown in Lecture 4, the amplitude equation reads

$$\frac{\partial A}{\partial T} = \mu A + \alpha\left(\frac{\partial}{\partial X} - \frac{i}{2k_c}\frac{\partial^2}{\partial Y^2}\right)^2 A - \beta|A|^2 A, \tag{5.18}$$

or in variational form

$$\frac{\partial A}{\partial T} = -\frac{\delta\mathcal{L}}{\delta\overline{A}} \tag{5.19}$$

whith

$$\mathcal{L}[A] = \int\left[-\mu|A|^2 + \frac{\beta}{2}|A|^4 + \alpha\left|\left(\frac{\partial}{\partial X} - \frac{i}{2k_c}\frac{\partial^2}{\partial Y^2}\right)A\right|^2\right] dX\,dY. \tag{5.20}$$

For anisotropic systems, the growth-rate is maximum for $|\mathbf{k}| = k_c$ with $\mathbf{k}$ along a prefered axis, x say. Thus

$$\sigma(\mathbf{k}) = r - r_c - \alpha(k_x - k_c)^2 + \alpha' {k_y}^2 + \cdots. \tag{5.21}$$

and

$$\Sigma(\mathbf{K}) = \mu - \alpha {K_X}^2 + \alpha' {K_Y}^2 + \cdots, \tag{5.21}$$

so the Ginzburg-Landau equation takes the form

$$\frac{\partial A}{\partial T} = \mu A + \alpha \frac{\partial^2 A}{\partial X^2} + \alpha' \frac{\partial^2 A}{\partial Y^2} - \beta |A|^2 A, \tag{5.23}$$

5.1.3 Two-dimensional patterns

We have already considered two-dimensional patterns in the previous lecture. Let us take the example of hexagons or more precisely of patterns with three basic wave-vectors, $\mathbf{k}_1, \mathbf{k}_2, \mathbf{k}_3$, such that $\mathbf{k}_p = k_c$ and $\mathbf{k}_1 + \mathbf{k}_2 + \mathbf{k}_3 = 0$,

$$\mathbf{U}(x, y, t) = \epsilon \sum_{p=1}^{3} [A_p \exp(i\mathbf{k}_p \cdot \mathbf{r}) + c.c.] \; \tilde{\mathbf{U}}_{kc} + \cdots, \tag{5.24}$$

without the $U \to -U$ invariance. Using symmetry considerations, the amplitude equations read

$$\frac{dA_l}{dT} = \mu A_l + \rho \overline{A}_m \, \overline{A}_n - \left[\beta |A_l|^2 + \delta(|A_m|^2 + |A_n|^2)\right] A_l, \tag{5.25}$$

Note that this equation is asymptotically valid only if the $U \to -U$ symmetry is slightly broken, so that the quadratic and cubic nonlinearities are obtained at the same order. The quadratic nonlinearities correspond to the resonant triad interaction $\mathbf{k}_1 + \mathbf{k}_2 + \mathbf{k}_3 = 0$. Although one can change the phase ϕ_p of each wave by shifting the origin in the horizontal plane along $\mathbf{k}_p$, the above relation implies

$$\phi_1 + \phi_2 + \phi_3 = \Phi = \text{constant}. \tag{5.26}$$

Φ determines the shape of the pattern (hexagons, triangles, ...). Using translational and reflection symmetry, one can restrict Φ to the interval $[0, \pi/2]$. Note that the leading order amplitude equations (5.25) select $\Phi = 0$.

5.2 Oscillatory instability

We now consider situations where the instability growth-rate has an imaginary part $\omega(k)$; thus, the unstable mode has an oscillatory behaviour with a pulsation $\omega(k_0)$ at onset. We begin with the case $k_0 = 0$.

5.2.4 *Oscillatory instability at zero wavenumber*

When the real part of the growth-rate is maximum at zero wavenumber, we have

$$\eta(k) = \sigma(k) + i\omega(k) \tag{5.27}$$

with

$$\begin{aligned} \sigma(k) &= r - r_c + \frac{1}{2}\left(\frac{\partial^2\sigma}{\partial k^2}\right)_0 k^2 + \cdots \\ \omega(k) &= \omega_0 + \left(\frac{\partial\omega}{\partial k}_0\right)_0 k + \frac{1}{2}\left(\frac{\partial^2\omega}{\partial k^2}\right)_0 k^2 + \cdots \end{aligned} \tag{5.28}$$

In the vicinity of the instability onset, $r - r_c = \mu\epsilon^2$,

$$\mathbf{U}(x,t) = \epsilon\left[A(X,T)\exp(\mathrm{i}\omega_0 t) + c.c.\right]\tilde{\mathbf{U}}_0 + \cdots, \tag{5.29}$$

where $\tilde{\mathbf{U}}_0 \exp(\mathrm{i}\omega_0 t)$ is the critical mode. As previously observed, the Fourier-Laplace transform of the dispersion relation gives the linear part of the amplitude equation, and translational invariance in time determines the form of the leading order nonlinear term, $|A|^2A$. We get

$$\frac{\partial A}{\partial T} = \mu A - c\frac{\partial A}{\partial X} + \alpha\frac{\partial^2 A}{\partial X^2} - \beta|A|^2 A, \tag{5.30}$$

where $c = (\partial\omega/\partial k)_0$ is the group velocity, $\alpha_r = -\frac{1}{2}\left(\partial^2\sigma/\partial k^2\right)_0$ is related to the diffusion of space-dependent perturbations ($\alpha_r > 0$), $\alpha_i = -\frac{1}{2}\left(\partial^2\omega/\partial k^2\right)_0$ corresponds to the dispersion, β_r is the nonlinear dissipation, and β_i is related to the nonlinear amplitude-dependence of the frequency. Note that, like for the nonlinear Schrödinger equation, one needs two slow time-scales T_1 and T_2 when deriving (5.30) with an asymptotic expansion. Transforming to the reference frame moving at the group velocity yields

$$\frac{\partial A}{\partial T} = \mu A + \alpha\Delta A - \beta|A|^2 A. \tag{5.31}$$

Equation (5.31) is a Ginzburg-Landau equation with complex coefficients α and β. This is a crucial difference from (5.6) for stationary cellular instabilities, that involves real coefficients. Indeed, no variational formulation is known for (5.31). Thus, A does not evolve in order to minimize a functional $\mathcal{L}[A]$ as for (5.6), but displays in some parameter range, periodic or even chaotic behaviours in space and time. Equation (5.31) has two simple limits, a "variational" one for α and β real

$$\frac{\partial A}{\partial T} = -\frac{\delta\mathcal{L}}{\delta\overline{A}}, \quad \frac{d}{dt}\mathcal{L}[A] = -2\int\left|\frac{\partial A}{\partial T}\right|^2 dX < 0,$$

and a conservative limit (the nonlinear Schrödinger equation), for α and β pure imaginary,

$$\frac{\partial A}{\partial T} = -\frac{\delta\mathcal{L}}{\delta\overline{A}}, \quad \frac{d}{dt}\mathcal{L}[A] = 0.$$

One method is to investigate (5.31) perturbatively, starting from one of these limit situations (lecture 8).

5.2.5 Oscillatory instability at finite wavenumber

Hydrodynamic instabilities often lead to time-dependent cellular patterns. The Couette-Taylor flow between concentric cylinders (DiPrima and Swinney, 1981), thermal convection in the presence of a salinity gradient or in binary fluid mixtures (Turner, 1973), thermal convection in a layer of fluid rotating about a vertical axis (Chandrasekhar, 1961), display a Hopf bifurcation at a finite wavenumber $k_0 \neq 0$. The growth-rate of the marginal modes read

$$\eta(k) = \sigma(k) + i\omega(k) \tag{5.32}$$

with

$$\begin{aligned} \sigma(k) &= r - r_c + \frac{1}{2}\left(\frac{\partial^2\sigma}{\partial k^2}\right)_0 (k-k_0)^2 + \cdots \\ \omega(k) &= \omega_0 + \left(\frac{\partial\omega}{\partial k}_0\right)_0 (k-k_0) + \frac{1}{2}\left(\frac{\partial^2\omega}{\partial k^2}\right)_0 (k-k_0)^2 + \cdots \end{aligned} \tag{5.33}$$

In the vicinity of the instability onset, $r - r_c = \mu\epsilon^2$,

$$\begin{aligned} \mathbf{U}(x,t) = {} & \epsilon\left[A(X,T)\exp(i\omega_0 t - k_0 x) + c.c.\right]\tilde{\mathbf{U}}_{-k_0} \\ & + \epsilon\left[B(X,T)\exp(i\omega_0 t + k_0 x) + c.c.\right]\tilde{\mathbf{U}}_{k_0} + \cdots, \end{aligned} \tag{5.34}$$

where A and B are the complex amplitudes of the waves propagating to the right and to the left, and obey the following amplitude equations

$$\begin{aligned} \frac{\partial A}{\partial T} &= \mu A - c\frac{\partial A}{\partial X} + \alpha\frac{\partial^2 A}{\partial X^2} - (\beta|A|^2 + \gamma|B|^2)A \\ \frac{\partial B}{\partial T} &= \mu B + c\frac{\partial B}{\partial X} + \alpha\frac{\partial^2 B}{\partial X^2} + (\gamma|A|^2 + \beta|B|^2)B. \end{aligned} \tag{5.35}$$

Equations (5.35) are invariant under the transformations

$$\begin{aligned} A \to A\exp(-i\phi), \quad B \to B\exp(i\phi), \\ A \to A\exp(i\theta), \quad B \to B\exp(i\theta), \end{aligned}$$

that reflect translational invariance in space and time, and under the transformation

$$X \to -X, \quad A \to B, \quad B \to A,$$

that traces back to space-reflection symmetry, $x \to -x$. Note that terms of the form $i\partial A/\partial X$, $i\partial B/\partial X$, satisfy symmetry requirements but are not involved because σ is maximum for $k = k_0$. Let us also remark that the group velocity c should be small in order to get all

the terms of (5.35) at the same order of an asymptotic expansion (see the discussion about counter-propagating waves in lecture 3).

Restricting the discussion to spatially homogeneous solutions, it is easy to check that (5.35) describe either :

- propagating waves ($|A| \neq 0, |B| = 0$, or $|A| = 0, |B| \neq 0$), which are stable if $\gamma_r > \beta_r > 0$,

- standing waves ($|A| = |B| \neq 0$, which are stable if $\beta_r > \gamma_r$.

When $\beta_r < 0$ or $\gamma_r < -|\beta_r|$, the bifurcation is subcritical.

5.3 Parametric instability

Parametric instabilities in spatially extended systems also generate waves. Let us consider for example the one-dimensional array of coupled pendula, already studied in lecture 3, with an additional damping and a parametric forcing. In the long-wavelength limit, the governing equation is

$$\frac{\partial^2 u}{\partial t^2} + 2\lambda \frac{\partial u}{\partial t} + (1 + f \sin \omega_e t) \sin u = \frac{\partial^2 u}{\partial x^2}. \tag{5.36}$$

In the limit of small dissipation ($\lambda \simeq 0$), the dispersion relation of the unforced array of pendula is

$$\omega(k)^2 = 1 + k^2. \tag{5.37}$$

The strongest parametric response being at $\omega_e/2$, a wavenumber k_0 is selected by the dispersion relation, such that

$$\omega_e \equiv 2\,\omega \simeq 2\,\omega(k_0).$$

In the vicinity of the instability onset,

$$u(x,t) = \epsilon\,[A(X,T) \exp i(\omega_0 t - k_0 x) + B(X,T) \exp i(\omega_0 t + k_0 x) + c.c.] + \cdots. \tag{5.38}$$

The symmetry requirements are,

- continuous translational invariance in space, that implies the invariance under the transformation

$$A \to A \exp(-i\phi), \quad B \to B \exp(i\phi),$$

- discrete translational invariance in time, $t \to t + 2\pi/\omega_e$, that implies

$$A \to -A, \quad B \to -B,$$

- space-reflection symmetry, $x \to -x$, that implies

$$X \to -X, \quad A \to B, \quad B \to A.$$

All the terms of (5.35) respect these requirements, but additional terms are allowed due to the less restrictive requirement about translational invariance in time (discrete instead of continuous). To leading order, two additional terms, proportional to the forcing, are allowed, $F\overline{A}$ and $F\overline{B}$. We get

$$\begin{aligned} \frac{\partial A}{\partial T} &= (-\Lambda + i\nu)A + F\overline{B} - c\frac{\partial A}{\partial X} + \alpha\frac{\partial^2 A}{\partial X^2} - (\beta|A|^2 + \gamma|B|^2)A \\ \frac{\partial B}{\partial T} &= (-\Lambda + i\nu)B + F\overline{A} + c\frac{\partial B}{\partial X} + \alpha\frac{\partial^2 B}{\partial X^2} - (\gamma|A|^2 + \beta|B|^2)B, \end{aligned} \tag{5.39}$$

where Λ is proportional to the dissipation and ν is proportional to the detuning from parametric resonance. Equations (5.39) show that the right-going wave is forced by the left-going wave, and vice-versa, so that only standing waves are parametrically generated in the vicinity of the instability onset. In other words, the phase of the parametric response being quenched by the external forcing in time, the only possibility at onset is a standing wave.

5.4 Neutral modes at zero wavenumber. Systems with Galilean invariance

Symmetry properties or conservation laws often imply the existence of neutral modes at zero wavenumber. Consider the following model of one-dimensional stationary cellular instability

$$\frac{\partial u}{\partial t} = \frac{\partial^2 u}{\partial x^2} + r\frac{\partial^4 u}{\partial x^4} + \frac{\partial^6 u}{\partial x^6} - u\frac{\partial u}{\partial x}. \tag{5.40}$$

The growth-rate $\sigma(k)$ for a perturbation of wavenumber k around the $u = 0$ solution reads

$$\sigma(k) = -k^2(1 - rk^2 + k^4)$$

and is displayed on Figure 5.2. For $r \simeq r_c = 2$, the nul state undergoes a stationary instability to a cellular structure of wavenumber k_c. The local behaviour of the growth-rate around k_c is thus similar to the one of the Swift-Hohenberg model (5.15).

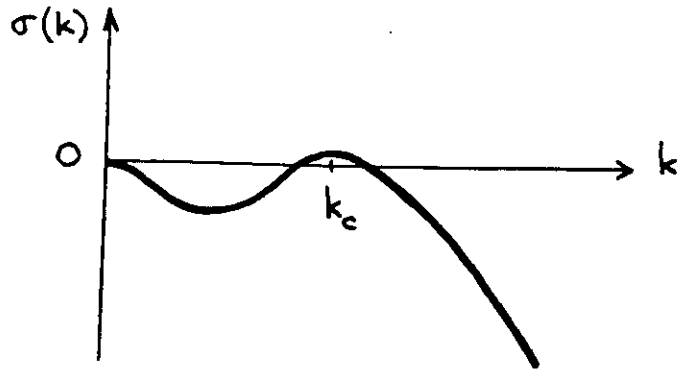

Figure 5.2. Growth-rate versus wave number for the model (5.40)

However, an important difference is that (5.40) can be written in a conservative form

$$\frac{\partial u}{\partial t} = \frac{\partial}{\partial x}\left(\frac{\partial u}{\partial x} + r\frac{\partial^3 u}{\partial x^3} + \frac{\partial^5 u}{\partial x^5} - \frac{1}{2}u^2\right). \tag{5.41}$$

If u is considered as a velocity field along the x-axis, this traces back to the Galilean invariance of (5.40), i. e. the invariance under the transformation

$$x \to x - vt, \quad u \to u + v.$$

This implies the existence of marginal modes at zero wavenumber, as shown by the dispersion relation of figure 5.2. In the vicinity of the instability onset, the amplitude of these slow modes should be taken into account, since it is generally coupled to the amplitude of the critical modes at k_c. Thus, we write

$$u(x,t) = \epsilon\left[A(X,T)\exp(ix) + c.c. + B(X,T)\right] + \cdots. \tag{5.41}$$

and get coupled evolution equations for A and B,

$$\frac{\partial A}{\partial T} = \mu A + 4\frac{\partial^2 A}{\partial X^2} - \frac{1}{36}|A|^2 A - iAB, \tag{5.42}$$

$$\frac{\partial B}{\partial T} = \frac{\partial^2 B}{\partial X^2} - \frac{\partial}{\partial X}|A|^2. \tag{5.43}$$

Note that all the terms in (5.42) and (5.43) cannot be obtained at the same order of an asymptotic expansion, and one should again use two different time-scales. If u is considered as a velocity field, B is a large-scale flow that advects the cellular pattern, thus shifting its phase through the term iAB in (5.41); in turn, the amplitude inhomogeneities of the cellular pattern, generates the large-scale flow B in (5.42). Note that u is a "compressible velocity field", but a similar effect occurs with Boussinesq convection rolls when two-dimensional perturbations are taken into account. The important point to remember is that the amplitude

of neutral modes couples to the one of the critical modes, and modify the dynamics described by the Ginzburg-Landau equation.

5.5 Conserved order parameter

Another class of stationary cellular instabilities where additional symmetries modify the form of the evolution equation for the amplitude of the critical modes, is when the amplitude obeys a conservation law. This situation is similar to a phase transition with a conserved order parameter, spinodal decomposition for instance (Langer, 1975). Let us consider again the example of Rayleigh-Bénard convection, but this time with upper and lower perfectly insulating boundaries. The Boussinesq equations are

$$\nabla \cdot \mathbf{v} = 0 \tag{5.44}$$

$$\frac{\partial \mathbf{v}}{\partial t} + (\mathbf{v} \cdot \nabla)\mathbf{v} = -\nabla \pi + P\nabla^2 \mathbf{v} + RP\theta \hat{\mathbf{z}} \tag{5.45}$$

$$\frac{\partial \theta}{\partial t} + \mathbf{v} \cdot \nabla \theta = \mathbf{v} \cdot \hat{\mathbf{z}} + \nabla^2 \theta, \tag{5.46}$$

with

$$\frac{\partial \theta}{\partial z} = 0, \tag{5.47}$$

$$\mathbf{v} = 0, \tag{5.48}$$

at the boundaries, $z = 0$ and $z = 1$. We consider rigid boundaries in order to avoid the coupling with a neutral mean flow at instability onset. We first consider a solution of equations (5.44 - 5.48),

$$\mathbf{U}_0 = [\mathbf{v}_0(\mathbf{r}, t), \theta_0(\mathbf{r}, t), \pi_0(\mathbf{r}, t)],$$

and note that

$$\mathbf{U}_\Theta = [\mathbf{v}_0, \theta_0 + \Theta(t), \pi_0 + RP\Theta(t)z],$$

is also a solution if

$$\frac{\partial \Theta}{\partial t} = 0.$$

In other words, $D\mathbf{U} = (0, 1, RPz)$ is an eigenmode with a zero eigenvalue. Thus, there is a neutral mode at zero wavenumber, that traces back to the existence of the above continuous family of solutions. To investigate the stability of the static state, $\mathbf{U} = 0$, we consider

$$\mathbf{U} = \Theta(X, Y, T)\, D\mathbf{U} + \cdots, \tag{5.49}$$

where $\Theta(X, Y, T)$ is slowly varying in space and time. When R is small, the space-dependent buoyancy in equation (5.45) is small and generates a small velocity field; thus, the coupling with velocity in equation (5.46) is weak, and Θ is damped because of thermal diffusion. The growth-rate is negative and the static state is stable in the long wavelength limit (see Figure 5.3). However, when R increases above a critical value R_c, the effective diffusivity in the equation for Θ changes sign due to the coupling with the velocity field that enhances the temperature perturbation Θ; we get a stationary instability at zero wavenumber (see Figure 5.3).

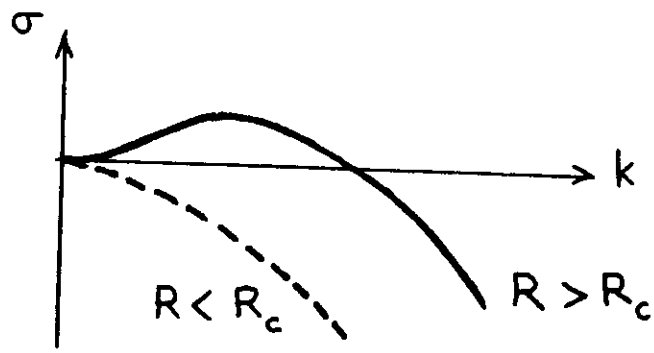

Figure 5.3. Dispersion relation for fixed-flux convection

The evolution equation for $\Theta(X, Y, T)$ can be obtained with a multiple-scale expansion (Chapman, 1978). We want to point out here that it should have the form of a conservation equation. Indeed, using the boundary conditions, the vertical average of (5.46) reads

$$\frac{\partial}{\partial t}\int_0^1 \theta dz + \nabla_h \cdot \left[\int_0^1 [(\theta - z)\mathbf{v}_h - \nabla_h \theta]\right] = 0. \tag{5.50}$$

In the vicinity of the instability onset, $R - R_c = \epsilon^2 R_c r$, the evolution equation for Θ is at leading order

$$\frac{\partial \Theta}{\partial T} = -r\nabla_h^2\Theta - \kappa\nabla_h^4\Theta + \gamma\nabla_h \cdot \left[(\nabla_h\Theta)^2\nabla_h\Theta\right]. \tag{5.51}$$

The absence of terms that involve explicitely Θ is related to the freedom of constant shift in temperature, that we have with the Boussinesq equations with insulating boundary conditions. The even number of space-derivatives is due to x and y-reflection symmetries in the horizontal plane. The absence of quadratic non-linearities traces back to the Boussinesq symmetry. We will find a lot of similar examples of stationary instability at zero wavenumber, when studying phase instabilities of cellular patterns (lecture 6).

5.6 Conservative systems and dispersive instabilities

Another additional symmetry that affects the form of the amplitude equation is the time reversal symmetry of conservative systems. A well-known example is that of two inviscid fluids layers of different densities, possibly moving at different velocities, in which Kelvin-Helmholtz or Rayleigh-Taylor instabilities can occur.

We restrict our attention to the Kelvin-Helmholtz instability. A layer of density ρ' moves at velocity U' above a layer of density ρ, $(\rho > \rho')$, moving at velocity U. The stability analysis is governed by the following dispersion relation (Chandrasekhar, 1961)

$$\frac{\eta}{k} = -i\frac{\rho U + \rho' U'}{\rho + \rho'} \pm i\left[\frac{g}{k}\frac{\rho - \rho'}{\rho + \rho'} - \frac{\rho\rho'}{(\rho + \rho')^2}(U - U')^2 + \frac{T}{\rho + \rho'}k\right]^{\frac{1}{2}} \tag{5.52}$$

where k is the wavenumber and T is the surface tension. Instability occurs when the term in the square brackets is negative, a result of the shear being large enough. The first term in the square brackets shows that the gravitational restoring force stabilizes low wavenumbers, whereas the last term shows that surface tension stabilizes high wavenumbers. The net effect is that in the presence of both a density step and surface tension, there is a critical velocity difference $(\Delta U^2)_c$ for the onset of instability, at which a critical wavenumber k_c becomes unstable first; at slightly higher values of ΔU^2 there is a narrow band of unstable wavenumbers.

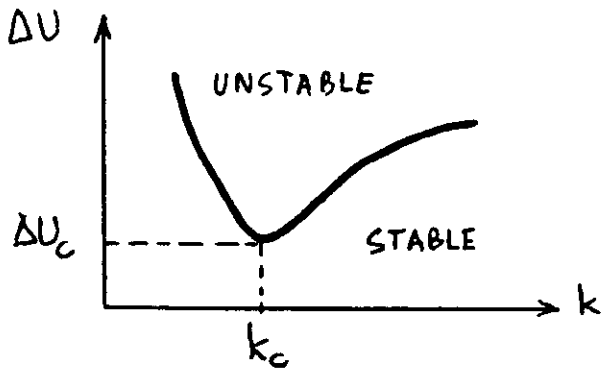

Figure 5.4. Marginal stability curve for the Kelvin-Helmholtz instability

This looks very similar to Rayleigh-Bénard convection, although the growth-rate for the Kelvin-Helmholtz has an imaginary part that corresponds to the frequency of the unstable waves, but the main difference is related to the conservative nature of the present problem. At the onset of the Kelvin-Helmholtz instability, four pure imaginary eigenvalues collide by pair and give rise to four complex eigenvalues, $(\pm\eta, \pm\overline{\eta})$, whereas for an instability in a dissipative system, a real eigenvalue, or pairs of complex-conjugate eigenvalues cross the imaginary axis. The former situation is a dispersive instability, and is related to time-reversal symmetry; indeed, this implies that, if η is an eigenvalue, then $-\eta$ is another eigenvalue. As the original problem involves real quantities, $\pm\overline{\eta}$ are also eigenvalues, and a conservative system involves either, pure imaginary eigenvalues (stable range), or complex eigenvalues $(\pm\eta, \pm\overline{\eta})$ (unstable range).

In the unstable range, the amplitude equation is also modified by the additional time-reversal symmetry constraint. Let us consider for instance the following conservative model of Swift-Hohenberg type.

$$\frac{\partial^2 u}{\partial t^2} = \left[\mu - \left(1 + \frac{\partial^2}{\partial x^2}\right)^2\right] u + u\frac{\partial u}{\partial x} \tag{5.53}$$

When $\mu \simeq 0$, the system is unstable about $k_c = 1$ and the linear growth-rate around k_c is

$$\eta^2 \simeq \mu - \alpha(k - k_c)^2.$$

Using the scalings

$$\frac{\partial}{\partial x} = \frac{\partial}{\partial x} + \sqrt{\mu}\frac{\partial}{\partial X}$$
$$\frac{\partial}{\partial t} = \sqrt{\mu}\frac{\partial}{\partial T},$$

show that the amplitude equation is

$$\frac{\partial^2 A}{\partial T^2} = \mu A + \alpha\frac{\partial^2 U}{\partial X^2} - \beta|A|^2 A.$$

This is a nonlinear Klein-Gordon equation.

References

Chandrasekhar, S. (1961) *Hydrodynamic and Hydromagnetic Stability*, Clarendon Press, Oxford.

Chapman, C. J. (1978) *Nonlinear Rayleigh-Bénard Convection Between Poorly Conducting Boundaries*, Woods Hole Oceanographic Institution Technical Report.

Coullet, P., Fauve, S. (1985) *Collective Modes of Periodic Structures, Combustion and Nonlinear Phenomena*, Les Editions de Physique.

DiPrima, R. C., Swinney, H. L., (1981) *Instabilities and Transition in Flow between Concentric Rotating Cylinders. Hydrodynamic Instabilities and the Transition to Turbulence*, Swinney, H. L. and Gollub, J. P. Editors. Topics in Applied Physics **45**, 97-137, Springer Verlag

Fauve, S. (1985) *Large Scale Instabilities of Cellular Flows*, Woods Hole Oceanographic Institution Technical Report.

Langer, J. S. (1975) *Spinodal Decomposition, Fluctuations, Instabilities, and Phase Transitions*, T. Riste Editor, NATO Advanced Study Institutes Series, Plenum Press.

Turner, J. S. (1973) *Buoyancy Effects in Fluids*, Cambridge University Press.

6. Secondary Instabilities of Cellular Flows: Eckhaus and zig-zag instabilities

6.1 Broken-symmetries and neutral modes

We have so far considered the onset of cellular structures as a control parameter is changed. We now consider the instability of such structures which occurs as the parameter is changed further. We call this a *secondary instability* of the system. In many cases, a secondary instability arises from a *neutral mode* associated with a symmetry of the governing equations broken by the primary instability.

For example, consider convection in container of infinite extent in the horizontal plane, or with periodic boundary conditions. The onset of convection breaks translational symmetry in the direction perpendicular to the rolls, the x-axis, say. However, one can imagine pushing the rolls along the x-axis without any expenditure of energy, since this only amounts to a shift of the x-axis origin. This translation is a neutral mode. In other words, one roll-solution breaks translational invariance, but the ensemble of all the possible roll-solutions should be invariant according to the Curie principle. Thus, as we noticed earlier, the phase of the periodic structure above the instability onset is arbitrary. Changing the phase amounts to move along the orbit of all the possible roll-solutions. This "motion" does not require any energy and is a neutral mode of the periodic structure, i. e. has a zero growth-rate.

Let us illustrate this concept with Swift-Hohenberg-type models. We first consider

$$\frac{\partial u}{\partial t} = \left[\mu - (1 + \frac{\partial^2}{\partial x^2})^2\right] u - u^3 \tag{6.1}$$

Suppose there exists a periodic solution $u_0(x)$ to the full nonlinear equation (6.1), that is,

$$L \cdot u_0 = {u_0}^3,$$

where $L = \left[\mu - (1 + \frac{\partial^2}{\partial x^2})^2\right]$. Taking derivatives yields

$$L \cdot \left(\frac{du_0}{dx}\right) = 3{u_0}^2 \frac{du_0}{dx}. \tag{6.2}$$

Now, we write

$$u = u_0(x) + \epsilon\, v(x,t)$$

in order to investigate the linear stability of u_0, and we get from equation (6.1)

$$\frac{\partial v}{\partial t} = L \cdot v - 3{u_0}^2\, v + O(\epsilon^2)$$

Comparison of equation (6.2) with equation (6.3) shows that

$$v = \frac{du_0}{dx}$$

is an eigenmode with a zero eigenvalue. A perturbation v proportional to this eigenmode corresponds to a translation $u_0(x+\epsilon)$. This can be shown differently by looking for a solution in the form

$$u(x,t) = u_0\,[x + \phi(t)] \tag{6.3}$$

where u_0 is our steady-state solution, and $\phi(t)$ is a time dependent phase. Substituting this into equation (6.1) yields

$$u_0' \frac{d\phi}{dt} = L \cdot u_0 - {u_0}^3$$

where u_0' is the derivative of u_0 with respect to its argument. We get

$$\frac{d\phi}{dt} = 0, \tag{6.4}$$

which confirms that the translational perturbation is a neutral mode of equation (6.1).

Translational invariance is of course not the only possible broken-symmetry at the onset of a pattern-forming instability. Consider for instance the model (5.40) of lecture 5

$$\frac{\partial u}{\partial t} = \frac{\partial^2 u}{\partial x^2} + r\frac{\partial^4 u}{\partial x^4} + \frac{\partial^6 u}{\partial x^6} - u\frac{\partial u}{\partial x}, \tag{6.5}$$

which is Galilean invariant, i. e. invariant under the transformation

$$x \to x - ct\ , \quad u \to u + c$$

We consider a periodic solution $u_0(x)$ of equation (6.5) and look for a perturbation in the form

$$u = u_0[x + \phi(t)] - \psi(t). \tag{6.6}$$

We get from (6.4)

$$\frac{d\phi}{dt}u_0' - \frac{d\psi}{dt} - \psi u_0' = 0,$$

thus:

$$\begin{aligned} \frac{d\phi}{dt} &= \psi \\ \frac{d\psi}{dt} &= 0. \end{aligned} \tag{6.7}$$

Two neutral modes are now involved, and trace back to the broken translational and Galilean invariances. The form of the coupling between ϕ and ψ can be understood as follows: if one pushes the pattern $u_0(x)$ at a constant velocity ψ along the x-axis, one observes a spatial phase ϕ that increases linearly in time.

6.2 Phase-dynamics

We could have imposed perturbations of the form (6.3) but with the phase ϕ slowly varying both in time and space, $\phi(X,T)$, where $X = \epsilon x$ and $T = \epsilon^\tau t$ are slow variables (for a diffusive behaviour for instance, $\tau = 2$). More generally, a long wavelength perturbation of the perfectly periodic pattern $u_0(x)$ can be writen in the form

$$u(x,t) = u_0\left[x + \phi(X,T)\right] + u_\perp(X,T), \tag{6.8}$$

where

$$u_0\left[x + \phi(X,T)\right] - u_0 \simeq \phi(X,T)\frac{du_0}{dx}$$

represents perturbations along the orbit of the symmetry group corresponding to translational invariance, i.e. phase perturbations, and $u_\perp$ consists of perturbations transverse to the group orbit, i.e. amplitude perturbations. A constant phase perturbation is neutral, and correspondingly weakly damped in the long wavelength limit, whereas amplitude perturbations decay on a faster timescale when the perfectly periodic pattern is stable. Adiabatic elimination of the amplitude modes leads to an evolution equation for the phase, that can be derived assuming that an expansion in powers of the gradients of the phase is valid,

$$\frac{\partial\phi}{\partial T} = \mathcal{F}\left[\frac{\partial\phi}{\partial X}, \frac{\partial^2\phi}{\partial X^2}, \ldots\right]. \tag{6.9}$$

The linear part of this equation is the Fourier-Laplace transform of the dispersion relation for the growth-rate of the phase modes. The growth-rate is zero at zero wavenumber due to translational invariance. If it is negative in the long wavenumber limit, the phase perturbation is damped; however, due to the coupling with amplitude modes, the growth-rate may be positve in the long wavelength limit, thus describing a phase instability of the perfectly periodic pattern.

In the case of model (6.5), long wavelength perturbations should be considered in the form

$$u(x,t) = u_0\left[x + \phi(X,T)\right] - \psi(X,T) + u_\perp(X,T). \tag{6.10}$$

This leads to phase equations of the form

$$\frac{\partial \phi}{\partial T} = \omega + \mathcal{F}\left[\frac{\partial \phi}{\partial X}, \frac{\partial^2 \phi}{\partial X^2}, \cdots\right]$$
$$\frac{\partial \psi}{\partial T} = \mathcal{G}\left[\frac{\partial \phi}{\partial X}, \frac{\partial^2 \phi}{\partial X^2}, \cdots\right] \tag{6.11}$$

Thus phase-dynamics is second order in time, and propagative modes may result from the coupling between the phases associated to broken translational and Galilean invariances.

Before we pursue phase dynamics further, it is worth pointing out that it is only useful for secondary instabilities with wavenumbers much smaller than those of the primary instability. In other words, we can only investigate variations of the underlying pattern which are much larger in scale than the basic pattern wavelength. Furthermore, we had earlier said that amplitude and phase ought to vary together, but here we have considered phase variations in isolation. This turns out to be reasonable when the secondary instability is well separated from the onset of the primary instability. In this case, the amplitude follows adiabatically the phase-gradients, so no additional equation for the amplitude is needed. However, in the vicinity of the primary instability, coefficients in the phase equation diverge, and we must use the full amplitude equation instead.

Other symmetries besides translation and Gallilean invariance can be found in the basic equations, but all symmetries do not, in general, lead to slowly-varying local dynamics, and so are not amenable to the method of phase-dynamics. For example, rotational and dilatational invariances, regardless how small the rate of transformation, both result in arbitrarily large effects at sites sufficiently distant from the center, and do not lead, in general, to additional phase modes.

6.3 Eckhaus Instability

6.3.1 Compression mode of a one-dimensional pattern

We considered stationary cellular instability earlier, and derived the amplitude equation, that reads in the supercritical case with appropriate amplitude and x scales,

$$\frac{\partial A}{\partial T} = \mu A + \frac{\partial^2 A}{\partial X^2} - |A|^2 A. \tag{6.12}$$

Equation (6.12) has stationary solutions

$$A_q = Q \exp(iqX) \quad \text{where} \quad Q^2 = \mu - q^2, \tag{6.13}$$

that represent all the possible roll-solutions which correspond to the unstable band of modes above the instability onset.

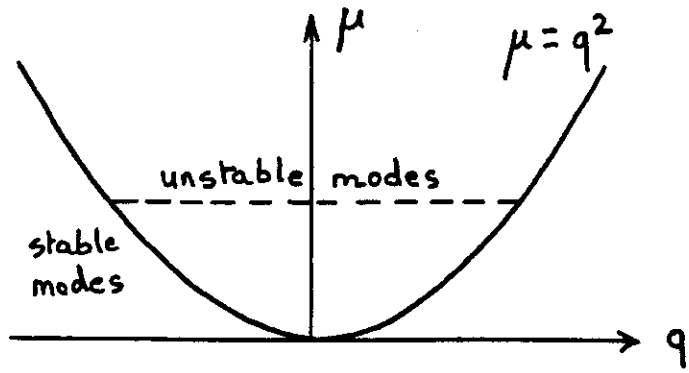

Figure 6.1. Cellular Instability: Cellular patterns exist only for parameters within the parabola.

We investigate the stability of these stationary patterns by perturbing their amplitude and phase, thus writing

$$A = [Q + r(X,T)] \exp i[qX + \phi(X,T)] \tag{6.14}$$

in equation (6.12). Expanding and separating real and imaginary parts yields

$$\frac{\partial r}{\partial T} = \mu[Q+r] + \frac{\partial^2 r}{\partial X^2} - [Q+r]\left[q + \frac{\partial \phi}{\partial X}\right]^2 - [Q+r]^3$$
$$[Q+r]\frac{\partial \phi}{\partial T} = 2\frac{\partial r}{\partial X}\left[q + \frac{\partial \phi}{\partial X}\right] + [Q+r]\frac{\partial^2 \phi}{\partial X^2}$$

If we linearize in r and ϕ, and use $Q^2 = \mu - q^2$, we obtain

$$\begin{aligned} \frac{\partial r}{\partial T} &\simeq -2Q^2 r + \frac{\partial^2 r}{\partial X^2} - 2Qq\frac{\partial \phi}{\partial T} \\ \frac{\partial \phi}{\partial T} &\simeq 2\frac{q}{Q}\frac{\partial r}{\partial X} + \frac{\partial^2 \phi}{\partial X^2} \end{aligned} \tag{6.15}$$

We consider modes proportional to $\exp(\eta t + iKX)$ and get from equation (6.15) the dispersion relation

$$\begin{vmatrix} \eta + 2Q^2 + K^2 & 2iQqK \\ -2\frac{q}{Q}iK & \eta + K^2 \end{vmatrix} = 0 \tag{6.16}$$

which has solutions

$$\eta(K) = -(Q^2 + K^2) \pm \sqrt{Q^4 + 4K^2q^2}$$

Thus, for small K, we have two different branches:

- the "amplitude modes", $\eta_-(K) = -2Q^2 + O(K^2)$, that are damped,

- the "phase modes", $\eta_+(K) = -K^2(1 - 2q^2/Q^2) + O(K^4)$, that are marginal. The phase modes

$$\eta_+(K) = -\left(\frac{\mu - 3q^2}{\mu - q^2}\right) K^2 - 2\frac{q^4}{(\mu - q^2)^3} K^4 + O(K^6) \tag{6.17}$$

lead to an instability when

$$D_{\parallel} = \left(\frac{\mu - 3q^2}{\mu - q^2}\right) < 0$$

so when $q^2 < \mu < 3q^2$; this is the Eckhaus instability. We can thus nest this secondary instability curve in the earlier stability diagram.

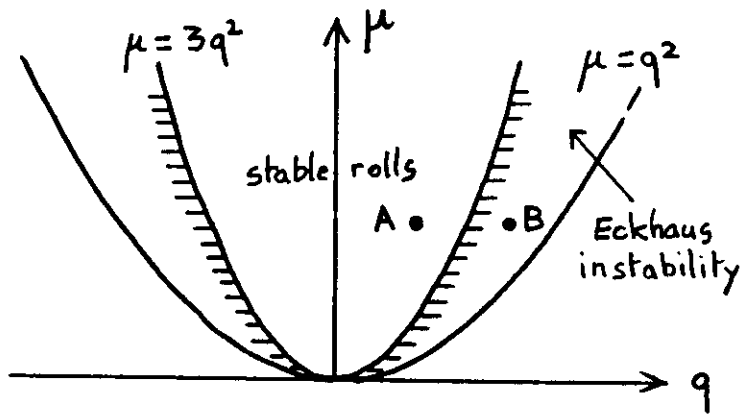

Figure 6.2. Eckhaus instability diagram. The pattern generating primary instability occurs inside the outer parabola, but the resulting pattern is stable only within the inner parabola.

6.3.2 Nonlinear phase equation for the Eckhaus instability

We now derive the phase equation of the Eckhaus instability in order to describe pattern-dynamics through the evolution of its slowly varying phase. As said above, this is possible in the long wavelength limit because we have two types of perturbations with different timescales (see Figure 6.3): adiabatic elimination of the amplitude modes leads to an evolution equation for the phase.

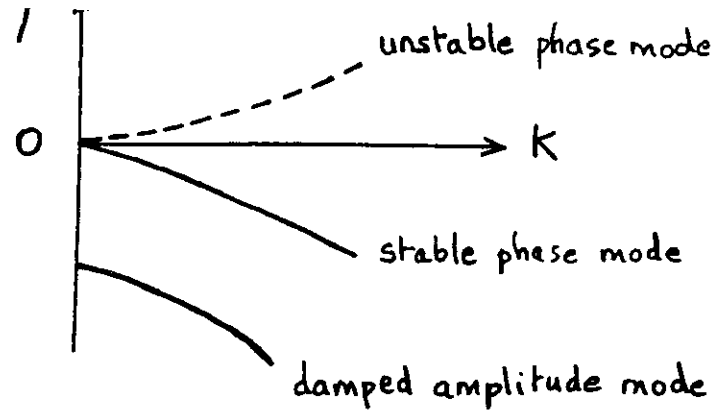

Figure 6.3. Amplitude and phase perturbations have different timescales in the long wavelength limit.

For a better understanding, let us consider again the linear equations (6.15). For spatially homogeneous perturbations, as already observed, the amplitude perturbation r decays exponentially whereas the phase perturbation ϕ is neutral. For perturbations slowly varying in space, r is non-zero only because it is forced by phase-gradients; thus, the amplitude follows adiabatically the phase-gradients, and the dominant balance in the evolution equation for r in (6.15) is

$$2Q^2 r \approx -2Qq\frac{\partial \phi}{\partial T}.$$

Substituting this into the phase equation of (6.15) we obtain

$$\frac{\partial \phi}{\partial T} \approx (1 - \frac{2q^2}{Q^2})\frac{\partial^2 \phi}{\partial X^2} \equiv D_{\parallel}\frac{\partial^2 \phi}{\partial X^2}.$$

We see that the Eckhaus instability shows up as a negative diffusivity in the phase equation; the small-scale flow generated by the primary instability, acts as a negative diffusivity for large scale perturbations, when the primary pattern wavenumber is far enough the critical one.

The higher order linear terms of the phase equation can be obtained from higher order balances in (6.15), or in a simpler way from the Fourier-Laplace transform of the small K expansion of the dispersion relation (6.17),

$$\frac{\partial \phi}{\partial T} = D_{\parallel}\frac{\partial^2 \phi}{\partial X^2} - \kappa\frac{\partial^4 \phi}{\partial X^4},$$

where $\kappa = 2q^4/Q^6$. In the vicinity of the Eckhaus instability onset, $D_{\parallel} \simeq 0$, then $\kappa \simeq \frac{3}{4\mu}$.

We next derive the leading order nonlinear term of the phase equation. Let us first see from symmetry arguments what form the nonlinear term might have. Translational invariance, $x \to x + x_0$, implies that the phase equation should be invariant under $\phi \to \phi + \phi_0$. This precludes any terms explicitely depending on ϕ such as ϕ^2 or $\phi\phi_X$. Reflection invariance

($x \to -x$) implies $\phi \to -\phi$, eliminating terms such as $\phi_X \phi_X$. The lowest order term possible is therefore $\phi_X \phi_{XX}$. The weakly nonlinear phase equation would then be (if the coeficient of this nonlinear term does not vanish)

$$\frac{\partial \phi}{\partial T} = D_{\|} \frac{\partial^2 \phi}{\partial X^2} - \kappa \frac{\partial^4 \phi}{\partial X^4} + g \frac{\partial \phi}{\partial X} \frac{\partial^2 \phi}{\partial X^2}. \tag{6.18}$$

Factoring the diffusive term, $(D_{\|} + g\phi_X)\phi_{XX}$, we see that the nonlinearity acts as an effective space-dependent diffusivity; however, we will see that it cannot compensate the negative diffusivity in the unstable regime, and does not saturate the Eckhaus instability which is thus a subcritical one whatever the sign of g. To find the coefficient g one can proceed formally with a multiple scale expansion from the nonlinear equations for r and ϕ. There is however a much simpler procedure: we first notice that $\phi = pX$ is a paticular solution of (6.18), that simply represents a homogeneous roll-solution of wavenumber $k_c + \epsilon(q + p)$; its linear stability is thus governed by the dispersion relation

$$\eta = -D_{\|}(q + p)K^2 + O(K^4).$$

We can also compute η by linearisation of (6.18) near $\phi = pX$; we get

$$\eta = -\left[D_{\|}(q) + gp\right] K^2 + O(K^4).$$

Identifying the two expressions to leading order in p, we obtain

$$g = \frac{\partial D_{\|}}{\partial q}.$$

We see that, at the Eckhaus instability onset ($D_{\|} = 0$), all the cefficients of the higher order terms of the phase equation (6.18) diverge as $\mu \to 0$, showing that, as already mentionned, the phase approximation becomes invalid, because near the primary cellular instability the amplitude mode also becomes neutral and thus cannot be eliminated. The full amplitude equation (6.12) should be used to capture the correct behaviour. However, one expects that for long wavelength perturbations of rolls, the form of the phase equation (6.18) remains valid along the Eckhaus instability curve, even for rather large values of $r - r_c$ out of the range of validity of the amplitude equation.

Let us now analyse the behaviour of the phase equation (6.18) in the vicinity of the Eckhaus instability onset. If we look at the linear dispersion relation for a mode $\exp(\eta T + iKX)$ we find (see Figure 6.4) that when $D_{\|} < 0$ there is a band of unstable modes for $0 < K < K_*$.

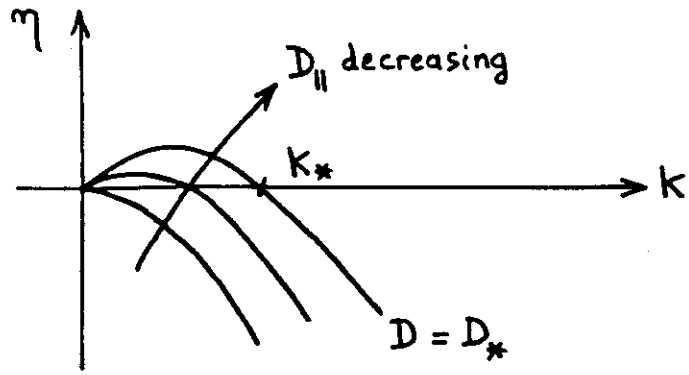

Figure 6.4. Dispersion relation for the phase equation.

We will focus on the neutral mode at $K = K_*$ since it is the first to go unstable ir an experiment with periodic boundary conditions (the first unstable mode is such that $K_* = 2\pi/L$, where L is the size of the periodic domain). The finite geometry thus delays the instability until $D_{\|} = -|D_*|$ when the mode K_* becomes neutral. The pattern is then unstable to the compression mode of wavenumber K_*; let us now study the finite amplitude behaviour of this mode.

We obtain this amplitude equation as usual, by inserting a mode

$$\phi = a(T)\exp(iK_*X) + c.c.$$

The resulting equation for $a(T)$ is

$$\frac{da}{dT} = -(D_{\|} - D_*)K_*^2\, a + 2\frac{\mu}{9}g^2K_*^2|a|^2a.$$

We see that there is no stabilization from the nonlinear term (since its coefficient is positive). This is shown on the bifurcation diagram (Figure 6.5).

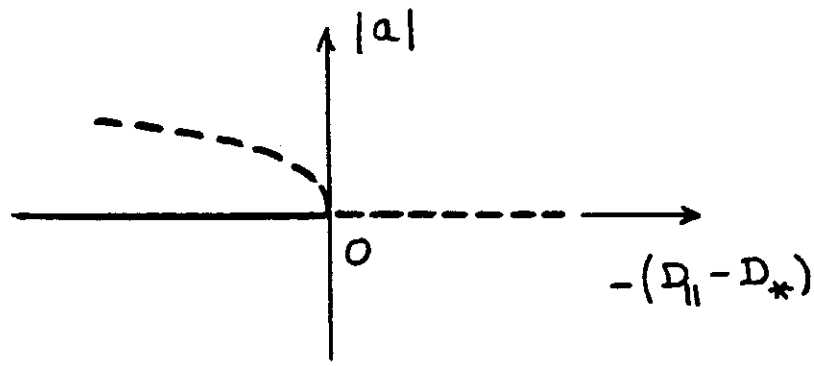

Figure 6.5. Bifurcation diagram of Eckhaus instability

Thus linearly stable rolls ($D_\parallel > D_*$) can be nonlinearly unstable to finite amplitude perturbations, a localized compression or dilatation of the pattern for instance. We will evaluate the critical size of the perturbation that generate the finite amplitude Eckhaus instability; this is analogous to a nucleation energy in first order phase transitions.

We look first for stationary solutions of the phase equation (6. 18). Setting $\partial\phi/\partial T = 0$, we obtain by integrating (6.18)

$$\lambda = D_\parallel \psi - \kappa \frac{\partial^2 \psi}{\partial X^2} + \frac{g}{2}\psi^2 \tag{6.19}$$

where ψ is the phase gradient,

$$\psi = \frac{\partial \phi}{\partial X},$$

i. e. the variation of the local wavenumber, and λ is a constant of integration related to the wavenumber at infinity. We can recast the problem as the motion of a particle of mass κ in a potential $U(\psi)$ such that

$$\begin{aligned} \kappa \frac{\partial^2 \psi}{\partial X^2} &= -\frac{dU}{d\psi} \\ U(\psi) &= \lambda\psi - \frac{D_\parallel}{2}\psi^2 - \frac{g}{6}\psi^3. \end{aligned} \tag{6.20}$$

The potential U can be simplified by eliminating the quadratic term with $\tilde{\psi} = \psi + D_\parallel/g$ to obtain

$$U(\tilde{\psi}) - U_0 = \left(\lambda + \frac{D_\parallel^2}{2g}\right)\tilde{\psi} - \frac{g}{6}\tilde{\psi}^3,$$

where U_0 is a constant. This potential is indicated in Figure 6.6. The solutions are graphically obvious but it should be recalled that these correspond to the X dependance of steady solutions. Nothing has been said as yet about their stability. We have two stationary solutions homogeneous in space (points A and B in Figure 6.6), and oscillatory solutions around B that represent patterns with a periodically modulated wavenumber. One solution of particular interest is the limiting solitary wave solution, where one imagines the particle travelling from the local maximum to the left and taking an infinite time to return. This motion is shown in Figure 6.7 and we see that it corresponds to a localized compression of the rolls.

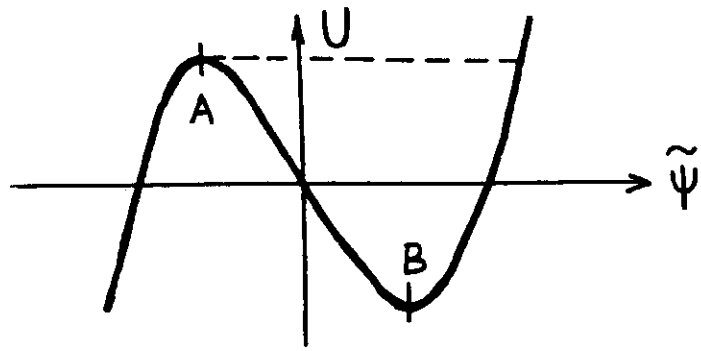

Figure 6.6. Potential well of stationary solutions of the phase equation.

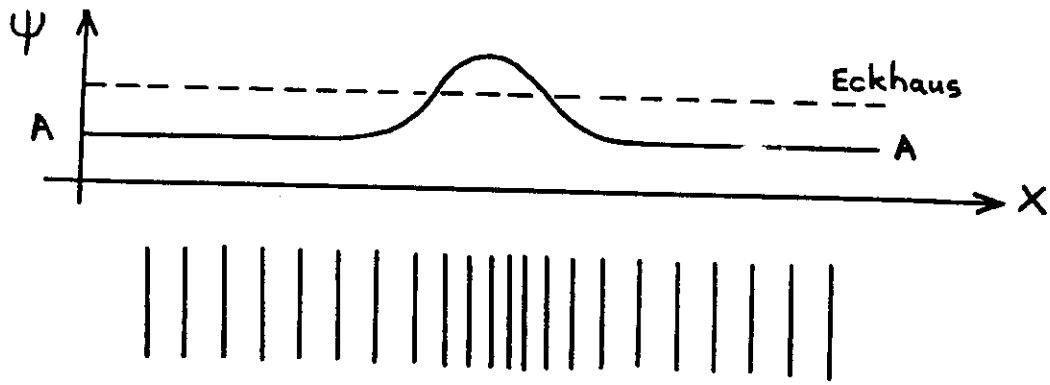

Figure 6.7. Solitary compression wave in the roll pattern.

We now try to find a Lyapunov functional in order to study the stability of the above stationary solutions. To wit we multiply equation (6.18) by $\partial\phi/\partial T$ and integrate over a wavelength in X. Integrating by parts we obtain

$$\int_0^L \left(\frac{\partial\phi}{\partial T}\right)^2 dX = \int_0^L \left[-D_{\|}\frac{\partial\phi}{\partial X}\frac{\partial^2\phi}{\partial X\partial T} - \kappa\frac{\partial^3\phi}{\partial X^2\partial T}\frac{\partial^2\phi}{\partial X^2} - \frac{g}{2}\left(\frac{\partial\phi}{\partial X}\right)^2\frac{\partial^2\phi}{\partial X\partial T}\right] dX.$$

Thus,

$$\frac{d}{dT}\mathcal{F} \equiv \frac{d}{dT}\int_0^L \left[\frac{D_{\|}}{2}\left(\frac{\partial\phi}{\partial X}\right)^2 + \frac{\kappa}{2}\left(\frac{\partial^2\phi}{\partial X^2}\right)^2 + \frac{g}{6}\left(\frac{\partial\phi}{\partial X}\right)^3\right] dX = -\int_0^L \left(\frac{\partial\phi}{\partial T}\right)^2 dX \leq 0.$$

$\mathcal{F}[\phi(X,T)]$ is decreasing during the phase dynamics but is not a proper Lyapunov functional because it is not bounded from below. Moreover, we should take into account an additional constraint imposed by the conservation form of the phase equation (6.18) or of the equation for the phase gradient ψ

$$\frac{\partial\psi}{\partial T} = \frac{\partial^2}{\partial X^2}\left[D_{\|}\psi - \kappa\frac{\partial^2\psi}{\partial X^2} + \frac{g}{2}\psi^2\right]. \tag{6.21}$$

This imposes the constraint

$$\frac{d}{dt}\int \psi dX = 0 \tag{6.22}$$

on the evolution, i. e. the conservation of the mean wavenumber. Therefore, the form of the phase equation shows that a pattern cannot evolve by continuously changing its wavelength.

When $\mathcal{F}[\phi(X,T)]$ has a local minimum, we can study the dynamics by minimising this functional where the above constraint enters with its Lagrange multiplier λ,

$$\mathcal{F}_\lambda = \int_0^L \left[\frac{D_\parallel}{2}\psi^2 + \frac{\kappa}{2}\left(\frac{\partial\psi}{\partial X}\right)^2 + \frac{g}{6}\psi^3 - \lambda\psi\right] dX.$$

Thus,

$$\mathcal{F}_\lambda = \int_0^L \left[\frac{\kappa}{2}\left(\frac{\partial\psi}{\partial X}\right)^2 - U(\psi)\right] dX, \tag{6.23}$$

and, to minimize $\mathcal{F}_\lambda$, we should maximize U. This means that the local maximum of U in Figure 6.6 is metastable whereas the local minimum is unstable. Indeed, points A and B in Figure 6.6 correspond to the same points on the Eckhaus stability diagram (Figure 6.2). Note that the oscillatory solutions about B are unstable. The solitary wave solution represents the "critical nucleus", i. e. the critical localized perturbation to the linearly stable pattern represented by A, that generates the finite amplitude Eckhaus instability. The corresponding value of $\mathcal{F}_\lambda$ minus its evaluation for the homogeneous stable pattern, represents the "energy barrier" of a pattern changing process from the homogeneous pattern A; this barrier vanishes at the linear Eckhaus instability onset. These points will be further covered next by studying the amplitude equation (6.12) directly.

6.3.3 Localized solutions of the one-dimensional Ginzburg-Landau equation

We now investigate in more detail the the amplitude equation (6.12). We first rescale the time scale so that (6.12) can be written as

$$A_T = \pm A + \frac{\partial^2 A}{\partial X^2} - |A|^2 A, \tag{6.24}$$

where the plus or minus sign corresponds to the sign of μ. As already mentionned in lecture 5, (6.24) is a variational problem, i. e.

$$\begin{aligned} \frac{d}{dT}\mathcal{L}[A] &= -2\int_0^L \left|\frac{\partial A}{\partial T}\right|^2 dX \le 0, \\ \mathcal{L}[A] &= \int_0^L \left[\left|\frac{\partial A}{\partial X}\right|^2 \mp |A|^2 + \frac{1}{2}|A|^4\right] dX. \end{aligned} \tag{6.25}$$

The Lyapunov functional $\mathcal{L}$ is a decreasing function and has a minimum value for the homogeneous solution ($A_X = 0$) that maximizes $U(A) = \pm A^2 - \frac{1}{2}A^4$. For $\mu < 0$, the stationary solutions of (6.24) are

$$A = Q\exp(iqX), \quad \text{with} \quad Q^2 = 1 - q^2, \tag{6.26}$$

and the Lyapunov functional (6.25) may be rewritten as

$$\mathcal{L} = \int_0^L l(q)dX,$$

where

$$l(q) = -\frac{1}{2}(q^2 - 1)^2.$$

We check that the periodic pattern with the critical wavenumber k_c, i. e. $q = 0$, correponds to the absolute minimum of $l(q)$. The inflection points of $l(q)$ correspond to $l''(q) = -2(3q^2 - 1) = 0$, which is the Eckhaus instability limit $q_E^2 = 1/3$. In solid state physics $l(q)$ is the free energy density and $l''(q) < 0$ corresponds to negative compressibility. Thus, the Eckhaus instability corresponds to a negative compressibility of the periodic pattern (Figure 6.8).

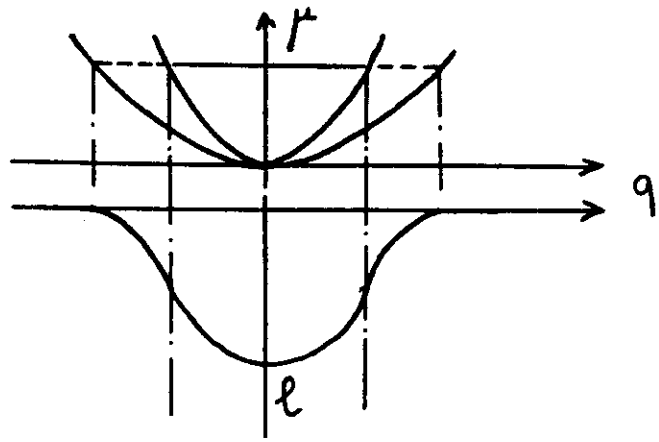

Figure 6.8. Plots of $\mu(q)$ and $l(q)$

We now investigate the wavenumber changing process. Substituting $A = Re^{i\phi}$ into the amplitude equation (6.24) and equating real and imaginary parts we get

$$\begin{aligned} \frac{\partial R}{\partial T} &= R - R^3 + \frac{\partial^2 R}{\partial X^2} - R\left(\frac{\partial \phi}{\partial X}\right)^2, \\ R\frac{\partial \phi}{\partial T} &= 2\frac{\partial R}{\partial X}\frac{\partial \phi}{\partial X} + R\frac{\partial^2 \phi}{\partial X^2}. \end{aligned} \tag{6.27}$$

For stationary solutions the second equation gives

$$R^2\frac{\partial \phi}{\partial X} = h, \tag{6.28}$$

where h is a constant. This conservation of "angular momentum" arises from the rotational invariance of the amplitude equation. The constraint (6.28) is the reason why the pattern-wavenumber changing process cannot occur by homogeneously modifying the wavenumber at constant amplitude.

Substituting (6.28) into (6.27), we get for stationary solutions

$$\frac{\partial^2 R}{\partial X} = -R + R^3 + h^2/R^3,$$

which is of the form

$$\begin{aligned} \frac{\partial^2 R}{\partial X} &= -\frac{\partial V}{\partial R}, \\ V(R) &= \frac{1}{2}R^2 - \frac{1}{4}R^4 + \frac{h^2}{2R^2}, \end{aligned} \tag{6.29}$$

thus corresponding again to the motion of a particle in the potential $V(R)$ (Figure 6.9 a). Bounded solutions exist for $h^2 < 4/27$; the two extrema $R_\pm$ of V correspond to homogeneous stationary solutions, such that

$$h^2 = R_\pm^4(1 - R_\pm^2).$$

Their stability can be determined using the Lyapunov functional (6.25); R_+ is the stable solution corresponding to the point A in Figures 6.2 and 6.6, and R_- is the unstable one corresponding to B.

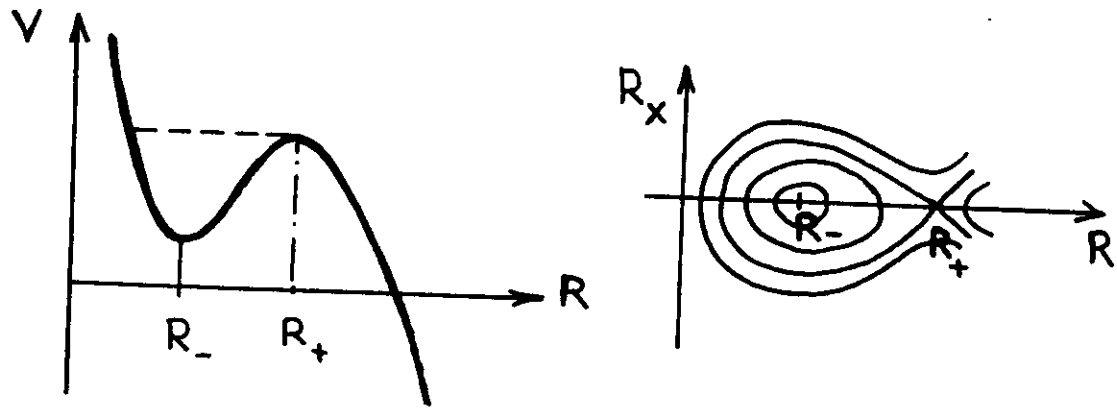

Figure 6.9. Potential well $V(R)$ for stationary solutions of the amplitude equation (6.24) and corresponding phase-space

Figure 6.9 b shows the phase space of the stationary solutions of amplitude equation (6.24). The homoclinic orbit passing through R_+ corresponds to the solitary wave solution that describes a localized compression (or dilatation) of the pattern, already found within the phase equation approach. The constraint (6.28) shows that the amplitude R decreases in these regions. When the localized compression (or dilatation) of the pattern is too large, the amplitude vanishes and this allows the anihilation (or creation) of pair of rolls; this

wavenumber changing mechanism involves length-scales comparable to the wavelength of the primary pattern, and is out of the range of validity of the amplitude equation (6.12) or of the phase equation (6.18). However, we were able to obtain the qualitative behaviour of the Eckhaus instability from these long-wavelength approximations.

6.4 The zig-zag instability

6.4.4 Torsion mode of a one-dimensional pattern

Like the Eckhaus instability, the zig-zag instability, shown in Figure 6.10 is associated with the broken translational invariance which a stationary roll-solution exhibits. In this case however the perturbation to the rolls is a transverse one, and can be writen in the long wavelength limit,

$$u(x,y,t) = u_0\left[x + \phi(Y,T)\right] + u_\perp(X,Y,T). \tag{6.30}$$

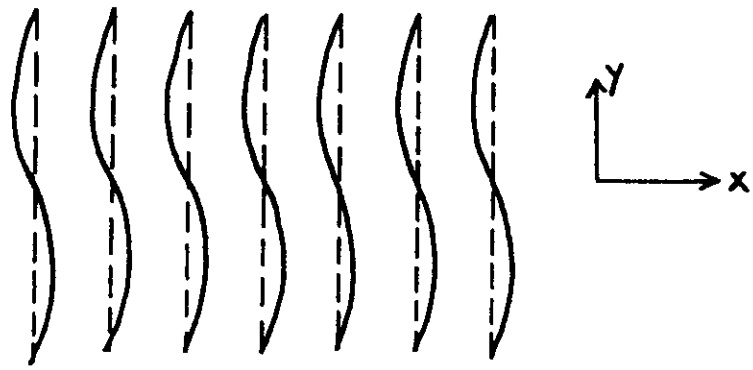

Figure 6.10. The form of the zig-zag instability: unperturbed rolls (dashed lines) and zig-zag mode (solid lines).

To investigate the dynamics of this torsion mode in the framework of the amplitude equation, we should use

$$\frac{\partial A}{\partial T} = \mu A + \left(\frac{\partial}{\partial X} - \frac{i}{2k_c}\frac{\partial^2}{\partial Y^2}\right)^2 A - |A|^2 A, \tag{6.31}$$

obtained in lecture 5.

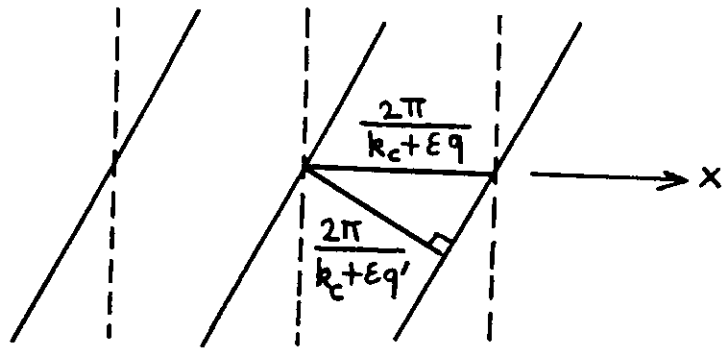

Figure 6.11. The effect of rotation of the roll planform

Figure(6.11 shows that rotation of the rolls leads to a decrease in the wavelength of the pattern, and hence an increase in the wavenumber. The zig-zag mode locally corresponds to a rotation of the pattern, so we can deduce that it will result in a local increase of the wavenumber. Referring to Figure 6.8, we see that for $q < 0$ an increase in q corresponds to a decease in $l(q)$, the Lyapunov functional, so in this region the pattern is unstable to zig-zag perturbations. However, for $q > 0$, $l(q)$ increases as q increases, demonstrating that the pattern is stable to local rotations. The zig-zag instability thus occurs for $k < k_c$ in the framework of (6.31). Indeed, if we look for a perturbation varying slowly in y,

$$A = [Q + r(Y,T)] \exp i[qX + \phi(Y,T)],$$

we get to leading order

$$\frac{\partial \phi}{\partial T} \simeq D_\perp \frac{\partial^2 \phi}{\partial Y^2}, \quad \text{where} \quad D_\perp = \frac{q}{k_c}.$$

6.4.5 Nonlinear phase equation for the zig-zag instability

Using symmetry considerations, translational invariance, that implies the invariance under $\phi \to \phi + \phi_0$, x-reflection symmetry, that implies the invariance under the transformation $X \to -X, \phi \to -\phi$, and y-reflection symmetry, that implies the invariance under the transformation $Y \to -Y$, we obtain to leading nonlinear order, the phase equation

$$\frac{\partial \phi}{\partial T} = D_\perp \frac{\partial^2 \phi}{\partial Y^2} - \kappa \frac{\partial^4 \phi}{\partial Y^4} + g \left(\frac{\partial \phi}{\partial Y} \right)^2 \frac{\partial^2 \phi}{\partial Y^2}. \tag{6.32}$$

Note the scaling $\phi \sim O(1)$, contrary to the Eckhaus instability where ϕ should be small. Rearranging (6.32) results in

$$\frac{\partial \phi}{\partial T} = \left[D_\perp + g \left(\frac{\partial \phi}{\partial Y} \right)^2 \right] \frac{\partial^2 \phi}{\partial Y^2} - \kappa \frac{\partial^4 \phi}{\partial Y^4}.$$

Now, $D_\perp < 0$ for instability; if the instability is to be saturated, the effective diffusivity must be positive, and hence g must be positive. Let us compute g, using a similar method as for the Eckhaus instability: first, note that $\phi = pY$ is a particular solution of (6.32) that corresponds to a tilted roll pattern. Writing, $\phi = pY + \tilde{\phi}$, and linearising in $\tilde{\phi}$, results in

$$\frac{\partial \tilde{\phi}}{\partial T} = (D_\perp + gp^2)\frac{\partial^2 \tilde{\phi}}{\partial Y^2} - \kappa \frac{\partial^4 \tilde{\phi}}{\partial Y^4}.$$

However, the tilted roll-solution is simply another roll pattern with a new wavenumber, q', where $q' = q + p^2/2k_c$. So we can also write

$$\frac{\partial \tilde{\phi}}{\partial T} = D_\perp(q')\frac{\partial^2 \tilde{\phi}}{\partial Y'^2} - \kappa \frac{\partial^4 \tilde{\phi}}{\partial Y'^4},$$

and matching the two previous equations gives

$$g = \frac{1}{2k_c}\frac{\partial D_\perp}{\partial q} = \frac{1}{2k_c^2}.$$

Hence $g > 0$, and the zig-zag instability is supercritical in the framework of the amplitude equation (6.31).

We now use the phase equation (6.32) to study the pattern generated by the zig-zag instability in the supercritical regime. If we let $\phi \propto \exp(\eta T + iKY)$ and linearise about $\phi = 0$, we obtain

$$\eta = -D_\perp K^2 - \kappa K^4.$$

This dispersion relation is similar to the one of the Eckhaus instability (see Figure 6.4; it might be thought that the mode with the maximum growth-rate, k_{max}, corresponds to the characteristic length-scale of the zig-zag instability in the supercritical regime, but a nonlinear analysis will show that this is not so.

The stationary solutions of (6.32) satisfy

$$\lambda = D_\perp \psi - \kappa \frac{\partial^2 \psi}{\partial Y^2} + \frac{g}{3}\psi^3,$$

where

$$\psi = \frac{\partial \phi}{\partial Y},$$

is the phase gradient, and λ is a constant of integration related to the wavenumber at infinity. This can be writen

$$\begin{aligned} \kappa \frac{\partial^2 \psi}{\partial Y^2} &= -\frac{dU}{d\psi} \\ U(\psi) &= \lambda\psi - \frac{D_\perp}{2}\psi^2 - \frac{g}{12}\psi^4, \end{aligned} \tag{6.33}$$

showing again that the determination of the stationary solutions amounts to find the trajectories of a particle of mass κ in the potential well $U(\psi)$. We look for a Lyapunov functional in order to determine their stability ; multiplying (6.32) by $\partial\phi/\partial T$ and integrating by part gives

$$\begin{aligned} \frac{d}{dT}\mathcal{F} &= -\int_0^L \left(\frac{\partial\phi}{\partial T}\right)^2 dY \leq 0 \\ \mathcal{F} &= \int_0^L \left[\frac{\kappa}{2}\frac{\partial\psi}{\partial Y}^2 + \frac{D_\perp}{2}\psi^2 + \frac{g}{12}\psi^4\right] dY. \end{aligned} \tag{6.34}$$

Thus, $\mathcal{F}[\psi(Y,T)]$ decreases; however, the governing equation for ψ has a conservative form

$$\frac{\partial\psi}{\partial T} = \frac{\partial^2}{\partial Y^2}\left[D_\perp\psi + \frac{g}{3}\psi^3 - \kappa\frac{\partial^2\psi}{\partial Y^2}\right], \tag{6.35}$$

which implies the constraint

$$\frac{d}{dT}\int_0^L \psi dY = 0 \tag{6.36}$$

on the phase dynamics. Thus, λ appears like a Lagrange multiplier, and we have to minimize

$$\mathcal{F}_\lambda = \int_0^L \left[\frac{\kappa}{2}\frac{\partial\psi}{\partial Y}^2 - U(\psi)\right] dY.$$

If we start from rolls perpendicular to the x-axis, i.e. $\psi = 0$, in the unstable regime, $D_\perp < 0$, we can take $\lambda = 0$ and the potential $U(\psi)$ is symmetric (Figure 6.12).

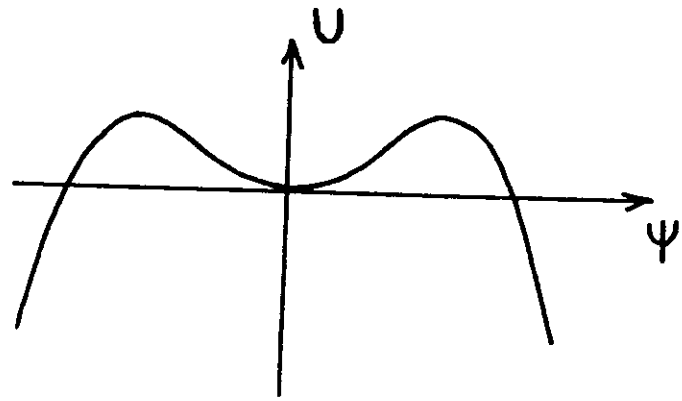

Figure 6.12. The potential $U(\psi)$ for $D_\perp < 0$ and $\lambda = 0$

The fastest growing mode is the one with wavenumber k_{max} and generates a wavy pattern as the one displayed in Figure 6.10. This pattern corresponds to an oscillatory solution about $\psi = 0$ in the potential well of Figure 6.12; thus it is unstable. The stable pattern which satisfies the constraint (6.36) corresponds to the limiting solitary-wave solution that connects the two opposite values $\psi = \pm\sqrt{3|D_\perp|/g}$, i.e. two sets of rolls with different orientations, symmetric with respect to the y-axis (see Figure 6.13). Note that this solution cannot be observed if we assume periodic boundary conditions in Y; the dynamics lead to a two-kink pattern in that case.

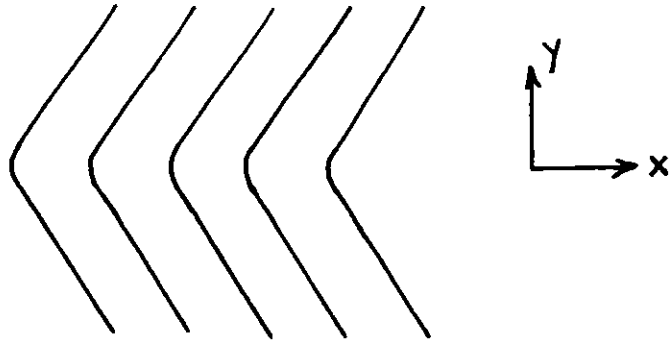

Figure 6.13. The solitary wave solution selected by the system to preserve the mean value of v

Thus, in the nonlinear regime, the zig-zag instability generates the largest possible domains with parallel rolls, compatible with the mean wavenumber conservation and the constraints related to boundary conditions. Although the Eckhaus and the zig-zag instabilities have similar dispersion relations, their nonlinear dynamics are different: the linearly unstable perturbations cascade to short scales in the Eckhaus instability, whereas larger and larger domains are created during the nonlinear evolution of the zig-zag instability.

References

Eckhaus, V. (1965) *Studies in Nonlinear Stability Theory*, Springer Verlag.

Fauve, S. (1985) *Large Scale Instabilities of Cellular Flows*, Woods Hole Oceanographic Institution Technical Report.

Kramer, L., Zimmermann, W. (1985) *On the Eckhaus Instability for Spatially Periodic Patterns*, Physica **D 16**, 221.

Kuramoto, Y. (1984) *Phase Dynamics of Weakly Unstable Periodic Structures*, Prog. Theor. Phys. **71**, 1182-1196

Pomeau, Y., Manneville, P. (1979) *Stability and Fluctuations of a Spatially Periodic Convective Flow*, J. Phys. Lettres **40**, 609-612

Stuart, J. T., DiPrima, R. C., (1978) *The Eckhaus and Benjamin-Feir Resonance Mechanisms*, Proc. Roy. Soc. Lond. **A 362**, 27-41

7. Drift Instabilities of Cellular Patterns

7.1 Introduction

Another type of secondary instability that occurs in many systems is the "drift instability". After a first bifurcation to a stationary cellular structure, $\mathbf{u}_0(x)$, further increase in the bifurcation parameter generates a secondary bifurcation to a traveling pattern of the form $\mathbf{u}_D(x \pm ct)$. The motion of the pattern in one of the preferential directions, $\pm x$, breaks the space reflection symmetry. As we observed in lecture 5 (model (5.14)), a stationary bifurcation may generate a traveling pattern at onset when the system is not invariant under reflection symmetry $x \rightarrow -x$. Here, we consider systems which are invariant under reflection symmetry and give rise to a symmetric primary pattern; the reflection symmetry is spontaneously broken at finite amplitude when the static pattern undergoes the secondary drift bifurcation.

Drift instabilities of cellular patterns have been widely observed in various experimental situations. Couette flow between two horizontal coaxial cylinders with a partially filled gap (Mutabazi et al., 1988), displays transitions from stationary to traveling rolls ; as clearly noticed, the traveling rolls are tilted and the direction of the propagation is determined by this asymmetry. The traveling-roll state is either homogeneous in space, or there exist domains of inclined rolls with opposite tilt and thus opposite propagation direction. Similar results have been found recently in a film draining experiment (Rabaud et al., 1990). Drift instabilities have been also observed in directional crystal growth experiments. Above the onset of the Mullins-Sekerka instability of liquid crystals, "solitary modes" propagating along the interface have been observed (Simon et al., 1988). These "solitary modes" consist of domains of stretched asymmetric cells that connect two regions with symmetric cells. Similarly, domains of tilted lamelae moving tranversally along the growth front have been observed during directional solidification of eutectics (Faivre et al., 1989), and the relationship of the tilt direction to the one of propagation has been also emphasized. Finally, a drift instability was observed recently for a standing surface wave excited parametrically in a horizontal layer of fluid contained in a thin annulus, submitted to vertical vibrations (Douady et al., 1989). It was observed that, as the driving amplitude is increased, the standing wave pattern either begins to move at a constant speed in one direction, or undergoes an oscillatory instability that corresponds to a compression mode of the periodic structure (i. e. a wavenumber modulation in space and time).

On the theoretical side, it is interesting to note that a secondary bifurcation that transforms a stationary structure into a traveling one has been predicted by Malomed and Tribelsky (1984) before the experimental results quoted above. They used a Galerkin approximation for model equations of the Kuramoto-Sivashinsky type, and pointed out that the drift instability arises in that case from the coupling between the spatial phase of the basic structure with the second harmonic generation. Recently this bifurcation was understood in a more general way from symmetry considerations (Coullet et al., 1989). Finally, a drift instabilty has been observed by numerical integration of the Kuramoto-Sivashinsky equation (Thual and Bellevaux, 1988).

We first propose a model that describes the drift instability of a stationary cellular pattern. We then show that a drift instability of a standing wave, as the one observed in the Faraday experiment, can be understood as a secondary bifurcation described by the evolution equations for the amplitudes of the right and left propagating waves (equations 5.39). In all cases, we will show that the basic mechanism consists of the coupling between the spatial phase ϕ of the primary pattern, with the order parameter V associated with the space-reflection broken-symmetry, and we will give the general governing equations for the drift bifurcation. The notations should be considered indenpendently in each section except in section (7.3) and (7.4).

7.2 A drift instability of stationary patterns

In their Galerkin approximation of a model equation, Malomed and Tribelsky found that the drift instability occurs when the second harmonic of the basic pattern is not linearly damped strongly enough. We thus consider a situation where two modes k and $2k$ interact resonantly,

$$\mathbf{u}(x,t) = [A(X,T)\exp(ikx) + \text{c.c.}]\,\mathbf{u}_k + [B(X,T)\exp(2ikx) + \text{c.c.}]\,\mathbf{u}_{2k} + \cdots \qquad (7.1)$$

From symmetry argument (translational invariance in space), the evolution equations for A and B read, to third order,

$$\begin{aligned} \frac{\partial A}{\partial T} &= \mu A - \bar{A}B - \alpha|A|^2 A - \beta|B|^2 A \\ \frac{\partial B}{\partial T} &= \nu B + \varepsilon A^2 - \gamma|A|^2 B - \delta|B|^2 B. \end{aligned} \qquad (7.2)$$

The quadratic coupling terms describe the resonant interaction between the modes k and $2k$. Their coefficients can be taken equal to $\varepsilon = \pm 1$ by appropriate scaling of the amplitudes; the coefficient of $\bar{A}B$ can be taken equal to -1, making the transformation $\mathbf{u} \to -\mathbf{u}$, if necessary. Positive values of α, β, γ and δ ensure global stability. The bifurcation diagram of equations

(7.2) have been studied by several authors in the context of resonant wave interaction (see for instance, Proctor and Jones (1988) and references therein). We thus refer to these papers for the mathematical aspects and discuss equations (7.2) in the restricted context of the "drift bifurcation".

Writing

$$A = R\exp(i\phi), \qquad B = S\exp(i\theta), \qquad \Sigma = 2\phi - \theta,$$

we get from (7.2)

$$\frac{\partial R}{\partial T} = (\mu - \alpha R^2 - \beta S^2)R - RS\cos\Sigma \tag{7.3a}$$

$$\frac{\partial S}{\partial T} = (\nu - \gamma R^2 - \delta S^2)S + \varepsilon R^2\cos\Sigma \tag{7.3b}$$

$$\Sigma_t = \left(2S - \varepsilon\frac{R^2}{S}\right)\sin\Sigma \tag{7.3c}$$

$$\phi_t = S\sin\Sigma \tag{7.3d}$$

In the context of our study we must take $\nu < 0$ (the second harmonic is linearly damped) and increase the bifurcation parameter μ. When μ becomes positive, the null state bifurcates to an orbit of stable stationary patterns related to each other by space translation:

$$R = R_0 \neq 0, \qquad S = S_0 \neq 0, \qquad \Sigma = \Sigma_0 = 0, \qquad \text{and} \quad \phi \text{ arbitrary.}$$

A cellular pattern drifting with a constant velocity, corresponds to :

$$\frac{\partial R}{\partial T} = 0, \qquad \frac{\partial S}{\partial T} = 0, \qquad \frac{\partial \Sigma}{\partial T} = 0, \quad \frac{\partial \phi}{\partial T} = \text{constant} \neq 0.$$

This implies $2S - \varepsilon R^2/S = 0$, and thus $\varepsilon = 1$. So the coefficients of the quadratic terms must have opposite signs in order to observe the drift instability. Note that this means that the second harmonic does not enhance the stationary instability near onset ; indeed, for $\mu \simeq 0$ and $\nu < 0$. B follows adiabatically A ($B \propto A^2$), and the quadratic terms of equation (7.2) contributes to saturate the primary instability. The stationary pattern is destabilized when $2S_0 + R_0^2/S_0$ vanishes as μ is increased. This happens if the condition $1 + \nu(2\gamma + \delta) > 0$ is satisfied, which corresponds to the condition that the second harmonic is not strongly damped ($|\nu|$ not too large). The system of equations (7.3 a, b, c) then undergoes a supercritical pitchfork bifurcation. The two bifurcated stationary states are such that $R_D^2 = 2S_D^2$, $\Sigma = \pm\Sigma_D \neq 0$. Above the instability onset, ϕ increases linearly in time according to equation (7. 3 d). As noted earlier, this state represents traveling waves .

The bifurcation from the stationary pattern to the traveling one has the following characteristics: Its order parameter, $\Sigma = 2\phi - \theta$, undergoes a pitchfork bifurcation that breaks the basic pattern reflection symmetry. The coupling with the basic pattern spatial phase ϕ induces the drift motion according to equation (7.3 d), and the direction of propagation is

determined by the sign of Σ. Thus the mechanism described by Malomed and Tribelsky for their model equations appears to be a general one. We expect that this k - $2k$ interaction mechanism is relevant for most of the experiments quoted above.

7.3 The drift instability of a parametrically excited standing wave

Let us now consider the drift instability of a standing surface wave, generated by parametric excitation in a horizontal layer of fluid contained in a thin annulus, submitted to vertical vibrations (Douady et al., 1989). It was observed that, as the driving amplitude is increased, the standing wave pattern, either begins to move at a constant speed in one direction, or undergoes an oscillatory instability that corresponds to a wavenumber modulation in space and time. We first consider the drift bifurcation and discuss the oscillatory instability next.

Close to the onset of instability, we write the surface deformation in the form

$$\xi(x,t) = A(X,T)\exp i(\omega t - kx) + B(X,T)\exp i(\omega t + kx) + c.c. + \cdots, \qquad (7.4)$$

where A and B are the slowly varying amplitudes of the right and left waves at frequency $\omega = \omega_e/2$, where ω_e is the external driving frequency. The equations for A and B are at leading order (see lecture 5),

$$\begin{aligned}
\frac{\partial A}{\partial T} + c\frac{\partial A}{\partial X} &= (-\lambda + i\nu)A + \mu\bar{B} + \alpha\frac{\partial^2 A}{\partial X^2} + (\beta|A|^2 + \gamma|B|^2)A \\
\frac{\partial B}{\partial T} - c\frac{\partial B}{\partial X} &= (-\lambda + i\nu)B + \mu\bar{A} + \alpha\frac{\partial^2 B}{\partial X^2} + (\beta|B|^2 + \gamma|A|^2)B,
\end{aligned} \qquad (7.5)$$

where λ is the dissipation ($\lambda > 0$), ν corresponds to the detuning between the surface wave frequency ω_0 and $\omega_e/2$. μ is proportional to the external forcing amplitude. The imaginary parts of β and γ describe the nonlinear frequency variation of the wave as a function of the amplitude, whereas the real parts correspond to nonlinear dissipation. α_i corresponds to dispersion.

When $\mu \geq 0$, a standing wave regime is observed. To analyze its stability we write,

$$A = \exp(S + R)\exp i(\Theta + \Phi) \qquad \text{and} \qquad B = \exp(S - R)\exp i(\Theta - \Phi),$$

and get from equations (7.5) for spatially homogeneous waves :

$$\frac{\partial S}{\partial T} = -\lambda + \cosh 2R\,[\mu\cos 2\Theta + (\beta_r + \gamma_r)\exp 2S] \qquad (7.6a)$$

$$\frac{\partial \Theta}{\partial T} = \nu + \cosh 2R\,[-\mu\sin 2\Theta + (\beta_i + \gamma_i)\exp 2S] \qquad (7.6b)$$

$$\frac{\partial R}{\partial T} = \sinh 2R\,[-\mu\cos 2\Theta + (\beta_r - \gamma_r)\exp 2S] \tag{7.6c}$$

$$\frac{\partial \Phi}{\partial T} = \sinh 2R\,[\mu\sin 2\Theta + (\beta_i - \gamma_i)\exp 2S]. \tag{7.6d}$$

Θ and Φ are respectively the temporal and spatial phases of the pattern. Note that the equation for Φ decouples, because of the translation invariance of the system in space. The standing-wave solutions correspond to $(S_0, \Theta_0, R = 0)$. Their stability with respect to spatially homogeneous perturbations is simple to investigate from equations (7.6). We assume $\beta_r + \gamma_r < 0$ and the detuning small enough ($|\nu| < \lambda|\beta_r/\beta_i|$). Then, perturbations in S and Θ are damped. Perturbations in R and Φ obey the equations,

$$\frac{\partial \Phi}{\partial T} = 2\,[\nu + 2\beta_i \exp 2S_0]\,R + \cdots \tag{7.7a}$$

$$\frac{\partial R}{\partial T} = 2\,[-\lambda + 2\beta_r \exp 2S_0]\,R + \cdots \tag{7.7b}$$

When the standing wave pattern amplitude $\exp(S_0)$ is small, R is damped and the standing wave pattern is stable. As the driving amplitude is increased, S_0 increases and R becomes unstable for $\exp(2S_0) = \lambda/2\beta_r$, provided that $\beta_r > 0$. A non zero value of R breaks the $x \to -x$ symmetry (see equation (7.4) and the expressions of A and B versus S, R, Θ, Φ). Thus R is the order parameter of the "drift bifurcation" for this standing wave problem. The coupling with the spatial phase Φ generates the drift (7.7 a). The structure of the "drift bifurcation" is thus similar to that described previously for stationary a pattern. However, higher order terms in equations (7.7) show that the "drift bifurcation" is subcritical in this case. One can easily check this by noting that the drifting solution of equations (7.6), $\frac{\partial S}{\partial T} = \frac{\partial R}{\partial T} = \frac{\partial \Theta}{\partial T} = 0$, $\frac{\partial \Phi}{\partial T} \neq 0$, exists for $\exp(2S_0) < \lambda/2\beta_r$, i.e. only before the onset of the drift bifurcation. But additional terms of the form $|A|^4 A$, $|B|^4 B$, can stabilize the drifting solution, and even make the drift bifurcation supercritical.

7.4 The drift bifurcation

We observed in the above examples that the drift bifurcation consists of a secondary instability of the basic pattern that spontaneously breaks its reflection symmetry $x \to -x$. The eigenvalue λ of the corresponding eigenmode $\mathbf{u}_\pi(x)$ vanishes at the bifurcation. However, we have a persistent zero eigenvalue associated with translational symmetry; the drift instability results from the coupling between the reflection symmetry-breaking amplitude mode, and the phase mode associated with translational invariance. In the vicinity of this instability onset, we write

$$\mathbf{u}(x,t) = \mathbf{u}_0[x + \phi(X,T)] + V(X,T)\,\mathbf{u}_\pi(x) + \cdots, \tag{7.8}$$

and look for coupled equations for ϕ and V. The form of these equations is given by symmetry arguments, translational invariance in space ($\phi \to \phi + \phi_0$), and space reflection symmetry ($x \to -x, \phi \to -\phi, V \to -V$). We get to leading orders in the gradient expansion

$$\frac{\partial \phi}{\partial T} = V, \tag{7.9a}$$

$$\frac{\partial V}{\partial T} = \lambda V - V^3 + a\frac{\partial^2 \phi}{\partial X^2} + b\frac{\partial^2 V}{\partial X^2} + fV\frac{\partial \phi}{\partial X} + gV\frac{\partial V}{\partial X} + h\frac{\partial \phi}{\partial X}\frac{\partial^2 \phi}{\partial X^2} + \cdots. \tag{7.9b}$$

Higher-order terms in equation (7.9 a) can always be removed via a nonlinear transformation (Fauve et al. 1987). (The coefficient in equation (7.9 a) has been scaled in V). If the coefficients, a, b are positive, the $V = 0$ solution first bifurcates when λ vanishes and becomes positive. The homogeneous drifting pattern, $V_0 = \pm\sqrt{\lambda}$, $\phi_0 = V_0 T$, bifurcates supercritically; however its stability to inhomogeneous disturbances of the form $\exp(\eta T + iKX)$, is governed by the dispersion relation,

$$\eta^2 + (2\lambda - iKgV_0 + bK^2)\eta - iKfV_0 + aK^2 = 0(K^2), \tag{7.10}$$

that shows that the term $fV\partial\phi/\partial X$ destabilizes the homogeneous pattern independently of the sign of f. This may appear somewhat surprising, because at the drift instability onset, one bifurcates from the linearly stable static pattern to the linearly unstable static pattern whithout appearence of stable drifting patterns; this behaviour traces back to the existence of subcritical localized traveling solutions of equation (7.9), that describe localized drifting regions with tilted cells, widely observed in most experiments. Thus, even when the the drift bifurcation is supercritical if one only considers homogeneous patterns (as in section 7.2 for instance), the coupling term $fV\partial\phi/\partial X$ makes it generically subcritical when no restriction is imposed.

Another experimental observation can be understood in the framework of equations (7.9): it is the stationary pattern wavenumber selection often observed as the control parameter is increased. In most of the above quoted experiments, it is observed that a pattern wavenumber modification occurs by nucleation of a transient drifting domain that generates a phase gradient, say K, and leads to a new periodic pattern of wavenumber $k + \epsilon K$. Indeed, $V = 0$, $\phi = Kx$, is a particular solution of equations (7.9), for which the damping rate of perturbations in V is $\lambda + fK$. Consequently the drift of this new pattern is inhibited if $fK < 0$, for $|K| > \lambda/f$. The new periodic pattern thus remains stationary because of wavenumber modification. Within the framework of the model of section 7.2, this stabilization mechanism is associated to the increase of the second harmonic damping rate when the pattern wavenumber is increased.

7.5 Oscillatory phase modulation of periodic patterns

As said above, an oscillatory phase modulation of periodic patterns is observed as a secondary instability of parametrically generated surface waves (Douady et al., 1989). After this instability onset, the position of the wavecrests is modulated in space and time by a standing wave. This oscillatory instability is observed close to the "drift bifurcation" in the experimental parameter space. The numerical integration of equations (7.5) has shown that this oscillatory instability corresponds to a standing wave modulation of the basic pattern spatial and temporal phases, in agreement with the experimental observations.

We show that the coupling that generates the "drift bifurcation" is also a possible mechanism to describe phase modulation of periodic patterns, if the order parameter V is destabilized at a finite wavenumber. We consider equations (7.9), that govern the space dependent perturbations of the basic periodic pattern, with $\lambda \simeq -\lambda_0$, $\lambda_0 > 0$. Thus, the standing pattern is stable with respect to homogeneous perturbations. The growth rate of a perturbation of the form $\exp(\eta T + iKX)$, is governed by the dispersion relation,

$$\eta^2 + \eta\left(-\lambda + bK^2\right) + aK^2 = o(K^2). \tag{7.11}$$

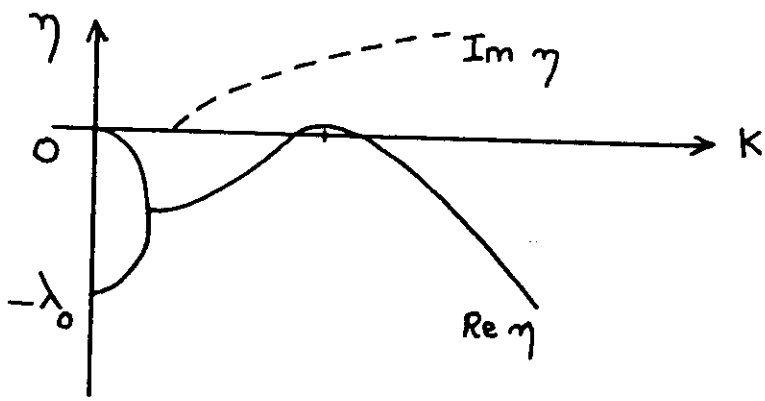

Figure 7.1. Perturbation growthrate as a function of the wavenumber of the oscillatory instability ($a > 0$, $b < 0$).

Stability at short wavelength requires higher order terms (fourth order gradients). For $a > 0$ and $b < 0$ an oscillatory instabilty occurs first. The corresponding growthrate is displayed on figure 7.1; it shows that the oscillatory instability results from the interaction of the neutral mode, because of the translation invariance in space, with the slightly damped, reflection symmetry-breaking mode associated with the "drift bifurcation" before its onset value. An instability leading to a stationary modulation of the basic pattern wavelength can occur for $a < 0$ and $b > 0$.

We have thus shown that a variety of recent experimental observations of periodic pattern secondary instabilities, can be understood in a simple framework : the coupling of the neutral mode associated with translational invariance in space, with a reflection symmetry-breaking bifurcation. Note that a similar singularity, with two zero eigenvalues at a secondary instability onset, occurs for the oscillatory instability of convection rolls and leads to traveling waves that propagate along their axis, although the underlying physical reasons are different (Fauve et al., 1987). Let us finally mention that the secondary instabilities described here fit in a general classification, proposed recently on the basis of symmetry arguments (Coullet and Iooss, 1989), but the present approach gives simple physical mechanisms that do generate these secondary instabilities.

References

Coullet, P., Goldstein, R. E., Gunaratne, G. H. (1989) Phys. Rev. Letters **63**, 1954-1957.

Coullet, P., Iooss, G. (1989) Phys. Rev. Letters **64**, 866.

Douady, S., Fauve, S., Thual, O., (1989) Europhysics Letters **10**, 309-315.

Fauve, S., Bolton, E. W., Brachet, M., (1987) Physica **29 D**, 202-214.

Faivre, G., de Cheveigné, S., Guthmann, C., Kurowski, P. (1989) Europhysics Letters **9**, 779-784.

Malomed, B. A., Tribelsky, M. I., (1984) Physica **14 D**, 67-87.

Mutabazi, I., Hegseth, J. J., Andereck, C. D., Wesfreid J. E., (1988) Phys. Rev. **A38**, 4752-4760.

Proctor, M. R. E., Jones, C., (1988) J. Fluid Mech. **188**, 301-335.

Rabaud, M., Michalland, S., Couder, Y. (1990) Phys. Rev. Letters **64**, 184.

Simon, A. J., Bechhoefer J., Libchaber, A. (1988) Phys. Rev. Letters **61**, 2574-2577.

Thual, O., Bellevaux, C., (1988) *Fifth Beer-Sheva Seminar on MHD Flows and Turbulence*, AIAA Progress in Astronautics and Aeronautics **112**, 332-354.

8. Nonlinear Localized Structures

8.1 Different types of nonlinear localized structures

Nonlinear interactions usually transfer energy to higher harmonics, thus making steeper a wave-front. Nonlinear effects can be balanced by dissipation; this is usually the case for shock waves. Let us consider a simple example, the Burgers equation

$$\frac{\partial \rho}{\partial t} + \rho \frac{\partial \rho}{\partial x} = \nu \frac{\partial^2 \rho}{\partial x^2}. \tag{8.1}$$

We look for a traveling solution of the form $\rho = \rho(x - ct)$, that connects two constant values of ρ, ρ_1 and ρ_2 for $x \to \pm\infty$. (8.1) becomes

$$-c\rho' + \rho\rho' = \nu\rho''.$$

Integrating once yields

$$-c\rho + \frac{1}{2}\rho^2 - \nu\rho' = \text{constant},$$

and consequently

$$c = \frac{\rho_1 + \rho_2}{2}.$$

Thus, although the shape of $\rho(x - ct)$ depends on the dissipation ν, this does not affect the shock velocity that depends only on the jump in ρ.

In conservative systems nonlinear effects may be balanced by dispersion: this is the basic mechanism that gives rise to solitary waves. We have already considered soliton-solutions of the nonlinear Schrödinger equation, and note that they can travel at any velocity because of Galilean invariance. This is not of course the case for all solitary waves; consider for instance the Sine-Gordon equation

$$\frac{\partial^2 u}{\partial t^2} = \frac{\partial^2 u}{\partial x^2} - \sin u, \tag{8.2}$$

which has kink type solitons of the form

$$u(x,t) = \pm 4\, tan^{-1}\left[\exp\frac{x - x_0 - ct}{\sqrt{1 - c^2}}\right]. \tag{8.3}$$

Unlike the solutions of the nonlinear Schrödinger equation, there is a speed limit 1 for the solutions (8. 3). However, there is a more important characteristic, associated with the discrete symmetry

$$u \to u + 2n\pi,$$

of the Sine-Gordon equation; the soliton solution (8.3) can be considered as a localized structure, connecting in space two states $u = 0$ and $u = \pm 2\pi$, related by this discrete symmetry transformation (Figure 9.1). This is called a topological soliton.

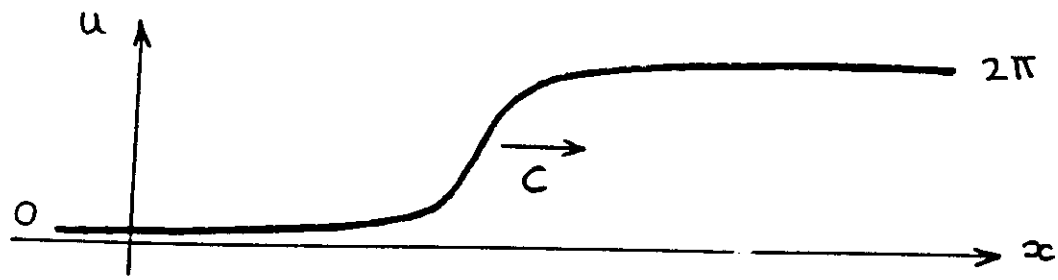

Figure 8.1. A kink soliton of the Sine-Gordon equation

Similar type of localized structures, from the symmetry point of view, exist in phase transitions or in patterns generated by instabilities; they are called topological defects. As we already mentionned, the amplitudes of unstable modes are analogous to order parameters in phase transition theory; indeed, a non zero amplitude is associated with the broken-symmetry at the instability onset. Thus, in the supercritical regime, it is natural to call defect, a region in space where the amplitude vanishes. A defect is said topologically stable, when a slight perturbation of the amplitude in space or time does not affect its characteristic shape (for instance only slightly translates it in space). We will only illustrate this concept with very simple examples (for a review, see Mermin 1979).

Let us consider the Ginzburg-Landau equation (5.16) for a real one-space-dimensional amplitude $R(X,T)$

$$\frac{\partial R}{\partial T} = \mu R + \frac{\partial^2 R}{\partial X^2} - R^3. \tag{8.4}$$

The broken symmetry at the instability onset ($\mu = 0$) is the $R \to -R$ symmetry. Correspondingly, there exist two homogeneous solutions, $R_0 = \pm\sqrt{\mu}$, that are related by this symmetry transformation. The space-dependent solution,

$$R(X) = \tanh\left(\sqrt{\frac{\mu}{2}}X\right),$$

connects these two solutions (Figure 8.2); it is a topological defect.

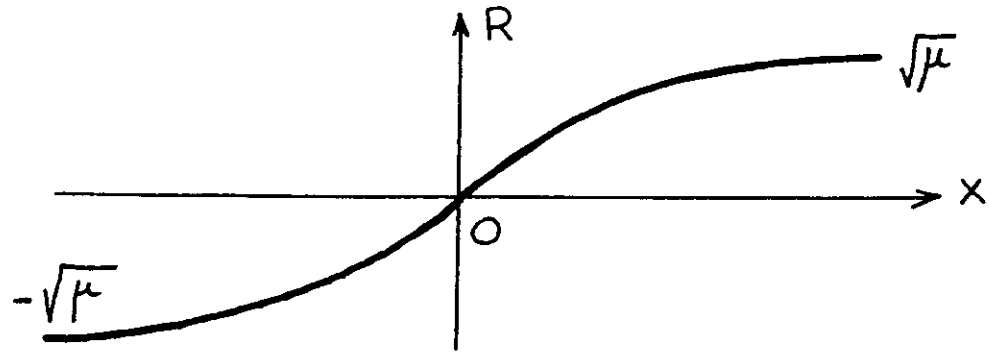

Figure 8.2. A topological defect for the real one-space-dimensional Ginzburg-Landau equation

This solution also exists for the complex Ginzburg-Landau equation,

$$\frac{\partial A}{\partial T} = \mu A + \Delta A - |A|^2 A. \tag{8.5}$$

However, it is not a topological defect since one can easily remove it with phase perturbations. On the contrary, for a two-space-dimensional field, $A(X, Y, T)$, there exists topologically stable point defects. Indeed, the complex amplitude $A(X, Y, T)$ vanishes if its real and imaginary parts vanish; at a given instant, Re $A(X, Y, T) = 0$ and Im $A(X, Y, T) = 0$ define one-dimensional curves in the $X - Y$ plane, that generically intersect at a point (Figure 8.3). If one slightly perturbs $A(X, Y, T)$, these curves move slightly and so does the defect, but it remains unchanged. Similarly, for a three-space-dimensional field, $A(X, Y, Z, T)$, topological defects of the complex Ginzburg-Landau equation are lines.

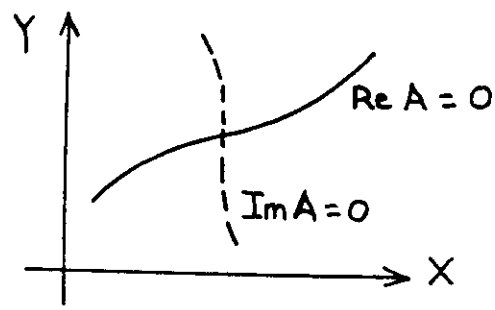

Figure 8.3. The location of a topological defect for a two-space-dimensional Ginzburg-Landau equation

If equation (8.5) is modified to

$$\frac{\partial A}{\partial T} = \mu A + \Delta A + |A|^2 A - |A|^4 A, \tag{8.6}$$

the bifurcation becomes subcritical. The interesting new feature is bistability; indeed, it is clear from the bifurcation diagram displayed in Figure 8.4 that two stable states coexist for μ negative. Obviously, these two solutions are not related by a symmetry transformation, but we can also consider an interface that separates in space these two stable states, or a droplet that consists of a region in one state surrounded by the other one. In a system with a Lyapunov functional, i.e. a free-energy, the interface moves such that the lowest energy state increases in size. Contrary to the situation with shock waves, the interface velocity does not depend only on the energy difference between the two homogeneous solutions, but also on the shape of the interface. With non-variational systems, interesting new phenomena occur (see section 8.3).

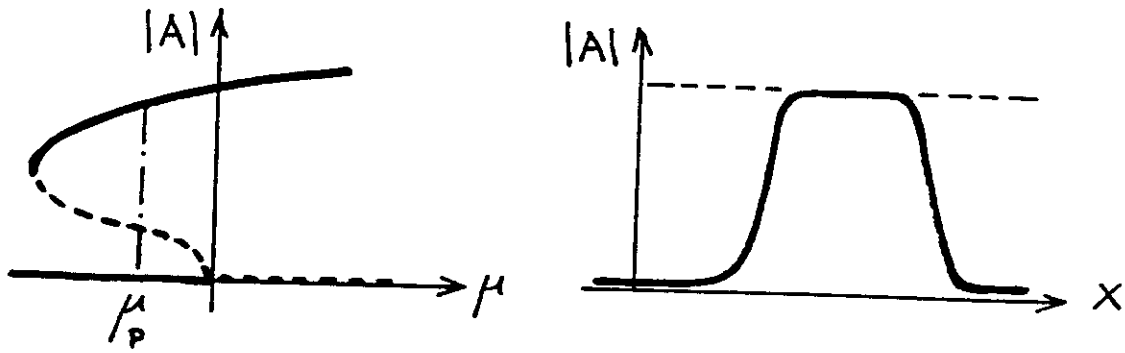

Figure 8.4. Bistability and localized structure in the vicinity of a subcritical bifurcation

8.2 Kink-dynamics

We consider equation (8.4) in the supercritical regime ($\mu > 0$); chosing appropriate time, space and amplitude scales, we get

$$\frac{\partial R}{\partial T} = 2R(1 - R^2) + \frac{\partial^2 R}{\partial X^2}. \tag{8.7}$$

This equation admits a kink type solution or defect,

$$R = \tanh X.$$

Consider a solution consisting of several kinks (Figure 8.4). Such a solution is unstable because the neutral translation mode, $\partial R/\partial X$, has a node; the only stable solution is the one with a single kink. What is the time evolution of such unstable structures? An interesting approach is to consider many topological defects, far one from the other, as a "gas" of such kinks and write an evolution equation for their density.

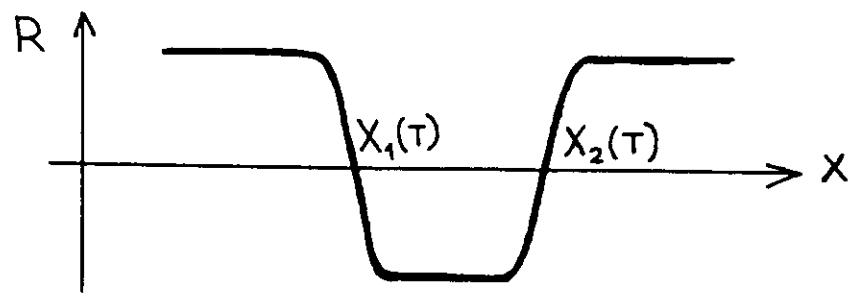

Figure 8.5. The two-kink solution (8.8)

We first derive an equation describing the interaction of two kinks that are far apart. Let us seek a solution in the form

$$R(X,T) = R_1\,[X_1(T)]\,R_2\,[X_2(T)]\,, \tag{8.8}$$

where

$$R_j\,[X_i(T)] = \tanh\,[X - X_i(T)] \tag{8.9}$$

and j is 1 or 2. Substituting (8.8) in (8.7) we obtain the equation

$$-\dot{X}_1 R_1' R_2 - \dot{X}_2 R_1 R_2' = 2R_1 R_2(1 - R_1^2 R_2^2) + R_1'' R_2 + 2R_1' R_2' + R_1 R_2'', \tag{8.10}$$

where a dot denotes time derivative and primes denote differentiation with respect to X_1 or X_2. By direct differentiation one can verify that

$$\begin{aligned} R_i' &= 1 - R_i^2 \\ R_i'' &= -2R_i(1 - R_i^2). \end{aligned}$$

At $X = X_i(T)$ we have $R_i = 0$, $R_i' = \pm 1$ and $R_j \approx \pm 1$. Substituting $X = X_i$ in (8.10) we derive the equations of motion for the kinks

$$\begin{aligned} \dot{X}_1 &\approx 2\,\left[1 - R_2^2(X_1)\right] \approx 2\exp\left(-2 \mid X_1 - X_2 \mid\right) \\ \dot{X}_2 &\approx -2\,\left[(1 - R_1^2(X_2)\right] \approx -2\exp\left(-2 \mid X_1 - X_2 \mid\right), \end{aligned} \tag{8.11}$$

which show that each kink feels the effect of the exponentially decreasing tail of the other at large separations. We can generalize this to consider the interaction of many kinks in the nearest neighbour approximation:

$$\dot{X}_i \approx 2\exp\left(-2 \mid X_{i+1} - X_i \mid\right) - 2\exp\left(-2 \mid X_i - X_{i-1} \mid\right). \tag{8.12}$$

Define

$$\rho_i = \exp\left(-2 \mid X_{i+1} - X_i \mid\right). \tag{8.13}$$

Then $-1/log\rho_i$ is the "kink density". Taking the logarithm of (8.12) and differentiating with respect to time, we have

$$\dot{\rho}_i = -2(\dot{X}_{i+1} - \dot{X}_i)\rho_i, \tag{8.14}$$

and on using (8.11) and (8.12),

$$\dot{\rho}_i = -4(\rho_{i+1} - 2\rho_i + \rho_{i-1})\rho_i. \tag{8.15}$$

Finally, passing to the continuum limit, we have the equation for a "rarefied kink gas"

$$\frac{\partial \rho}{\partial T} = -8\rho\frac{\partial^2 \rho}{\partial X^2}. \tag{8.16}$$

We see that this is a nonlinear diffusion equation where the diffusion coefficient $D = -8\rho$ is negative. It therefore describes a condensation process with all the kinks tending to clump together due to mutual attraction. Let us consider a train of kinks, equispaced with a distance a apart. Then, $X_{i+1}^{(0)} - X_i^{(0)} = a$, where the superscript zero denotes the initial state. Setting, $X_i = X_i^{(0)} + u_i$, and looking for normal modes, $u_n \propto \exp(\eta T - iKna)$, we have

$$\eta = 16e^{-a}\sin^2(Ka/2),$$

which shows that the mode with the largest growth rate is at $Ka = \pi$, i.e. an optical mode at twice the wavelength of the kink-array.

The important point to note here, is that we can describe a system at different approximation levels corresponding to equations (8.7), (8.11) and (8.16). Depending on the problem, one can consider localized structures as "particles" and use (8.11), or use a continuous description.

8.3 Localized structures in the vicinity of a subcritical bifurcation

Consider the following simple model equation describing a subcritical bifurcation:

$$\frac{\partial A}{\partial T} = \mu A + \alpha\frac{\partial^2 A}{\partial X^2} + \beta \mid A \mid^2 A + \gamma \mid A \mid^4 A. \tag{8.17}$$

If the coefficients of this equation are real, the steady state is given by the solution which minimizes the Lyapunov functional

$$\begin{aligned} \mathcal{L} &= \int_0^L \left[\alpha_r \mid A_x \mid^2 - V(\mid A \mid)\right] dX \\ V(\mid A \mid) &= \mu \mid A \mid^2 + \frac{\beta_r}{2} \mid A \mid^4 + \frac{\gamma_r}{3} \mid A \mid^6 . \end{aligned} \tag{8.18}$$

Since we are considering a subcritical bifurcation, $\beta_r > 0$ and $\gamma_r < 0$. The three possible situations are shown in Figure 8.6. The two states have the same energy and thus can coexist only if $\mu = \mu_P$; μ_P corresponds to the Maxwell plateau of first order phase transitions.

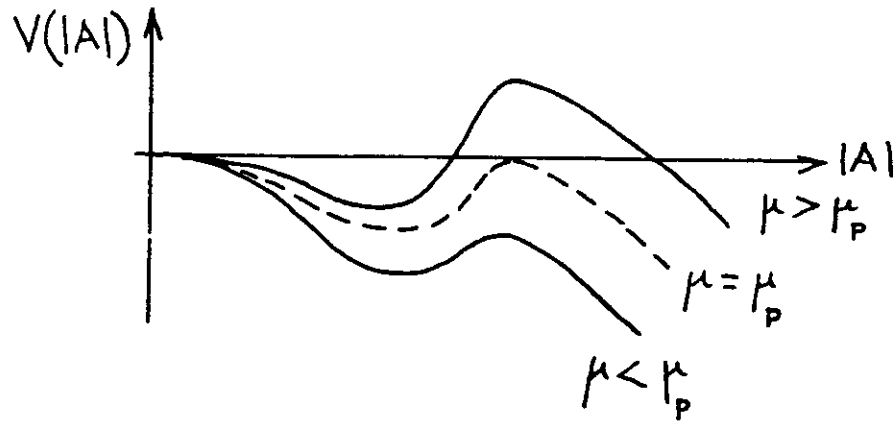

Figure 8.6. The Lyapunov functional (8.18) for $\mu \approx \mu_P$

Now consider the situation with α and β complex so that there is no longer a Lyapunov functional for the problem. In this situation stable localized structures are possible (Thual and Fauve, 1989). The stabilization can be explained by the following rough argument. Substituting

$$A = R(X,T)\exp\left[i\theta(X,T)\right]$$

in equation (8.17) and equating real and imaginary parts we have

$$\begin{aligned}
\frac{\partial R}{\partial T} &= \alpha_r \frac{\partial^2 R}{\partial X^2} + \left[\mu - \alpha_r \left(\frac{\partial \theta}{\partial X}\right)^2\right] R + \beta_r R^3 + \gamma_r R^5 - \alpha_i \left(2\frac{\partial R}{\partial X}\frac{\partial \theta}{\partial X} + R\frac{\partial^2 \theta}{\partial X^2}\right) \\
R\frac{\partial \theta}{\partial T} &= \alpha_r \left(2\frac{\partial R}{\partial X}\frac{\partial \theta}{\partial X} + R\frac{\partial^2 \theta}{\partial X^2}\right) + \alpha_i \frac{\partial^2 R}{\partial X^2} - \alpha_i R \left(\frac{\partial \theta}{\partial X}\right)^2 + \beta_i R^3 + \gamma_i R^5.
\end{aligned} \tag{8.19}$$

If the imaginary part of the coefficients are zero, (8.19) is solved by $\partial\theta/\partial X = 0$, and we have a variational problem for R. In the presence of a non-zero imaginary part, the amplitude and phase equations couple so that there is a nonzero $\partial\theta/\partial X$. This changes the effective value of μ in the coefficient of R in (8.19); we define

$$\mu_{eff} = \mu - \left(\frac{\partial \theta}{\partial X}\right)^2.$$

The effect of the phase gradient is to decrease μ_{eff} in the outer region, thus stabilisating the zero-solution, whereas the bifurcated solution is stabilisated in the core of the localized structure.

These localized structures can be obtained perturbatively in the variational and conservative limits; in the conservative limit, let us write (8.17) as

$$\begin{aligned}
\frac{\partial A}{\partial T} &= i\frac{\partial^2 A}{\partial X^2} + 2i \mid A \mid^2 A + \epsilon P(A) \\
P(A) &= \mu A + \alpha_r \frac{\partial^2 A}{\partial X^2} + \beta_r \mid A \mid^2 A + \gamma_r \mid A \mid^4 A.
\end{aligned} \tag{8.20}$$

For $\epsilon = 0$ this is simply the nonlinear Schrödinger equation and admits the one-parameter family of solutions

$$A_s = \Delta \, \mathrm{sech}(\Delta X) \exp(-i\Delta^2 T). \tag{8.21}$$

The existence of such a one-parameter family is due to the scale invariance of the nonlinear Schrödinger equation.

If ϵ is given a small but nonzero value, we look for slowly varying solitons of the form

$$A(X,T) = \Delta(T) \, \mathrm{sech}[\Delta(T)X] \exp[-i\Theta(T]. \tag{8.22}$$

The temporal evolution of a soliton under the action of a perturbation $P(A)$ is a well-known problem of soliton theory and can be solved with the inverse scattering method (see for instance Lamb, 1980). The temporal evolution of $\Delta(T)$ can be found in a simpler way here: multiplying equation (8.20) by $\bar{A}$ and integrating on space leads to the evolution equation

$$\frac{d}{dT} \int |A|^2 \, dX = \epsilon \int [\mu |A|^2 + \beta_r |A|^4 + \gamma_r |A|^6 - \alpha_r |A_x|^2] \, dX. \tag{8.22}$$

Substituting (8.21) in (8.22), we get to leading order, an evolution equation for Δ,

$$\frac{1}{2}\frac{d\Delta}{dT} = \mu\Delta + \frac{4}{3}(2\beta_r - \alpha_r)\Delta^3 + \frac{128}{15}\gamma_r\Delta^5 \tag{8.23}$$

For $\alpha_r < 2\beta_r$, equation (8.23) has two non-zero solutions $\Delta_\pm$ for $\mu_s < \mu < 0$, with $\mu_s = 5(-\alpha_r + 2\beta_r)^2/96\gamma_r$. Only the larger is stable, and gives the size of the selected pulse.

The above mechanism is a rather general one: the dissipative terms of equation (8.17) stabilize one of the soliton solutions among the continuous family (8.21) and select its size by breaking the scale-invariance associated with the corresponding conservative problem.

References

Fauve, S., Thual, O. (1990) Phys. Rev. Lett. **64** , 282-284

Hakim, V., Jakobsen, P. Pomeau, Y. (1990) Europhysics Lett.**11**, 19-24

Kawasaki, K., Ohta, T. (1982) Physica **116 A**, 573

Lamb, G. L. (1980) *Elements of Soliton Theory*,Wiley